Generation of anti-HER1/2 immunotoxins by protein ligation using split inteins

TECHNISCHE UNIVERSITÄT DARMSTADT

vom Fachbereich Chemie
der Technischen Universität Darmstadt

zur Erlangung des Grades
Doctor rerum naturalium (Dr. rer. nat.)

Dissertation

von

Thomas Pirzer, M.Sc.
aus Haßfurt

Erstgutachter: Prof. Dr. Harald Kolmar
Zweitgutachter: Prof. Dr. Henning D. Mootz

Darmstadt 2018

Pirzer, Thomas : Generation of anti-HER1/2 immunotoxins by protein ligation using split inteins
Darmstadt, Technische Universität Darmstadt,
Jahr der Veröffentlichung der Dissertation auf TUprints: 2018
URN: urn:nbn:de:tuda-tuprints-77542
Tag der mündlichen Prüfung: 02.08.2018
Veröffentlicht unter CC BY-SA 4.0 International

Tag der Einreichung: 14. Juni 2018
Tag der mündlichen Prüfung: 02. August 2018

Die vorliegende Arbeit wurde unter der Leitung von Herrn Prof. Dr. Harald Kolmar am Clemens-Schöpf-Institut für Organische Chemie und Biochemie der Technischen Universität Darmstadt im Zeitraum von Juni 2015 bis Juni 2018 angefertigt.

Publications derived from this work:

Pirzer T., Becher K-S., Rieker M., Meckel T., Mootz H. D., Kolmar H. Generation of potent anti-HER1/2 immunotoxins by protein ligation using split inteins. *ACS Chemical Biology* **2018**, 13 (8), 2058–2066

Further publications during PhD thesis:

Könning D.; Rhiel L.; Empting M.; Grzeschik J.; Sellmann C.; Schröter C.; Zielonka S.; Dickgießer S.; **Pirzer T**.; Yanakieva D.; Becker S.; Kolmar H. Semi-synthetic vNAR libraries screened against therapeutic antibodies primarily deliver anti-idiotypic binders. *Scientific Reports* **2017,** 7 (1), 1-13

Grzeschik J.; Hinz S., Könning D.; **Pirzer T**.; Becker S.; Zielonka S.; Kolmar H. A simplified procedure for antibody engineering by yeast surface display: Coupling display levels and target binding by ribosomal skipping. *Biotechnology Journal* **2017,** 12 (2)

Table of Content

1. Abstract

1.1. Zusammenfassung

Zellspezifische Proteintoxine haben durch die Möglichkeiten, das therapeutische Fenster zu vergrößern und die systemische Toxizität zu senken, zunehmendes Interesse in der Krebstherapie geweckt. Aufgrund limitierender Toxizität in eukaryotischen Expressionssystemen, beruhten die meisten Anwendungen bisher auf der Fusion von Antikörperfragmenten mit Toxinen, die in Bakterien, wie *Escherichia coli (E. coli)* hergestellt werden können. Diesen Fusionen fehlen jedoch häufig nützliche Eigenschaften von Volllängenantikörpern, wie eine verlängerte Serumhalbwertszeit oder effiziente endosomale Aufnahme durch Rezeptorgruppierung.

Ziel dieser Arbeit war die Herstellung neuartiger Immuntoxine, bestehend aus Volllängenantikörpern und verschiedenen Proteintoxinen, durch Proteinspleißen in *trans* mit geteilten Inteinen. Zunächst wurde die Toxinexpression durch Optimierung verschiedener Parameter, wie Expressionsstamm, Induktionskonditionen und Fusionspartnern, verbessert. Das pflanzliche Gelonin und das bakterielle *Pseudomonas* Exotoxin A wurden dafür in *E. coli* produziert. Fusionen mit Thioredoxin und Maltosebindeprotein erzielten reproduzierbare und akzeptable Ausbeuten. Der HER2 bindende Antikörper Trastuzumab wurde als Modell für therapeutisch relevante und gut beschriebene Antikörper verwendet. Zusätzlich wurde ein, aus zwei EGFR bindenden VHH Domänen bestehender, Antikörper entwickelt, welcher nur aus einer schweren Kette besteht. Beide Antikörper wurden in Säugetierzellen in guten Ausbeuten produziert.

Ein geteiltes Intein wurde verwendet, um Antikörper und Toxine zu verbinden und daraus biologisch aktive Immuntoxine zu generieren. Der kurze (11 Aminosäuren) *N*-terminale Teil des aus *Ssp* DnaB evolvierten M86 Inteins wurde rekombinant an die Antikörper fusioniert, während der längere (143 Aminosäuren) Teil an die Toxine fusioniert wurde. Durch das Mischen der beiden Reaktionspartner konnte sich das Intein in seine aktive Form falten und das Spleißen ausführen. Die Reaktionsbedingungen wurden in diversen *in vitro* Reaktionen getestet und optimiert. Zu ihnen gehörten die Konzentration des Reduktionsmittels, die Reaktionszeit und der Aggregationsstatus der Toxine. Beide Antikörper konnten mit Spleißeffizienzen von 50 – 70 % erfolgreich mit Gelonin und Exotoxin A verbunden werden. Diese Immuntoxine wurden durch Protein A und immobilisierte Metallaffinitätschromatographie gereinigt. Die Endkonstrukte waren durch ein Toxin/Antikörper Verhältnis von 1,3 gekennzeichnet und wurden daraufhin detaillierter analysiert.

Die spezifische Zellbindung konnte bei allen Immuntoxinen bestätigt werden. Außerdem wurde die enzymatische Aktivität von Gelonin in einem *in vitro* Translationsversuch bestätigt. Konfokalmikroskopie wurde angewandt, um die endosomale Aufnahme, die dort stattfindende Spaltung eines proteaselabilen Linkers und die anschließende Translokation des Toxins ins Zytoplasma zu bestätigen. Alle Immuntoxine

zeichneten sich in Zelltoxizitätsexperimenten auf verschiedenen Zelllinien durch IC_{50} Werte im mittleren pikomolaren bis hohen femtomolaren Bereich aus, wodurch sie zu den potentesten bisher publizierten Immuntoxinen gehören.

1.2. Abstract

Cell targeting protein toxins have gained increasing interest for cancer therapy, aimed at increasing the therapeutic window and reducing systemic toxicity. Since recombinant expression of immunotoxins consisting of a receptor-binding and a cell-killing moiety is hampered by their high toxicity in a eukaryotic production host, most applications rely on recombinant production of fusion proteins consisting of an antibody fragment and a protein toxin in bacterial hosts such as *Escherichia coli (E. coli)*. These fusions often lack beneficial properties of whole antibodies like extended serum half-life or efficient endocytic uptake via receptor clustering.

This work aimed to generate novel immunotoxins composed of full-length antibodies and different toxins by protein *trans*-splicing using split inteins. Initially, different toxins were optimized for expression by testing a variety of expression hosts, induction parameters and fusion partners. The plant toxin gelonin and variants of the bacterial *Pseudomonas* Exotoxin A were used and expressed in *E. coli*. Fusions to thioredoxin and maltose binding protein resulted in reproducible and acceptable yields.

The HER2 binding antibody trastuzumab was used as a model for therapeutic antibodies with known properties. Additionally, a new antibody was designed, composed of two VHH domains that were attached in tandem on an IgG1 Fc scaffold, resulting in a heavy-chain antibody with specificity towards EGFR. Both antibodies were produced in mammalian cells at good yields.

A split intein was used to connect both antibodies and toxins to form biologically active immunotoxins. To this end, the short (11 amino acids) *N*-terminal intein part of the artificially designed split intein M86, a derivative of the *Ssp* DnaB intein, was recombinantly fused to the heavy chain of the antibodies, while the longer (143 amino acids) *C*-terminal intein part was fused to the toxins. By mixing both reaction partners under reducing conditions, the intein assembled into its active form and splicing occurred.

Reaction conditions for protein splicing were optimized in *in vitro* reactions. Parameters included concentration of reducing agents, time and aggregation state of the toxin. Both antibodies could be linked to gelonin and exotoxin A with splicing efficacies of 50 – 70 %. Generated immunotoxins were purified by protein A chromatography and immobilized metal affinity chromatography. The resulting constructs were characterized by a toxin/antibody ratio of about 1.3 and were analyzed in more detail.

Specific cell binding was analyzed and confirmed for all immunotoxins. The activity of gelonin was confirmed by an *in vitro* translation assay with cell lysates. Confocal microscopy was used to follow

cellular uptake and confirmed endosomal uptake as well as cleavage of a protease-labile linker and subsequent translocation of the toxin out of the endosomes. All immunotoxins exhibited IC_{50} values in the mid- to subpicomolar range in cytotoxicity assays with different cell lines, numbering them among the most toxic immunotoxins reported to date.

1. Introduction

The human body is under constant attack from pathogens, ranging from viruses to bacteria. Additionally, mutations occur in each cell of the body, caused by external agents such as UV light, X-rays or chemicals as well as internal metabolites like reactive oxygen species.[1] This results in up to 70,000 DNA damages per day in each cell.[2] Although a variety of DNA repair mechanisms exist, some of these somatic mutations may diminish the genomic stability and follow-up mutations alter a cell's fate and drive its abnormal growth.[1] Once a threshold of mutations in cancer-driving genes, so-called oncogenes, has been reached, tumor progression takes place. Notably, the acquisition of further mutations doesn't stop but continues and complicates treatment, since a tumor is not a uniform cluster of clonal cells and each cell may acquire a different set of mutations.[3] Once a tumor has formed it is defined by several hallmarks consisting of i) sustaining proliferative signaling ii) evading growth suppressors iii) activating invasion and metastasis iv) enabling replicative immortality v) inducing angiogenesis and vi) resisting cell death.[4] Especially the outcome of hallmark iii) will lower the treatment success and survival prognosis. But how to fight a tumor that has no recognition sites that mark it as pathogenic or lethal?

In 1900 Paul Ehrlich proposed a concept called "magic bullets" to target specific pathogens or malignancies like cancer.[5] Inspired by his search for molecules that target specific structures or organelles – in his case with dyes – cancer researchers sought molecules that could kill pathogens or tumors specifically. The first chemotherapeutics were found by chance in the 1950s by Goodman and Gilman. They found that derivatives of nitrogen mustard caused a drastic anti-tumor effect in patients with non-Hodgekin lymphoma.[6,7] Based on the finding that tumor cells proliferate much faster than normal tissues and on the knowledge of the underlying molecular mechanisms of cell division, chemically modified DNA base analogues and DNA binding molecules with reduced host toxicity were developed, including 5-fluorouracil and cisplatin.[8–10] With the discovery of oncogenes and tumor suppressor genes in the 1970s and 80s another step was taken towards the specific targeting of cancer. In cancer overexpressed proteins critical for proliferation, invasion and metastasis were trying to be targeted with small-molecules. Imatinib, for example, the inhibitor of a tumor progressing tyrosine kinase originating from the bcr-abl gene fusion, showed great clinical success and spurred other researchers.[11] Further, inhibitors of protein-protein interactions of oncoproteins were invented, for example insulin-like growth factor 1 receptor or the p53-binding pocket of MDM2.[12,13]

Although several side effects and high systemic toxicity are known, chemotherapy is still a standard therapy in cancer. A better way would be to target tumors specifically by distinct markers. One of the main problems was the identification of surface exposed structures that discriminate tumor cells from healthy ones. Although biomarkers are defined as any structure, substance or progress that is involved in a disease, those that are targetable on the cell surface are most desired.[14] The current progress in high-throughput sequencing and proteomic methods leads to an exponential increase in studies, unfortunately

without a directly proportional verification of clinical valuable targets.[14] Some growth factor receptors that can be specifically targeted are nevertheless regularly overexpressed in several tumors. The molecule of choice used for targeting these structures are antibodies (Abs). These proteins are one of the key players in the recognition of pathogens in the human immune system. Their properties make them the optimal choice for cancer treatment: i) they can bind an antigen with high selectivity and affinity ii) they have a long natural half-life in the blood circulation iii) they have effector functions iv) they are almost not immunogenic when they are of human origin.[15,16] The key technology for the realization of antibody screening and production was the generation of hybridoma cells that could produce monoclonal antibodies (mAbs) with only one specificity.[17] After the identification of human epidermal growth factor receptor 2 (HER2) as an overexpressed biomarker in a subset of breast cancer patients the antibody trastuzumab was developed and displayed high clinical efficacy.[18]

Promising results from many other antibodies developed for cancer treatment also paved the way for the attachment of toxins to antibodies, creating antibody-drug conjugates (ADCs). In this concept, the targeting properties of the antibody are combined with the high cytotoxicity of a chemotherapeutic drug to directly kill tumor cells. Especially naturally derived cytotoxic agents that showed extremely high potency *in vitro* but had elusive clinical success, like maytansinoids, dolastatins or duocarmycins, were chemically linked to antibodies.[19] Due to the conjugation, the therapeutic window of the drug, which is the dose range between the minimum effective dose (MED) and the maximum tolerated dose (MTD), can be increased resulting in higher potency of an ADC compared to the drug alone.[20,21] Although ADCs show great potential in cancer treatment, only two are currently approved by the FDA: ado-trastuzumab emtansine for the treatment of HER2 positive metastatic breast cancer and Brentuximab vedotin, a CD30 specific ADC for the treatment of Hodgkin lymphoma and anaplastic large cell lymphoma.[22–25]

Instead of small molecular toxins protein toxins can be conjugated to antibodies or antigen-targeting fragments. In 1978 Thorpe *et al.* showed for the first time that the bacterial diphtheria toxin (DT) could be conjugated to an anti-lymphoblastoid antibody to increase the potency of the toxin.[26] Together with the development of mAbs a new class of “magic bullet” arose, so-called immunotoxins (ITs).[27] While the first ITs involved chemical linkage of isolated toxins to antibodies, molecular cloning techniques paved the way to recombinant and optimized fusion proteins composed of antibody fragments and active toxin domains.[28] From there on ITs were constantly improved in terms of safety and efficacy. The toxic portion is mostly derived from bacterial or plant toxins like DT, *Pseudomonas* Exotoxin A, ricin or gelonin.[28,29] In the same way ADCs still lack striking clinical efficacy, there are still problems with ITs in terms of side effects like immunogenicity. Nevertheless progress is made in the development of next generation ITs with reduced immunogenicity by identifying and exchanging prominent T- and B-cell epitopes.[30]

1.3. Antibodies as "magic bullets"

To defend itself, the body has evolved a range of mechanism for destroying pathogens. On the one hand, there is the innate immune system that is passed over from a mother to a child even before birth and is rather unspecific and includes immune cells like natural killer cells, macrophages as well as cytokines, complement and acute phase proteins. This system is primarily used for a fast response, for example when pathogens enter through a wound, because of the lack of a long lag phase. Therefore, it recognizes generally available pathogen-associated molecular patterns (PAMPs) that are detected on a multitude of microorganisms through pattern recognition receptors (PRRs). On the other hand, the adaptive immune system, which is present only in vertebrates, is antigen-specific with responses from T- and B-lymphocytes. In contrast to the innate immune response, the adaptive one takes days rather than hours to develop but retains a long lasting immunity up to several years. B-cells produce antibodies after being activated. Those molecules are characterized by a high specificity towards an antigen, high serum stability and several effector functions. By binding to an antigen it activates different immune pathways with the final outcome of killing the pathogen or the malign cell.[15,31] Currently they are widely used for the therapy of several indications like inflammatory diseases, hemophilia, autoimmune diseases and cancer. Besides classical antibodies that rely on their agonistic/antagonistic properties or intrinsic effector functions, antibody-drug conjugates have been developed.[32] These combine the specific targeting properties of antibodies with highly toxic small molecules.

1.3.1. Structure and function of antibodies

Antibodies or immunoglobulins are produced by activated B-cells and secreted into the blood serum. These proteins are heterodimers consisting of two heavy (HC) and two light chains (LC), each of them composed of constant (C) and variable (V) domains. The HC is generally composed of V_H, CH_1, CH_2 and CH_3 for IgG, IgA, and IgD classes, with a fourth constant domain (CH_4) for IgM and IgE.[33] The LC has only one variable (V_L) and one constant domain (C_L). The *N*-terminal variable domains are responsible for antigen binding. Each single domain is about 120 amino acids (aa) long, has a β-sandwich secondary structure, which is termed as classical immunoglobulin fold and is further stabilized by an intramolecular disulfide bridge.[33]

For antigen recognition, the variable domains have three hypervariable stretches (HV), called complementarity-determining regions (CDRs) that extend from the framework (FR) structure. The third CDR is typically the most variable one. In sum there are six CDRs forming the complementary binding site to the antigen. These loop structures can adapt a multitude of conformations, thus adapting to proteins, peptides or sugars. Although antibodies naturally recognize conformations on molecular surfaces, they sometimes bind to linear epitopes, as used for detection Abs binding His_6 or myc tags. The

diversity of variable domains is obtained by several mechanisms including gene recombinations, nucleotide deletions/insertions and somatic hypermutation. This results in a theoretic antibody diversity of $> 10^{11}$ receptors that can be produced by B-cells.[15]

Both variable domains of HC and LC (V_C and V_L), together with their neighboring constant domains (C_H1 and C_L) form the antigen binding fragment (Fab) of an antibody (Figure 1). If single V_C and V_L are genetically connected by a flexible linker, one speaks of a single-chain variable fragment (scFv), which doesn't occur naturally. A hinge region follows the C_H1 domain giving flexibility and two disulfide bridges connecting both HCs lead to extra stability.

Domains CH_2 and CH_3 make up the crystallizable fragment (Fc) and determine the different antibody isotypes and interactions. The predominant and simultaneously mostly studied isotype of antibodies in human serum is the IgG isotype. It is further divided into subtypes IgG1-4 based on structural and functional differences. These are numbered according to their abundance in serum. The IgG1 is the most studied isoform because of its high proportion and its many effector functions that makes it suitable as a therapeutic. Additionally, it has one of the highest half-lifes owing to its recycling in endothelial cells by binding to the neonatal Fc receptor (FcRn).[34,35] The following study is always referring to the IgG1 isotype unless otherwise stated. The characteristic *N*-glycosylation is located in the C_H2 domain at asparagine 297 and is characterized by a biantennary structure with a heptasaccharide core consisting of *N*-acetylglucosamine and mannose. Variability is achieved by terminal units of fucose, galactose, *N*-acetylglucosamine and sialic acid. Glycosylation profoundly influences stability of the Fc part and is critical for antibody pharmacokinetics and its interaction with Fc receptors.[33,35–37] The Fc fragment has adapter functions to induce effects like complement activation, half-life extension and Fc receptor binding that amongst others leads to acquisition of effector cells. IgG antibodies for example specifically trigger antibody-dependent cellular cytotoxicity (ADCC)[38] and complement-dependent cytotoxicity (CDC)[39], which is dependent on the unique glycan composition of this subtype. Fc gamma receptors (FcγR) bind to the IgG constant domain and induce macrophage phagocytosis, natural killer (NK) cell ADCC and neutrophil activation, depending on the type of FcγR.[40] Upon binding and clustering on FcγR an intracellular signaling cascade is activated by immunoreceptor tyrosine-based activation (ITAM) or inhibitory motifs (ITIM).[41] Since various IgG subtypes show different affinities to the activating or inhibiting receptors, it is an important setscrew for the selection of therapeutic antibodies.[42] For example when targeting a tumor cell and ADCC shall be activated leading to cell death, the subtypes IgG1 and 3 have to be used because of their affinity to the FcγRIII, which is present on natural killer (NK) cells and triggers the release of cytoplasmic granules containing perforin and granzymes.[15,43]

As mentioned previously, IgG bind to the well characterized neonatal Fc receptor (FcRn). Originally the receptor was found to transcytose IgGs from mother to fetus across the placenta thus giving the new born child a humoral immunity. In adults it is mainly responsible for the regulation of IgG distribution

and serum levels. The FcRn binds an IgG at acidic pH (pH 6 – 6.5) and releases it at physiological pH (pH 7.4). This primarily takes place in the endothelium or glomerular cells in the kidney where Abs are endocytosed unspecifically from the blood-stream. The endosomal complex of Ab and receptor are trafficked back to the cell surface or to the opposite cell membrane, thereby protecting the Ab from lysosomal degradation and extending its half-life to around 21 days.[15,34,44]

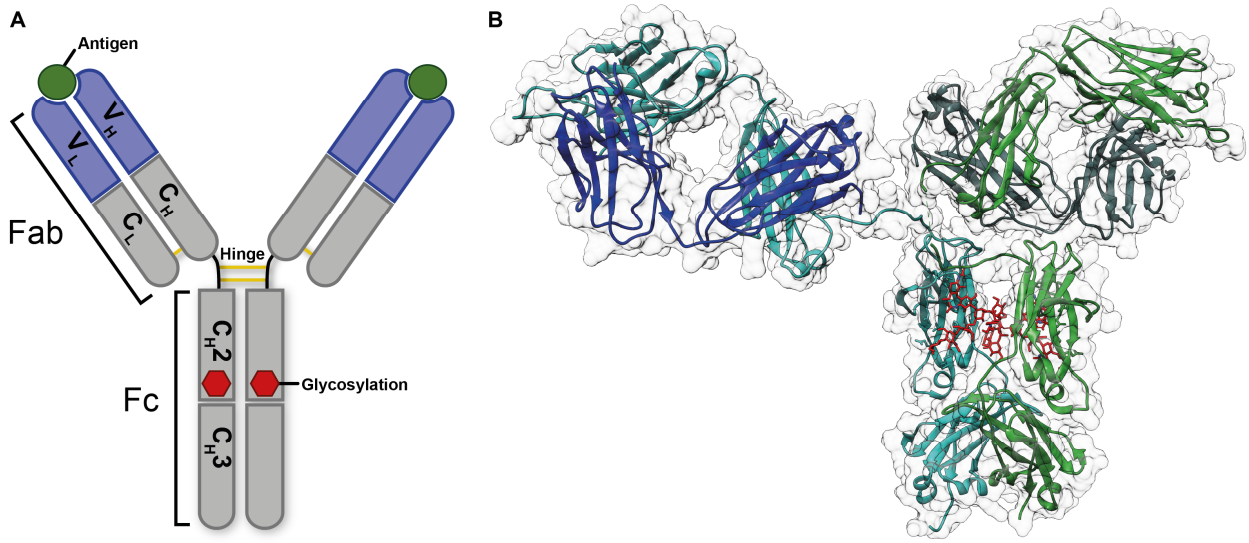

Figure 1: Structure of antibodies and antibody-drug conjugates.
A) Domains and fragments of a conventional IgG. The site of glycosylation is marked in red, intermolecular disulfide bridges are depicted in yellow. Intramolecular disulfide bridges in each domain are not shown. *B)* 3D structure of an ADC with linker-drug effector chemically bound to different residues of the Ab. The glycosylation is depicted in red. The model was created with from the published crystal structure (PDB: 1HZH) using UCSF Chimera software.

1.3.2. Monoclonal antibodies for cancer therapy

An activated B-cell will produce antibodies with a unique sequence after maturation. Since all antibodies that come from this single clone are identical, they are called monoclonal antibodies. With the development of the hybridoma technique in 1975, B-cells could be immortalized by fusion with a murine cancer cell and screened for single antibodies with preferable binding characteristics.[17] This led the way towards biochemically defined antibody therapeutics. The first therapeutic mAbs were derived from immunized mice and showed adverse effects due to their foreign origin.[45] Progress in DNA technology and cloning methods led to the development of chimeric (only V_H/V_L from mouse) and later completely humanized (only CDRs from mouse) mAbs.[46] Today, display techniques are at hand allowing the fast screening of mAbs also towards antigens that were beyond scope before, such as toxic or non-immunogenic ones.[47]

MAbs can exert their anti-tumor effect through different mechanisms like perturbation of tumor cell signaling, activation of CDC, ADCC and induction of adaptive immunity. Antagonistic effects on receptor signaling has been shown for cetuximab (Erbitux®) and trastuzumab (Herceptin®), both binding to epidermal growth factor receptors (EGFRs) and thereby inhibiting tumor growth. As described above, the activation of immune effects like CDC and ADCC is dependent on the Fc part of an antibody and varies between different therapeutic antibodies. While cetuximab and trastuzumab for example mainly activate ADCC for tumor killing[48,49], the CD20 targeting rituximab (MabThera®, Rituxan®) activates CDC and ADCC[50]. By investigating CD20 binding in more detail it was found that a hexamerization of IgGs needs to take place to recruit C1q complement protein and that certain residues in the Fc part are involved in this process, making antibody engineering possible.[51] Not only binding and effector properties are important for therapeutic efficacy, also other tumor markers play an important role. Thus cetuximab treatment revealed that therapy in a patient subgroup with wild type KRAS shows improved disease control, responses and survival. Additionally, trastuzumab is only administered to patients with high HER2 expression because of a maximum effect.[52] Another important mechanism that is currently under investigation is the antagonistic binding of immune checkpoint inhibitors. Cytotoxic T lymphocyte–associated protein 4 (CTLA-4) and programmed cell death 1 (PD-1) are both negative regulators of antitumor T cell responses. CTLA-4 blockage with Abs occurs in the lymph nodes where T cells are activated by antigen-presenting cells (APCs) and an inhibition with Abs leads to an increased immune response towards the tumor. Although initial success was reported, many side-effects mainly due to tissue-specific inflammations hindered its applicability and approval.[53] PD-L1 expression is induced upon an inflammation reaction in the tumor environment resulting in an exhaustion of T cells and thereby inhibiting a cytotoxic T cell response.[53] Since this resistance mechanism is mostly restricted to the tumor site, PD-1 blockage on activated T-cells or that of its ligand (PD-L1) on cancer cells is more specific, thus showing less side effects.[54,55] Since 2011 two antibodies targeting CTLA-4 and five antibodies targeting PD-1/PD-L1 have been approved by the FDA, further emphasizing the efficacy of this treatment concept.[53]

Unfortunately, monoclonal antibodies still suffer from several tumor escape mechanisms and antibody characteristics that diminish their activity. Downregulation of target receptors, ineffective receptor blocking or activation of compensatory pathways reduce the antitumor effect. Additionally, the large size of antibodies still limits their use in many solid tumors because of a limited tumor penetration.[52,56] Epitopes of certain mutated tumor-associated biomarkers may be hidden and cannot be addressed by Abs showing the need for alternative targeting scaffolds.[57]

1.3.3. Heavy-chain antibodies

A completely different type of antibodies is found in other forms of life. Camelids and sharks have evolved homodimeric, heavy-chain antibodies (HCAbs). The variable domains thereof are named VHH ($\mathbf{V_H}$ of **H**eavy chain antibody) and vNAR (**v**ariable domain of **N**ew **A**ntigen **R**eceptor), respectively. Sequences that are exchanged in the V_H-V_L interface are mutated to highly polar and charged amino acids, which makes these domains highly soluble.

1.3.3.1. vNAR

vNARs are derived from one of three antibody types in cartilaginous fish (IgM, IgNAR and IgW). IgNARs have one variable and five constant domains, C1-5. Although lacking a hinge region, the tilted dimerization domain C1 supports sufficient distance for antigen binding. The vNAR has sequence similarity with V_κ domains but is structurally related to V_α, V_λ, and V_H domains.[58] It shows an Ig superfamily related β-sandwich sheet with 8 instead of 10 beta strands due to the lack of a FR2-CDR2 region.[59] This leads to the smallest to date known antibody-like antigen binding domain with only 12 kDa. Since one CDR region is absent in vNARs the main antigen binding interactions are performed by the elongated CDR3. Additionally, a high rate of somatic hypermutation occurs in two hypervariable loops, therefore named HV2 and HV4. The latter was shown to contribute to antigen binding.[60] Compared to classical variable domains, vNARs can comprise non-canonical cysteine residues that form intramolecular disulfide bridges. Depending on the presence and connection of residues, vNARs are categorized in type I – IV.[59] The lack of two possible binding structures in IgNARs compared to IgGs (4 vs. 6, respectively) doesn't interfere with high affinity antigen binding. Binders in the picomolar range were reported.[61] Besides using immunized animals for library generation, naïve and synthetic libraries can be used and subsequently screened for antigen binding with different methods like phage, ribosome or yeast display.[59]

Because of their structural diversity vNARs are highly attractive alternatives to conventional antibodies. They are able to adapt different loop structures and have an additional level of alternations due to different disulfide bridge patterns (Figure 2B). They are highly thermostable and soluble that makes them even more attractive in therapeutics and diagnostics.[62] While the small size is especially suited for diagnostic purposes where the tracking molecule has to be cleared from the body rapidly, it counteracts the use as therapeutic. In this case a longer half-life is needed, which can be achieved by an Fc fusion[63,64] or a fusion to a human serum albumin binding vNAR[61]. These biomolecules are promising candidates for biotechnological applications like high affinity capturing agents for purification of biomolecules or as tools for diagnostic applications. VNARs can for example be coupled covalently and site-specifically to crystalline nanocellulose that serves as a protein-capturing nanoscaffold.[65]

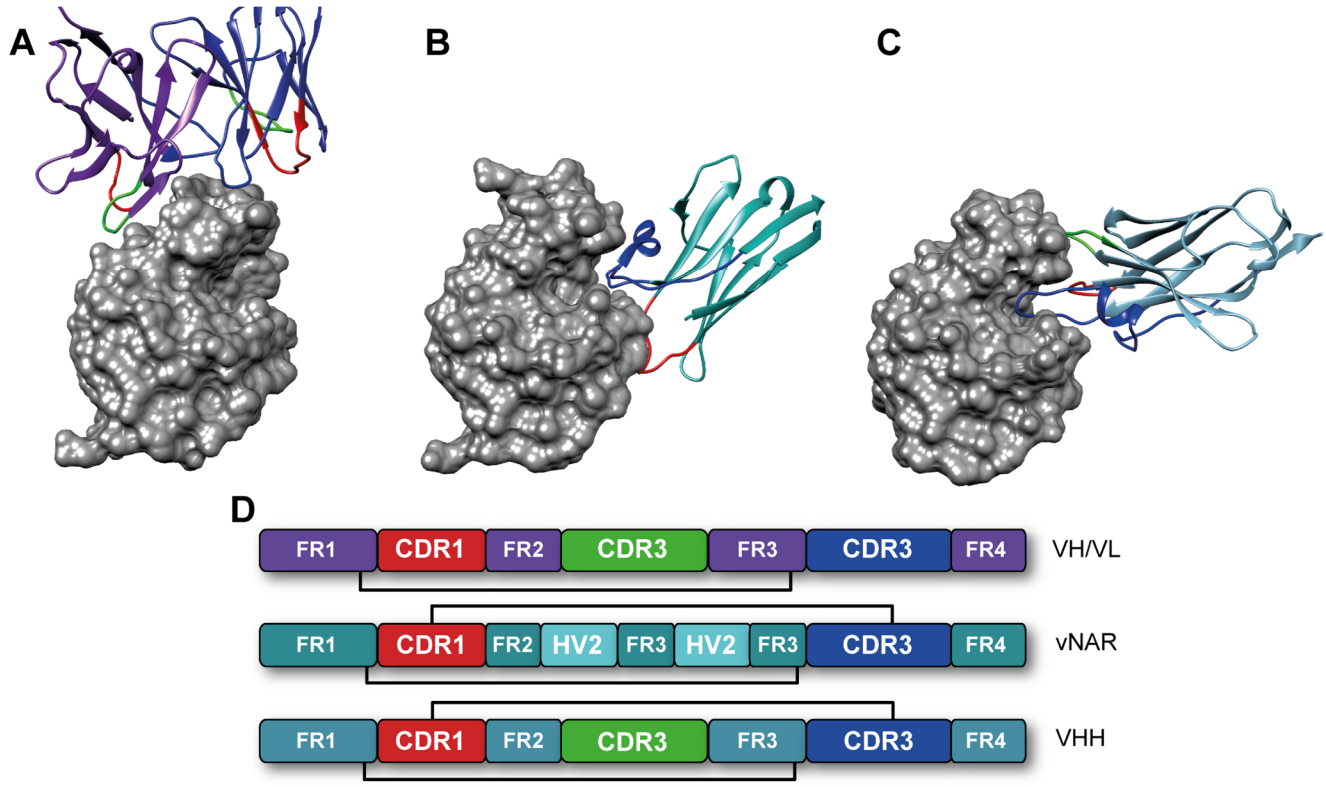

Figure 2: Structural comparison of the binding domains of mAbs and HCAbs.
A – C) 3D structures of hen egg lysozyme in complex with a Fab (PDB: 1mlc), a vNAR (PDB: 1mel) and a VHH (PDB: 1t6v), respectively. CDR regions 1 – 3 are shown in red, green and blue, respectively. Lysozyme is represented as grey surface model. *D)* Domain structure of the different antibodies. Colors correspond to the 3D structures. Black lines connecting domains show intramolecular disulfide bridges. Disulfide bridge pattern for the vNAR reflect type II and III.

1.3.3.2. VHH

HCAbs were first found in 1993 to complement the "standard" HC/LC antibodies in camelids.[66] In these animals the IgG1 antibodies are complemented by IgG2 and IgG3, both missing the LC and the C_H1 domain.[67] With a molecular mass of only 90 kDa compared to 150 kDa of a HC/LC antibody they are much smaller and comprise a more compact architecture than conventional antibodies. Since their variable domain, the VHH domain, has dimensions in the nanometer range and has a molecular weight of only 15 kDa, it was also termed nanobody. Despite their uncommon structure, these HCAbs contribute a lot to the immune protection of camelids. About 10 – 80 % of IgG in the sera of different camelid species are made up by HCAbs.[67]

Comparable to V_H or V_L domains, the major variability of VHH is located in three hypervariable loops between more conserved framework regions. The overall β–sheet structure is stabilized by an intramolecular disulfide bridge. While the overall organization of FR and HV regions is similar to the VH domain of conventional antibodies, some structural differences have been found. The FR2 domain is normally composed of several hydrophobic residues that interact with the V_L domain. These are

exchanged to smaller and/or more hydrophilic residues, which contributes to the solubility of the single domain.[67] Another difference is found in the hypervariable loops. To achieve a binding surface area of about 600 – 800 Å^2, which is in the same range of conventional antibodies, the loops HV1 and 3 are elongated (Figure 2C).[67,68] The elongation of both loops has additional effects. First, VHHs have been found to preferentially bind into clefts like active sites of enzymes due to their convex paratope surface (Figure 2C).[68,69] Second, the larger flexibility attributed to longer loops is expected to be entropically counterproductive for binding. Hence, camel VHHs sometimes constrain the long loops with an additional disulfide bond.[70] The strengthening is displayed in a high thermostability with melting points up to 90 °C.[71,72] The homology of over 80 % to human VH domains furthermore results in a low immunogenicity, which is important when considering the therapeutic applications.[73]

The singe-domain structure holds advantages towards screening and engineering. Cloning and screening libraries of conventional Abs is more demanding and time consuming because both HC and LC contribute to the binding. Therefore, synthetic or naïve library generation is a valuable method for the screening of VHHs towards new target.[74,75] VHH libraries from immunized animals are also commonly generated and hits often showed higher binding affinities than VHHs from non-immune libraries.[76] They can be screened by different methods like bacterial two-hybrid screening (intracellular usage), ribosome display and by yeast or bacterial surface display combined with fluorescence-activated cell sorting (FACS).[77] Production is simpler compared to Abs, since the small and robust VHH can be easily expressed in yeast or bacteria like *E. coli* in soluble form or as inclusion bodies.[78]

Due to their properties, VHHs were already used in a multitude of applications, like targeting extracellular targets for cancer therapy, delivering drugs, targeting of intracellular targets for mechanistic studies, use as biosensors for the detection of cancer biomarkers or bacterial toxins, molecular imaging and many more.[67,76–79] A trivalent nanobody targeting two distinct epitopes of EGFR and human albumin for an elongation of serum half-life was developed for cancer therapy but could not show superior effects compared to cetuximab, a FDA-approved mAb targeting the same receptor.[80] This may be attributed to the lack of intrinsic effector functions like ADCC activation by the Fc part. For tumor targeting, advantages like deeper tumor penetration and addressing new epitopes on cell surface receptors are often outbalanced by drawbacks like low affinity, fast blood clearance and the lack of effector functions.[79] Combining VHH domains in new formats that circumvent some of the disadvantages is, however, a feasible task, with several protein engineering techniques at hand. Therefore, they have a great therapeutic potential and thus were chosen for this study.

1.4. Antibody-drug conjugates and immunotoxins

1.4.1. Antibody-drug conjugates

The lack of effector functions of mAbs can be circumvented by conjugating effector molecules to the antibody. For the treatment of cancer, highly toxic small molecular drugs are attached that effectively kill a tumor cell after internalization of the antibody. The concept of antibody-drug conjugates combines the high specificity of an antibody with the cell killing properties of a cytotoxin. In Figure 5 a trend towards ADCs as future therapeutics is clearly visible as publications per year increased in eight years from 5 to 205. The concept of ADCs combines the preferential cell killing potential of chemotherapeutics with the specific targeting of mAbs. Chemotherapy is still the standard therapy for most tumors but suffers many side effects since these small molecules affect all fast dividing cells in the body, not only cancer cells.[18] This results in an insufficient therapeutic window. The minimum effective dose is just below the maximum tolerated dose (Figure 3), meaning no significant amount of tumor cells are killed without systemic toxicity. In fact it has been estimated that at least 99 % of the cells of a tumor have to be killed to achieve a complete remission, with significantly greater degree of cell killing required to achieve tumor eradication.[19,81]

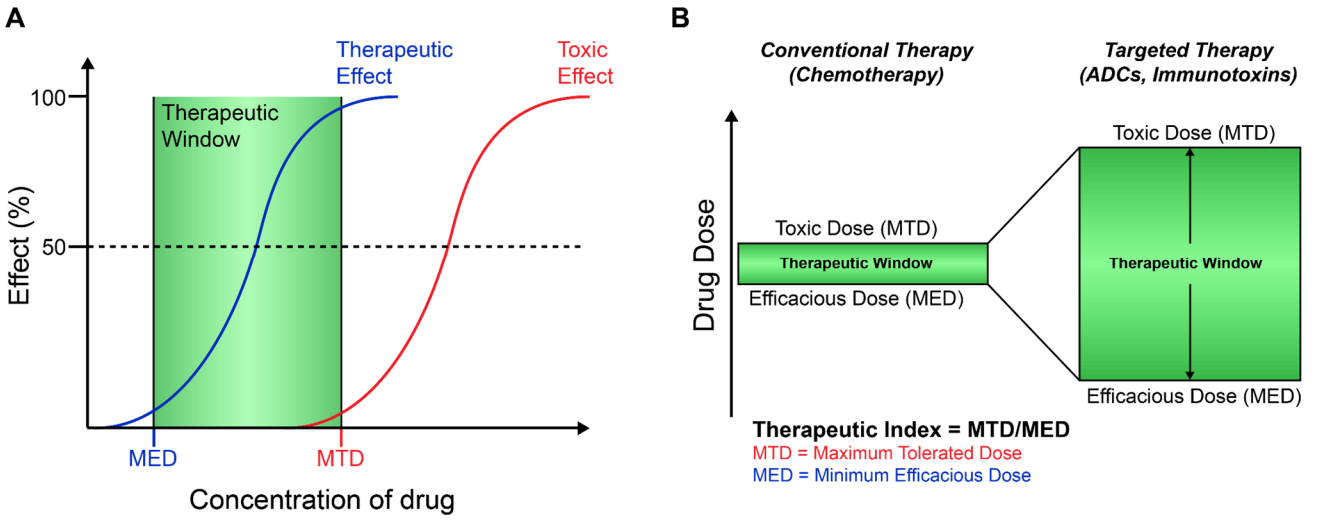

Figure 3: ADCs increase the therapeutic window of a drug.
Increasing the efficacy of a drug while maintaining or decreasing toxicity is beneficial for the therapeutic index and window. *A)* The therapeutic window is the concentration range between the minimum efficacious dose (MED) and maximum tolerated dose (MTD). Increasing the drug concentration leads to an increased therapeutic effect. At a specific dose, toxic effects occur and diminish the therapeutic effect. *B)* MED and MTD are representative markers for the calculation of the therapeutic index. Increased potency of a drug decreases the MED and higher specificity increases the MTD, both leading to an elevated therapeutic index and window.

The first ADCs included established chemotherapeutics like methotrexate or doxorubicin. These constructs lacked *in vitro* efficacy and were often less potent than the drugs alone. However, some conjugates were evaluated in mouse xenograft studies and showed increased potency. Encouraged from

these results researchers focused on the details of the ADC including the antibody and antigen, the linker and the cytotoxic drug (Figure 4).[19]

The antibody has to be highly specific for a tumor antigen that is ideally overexpressed and presented on the tumor cell surface of the cancerous tissue. Selectivity towards the tumor increases if the expression levels in comparison to healthy tissues is as high as possible. Additionally, the antigen should be homogeneously distributed on all tumor cells. In some cases, like hematological malignancies, the depletion of healthy cells can be tolerated if these regenerate as it was shown for rituximab.[82] The ADC has to be internalized by the cell to exert its toxic effect, which is achieved by receptor-mediated endocytosis. This process, however, is dependent on the nature of the antigen and can vary lot. EGFR is targeted by cetuximab and is known to be well internalized.[83] However, even targeting different epitopes on a suited target can lead to differential intracellular trafficking and lysosomal accumulation.[84] Once the antibody reaches the tumor site, its affinity has to be high enough to ensure tumor localization (K_D < 10 nM) but mustn't be too high to ensure tumor penetration.[19,85]

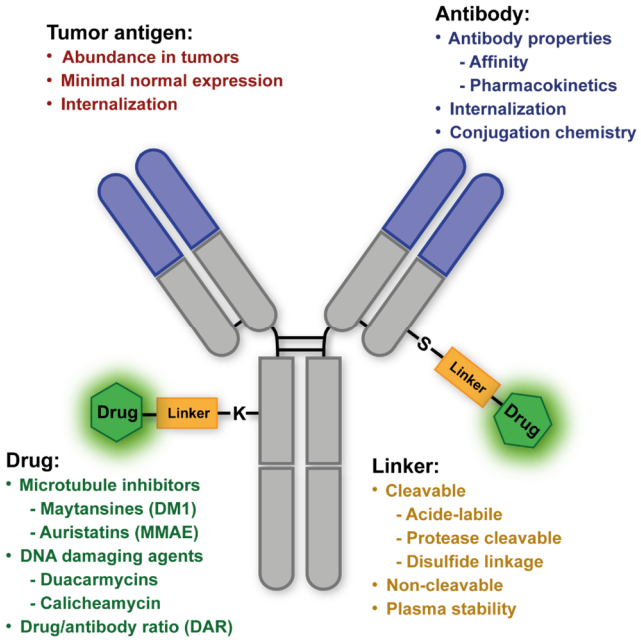

Figure 4: Critical influence factors for ADCs.
ADCs consist of a specific antibody format, a chemical linker and a cytotoxic drug. Together with the choice of a suited tumor antigen, 4 parameters have to be adjusted. Modified from Panowski *et al.* [85]

The linker itself plays a major role in the efficacy of an ADC. It has to be stable in the blood circulation but needs to release the drug in the acidic compartments of late endosomes or lysosomes. Both cleavable and uncleavable linkers have been developed and have advantages and disadvantages. Uncleavable linkers show reduced off-target toxicity but release the drug only upon complete proteolysis of the antibody. This is used for Kadcyla®, a trastuzumab-based ADC for the treatment of HER2 positive breast cancer.[25,86] Cleavable linkers dissemble upon a pH shift (e.g. acid labile hydrazone linkers), reducing conditions (disulfide linkers) or specific cleavage by a lysosomal protease like cathepsin B (valine citrulline linkers). The right linker has to be found for each antibody-drug combination and indication. Studies are underway to understand the rationales for linker design.[19,87,88]

After the discovery of highly potent toxins mainly from natural origin that showed IC_{50} values in the picomolar range[89], next generation ADCs were generated. These molecules were either inhibiting cell mitosis through inhibition of microtubule assembly like maytansinoids and auristatins or damaging DNA like duocarmycins.[89–91] The antimitotic agents further introduced some level of selectivity towards fast

dividing tumor cells and had less impact on cell types of noncancerous cells that may also take up antibody or ADC by nonspecific pinocytosis or through cell surface Fc receptors.[19,92] The maytansinoid DM1 is currently used in ado-trastuzumab emtansine and the auristatin MMAE is used in brentuximab vedotin.[85]

Most ADCs are produced by chemical linkage of the cytotoxic drug to reactive amino acid side chains like that of lysines or cysteines. The toxic agent is typically linked to reduced interchain cysteines or lysines on the antibody surface but also conjugations to sugars of the glycosylation sites are reported.[19,93] Lysine conjugation was applied for the generation of Mylotarg® and Kadcyla®. Simultaneous conjugation at various positions occurs because an IgG antibody typically contains more than 80 lysine residues, resulting in ADC mixtures. Although reaction conditions can be controlled to yield reproducible results, conjugates that vary in conjugation site and drug-to-antibody ratios (DAR) are produced.[94,95] This heterogeneity can impact solubility, stability and pharmacokinetics (PK).[96] Cysteines can be addressed by partial reduction of interchain disulfide bonds and subsequent toxin conjugation by maleimide coupling. This strategy yields a maximum of eight conjugation sites, which probably leads to reduced product heterogeneity. However, conjugation reactions still result in several different species with DARs up to 8.[85] Another better way is to use site-specific labeling that reduces heterogeneity and results in much more homogenious *in vivo* PK. ThioMab™ technology introduces additional cysteines in the heavy chains leading to drug/antibody ratios (DARs) of 2 resulting in very homogeneous products with comparable *in* vivo activity, increased therapeutic index and improved PK.[20,97] Other conjugation strategies include introduction of unnatural amino acids like selenocysteine or *p*-acetylphenylalanine (pAcPhe) that can be modified in a next step using biorthogonal chemistry. Last but not least enzymatic approaches can be utilized for site-specific conjugation.[98–100] Microbial transglutaminase (mTG) and sortase A have been shown to yield homogeneous ADCs and will be described in more detail.

1.4.2. Immunotoxins

Beside small molecules, bacterial and plant proteins have been investigated in detail for their toxic potential as antibody conjugates in therapy.[101] Already in the 1970s first approaches to use highly toxic bacterial proteins were made. In 1978 Thorpe *et al.* chemically conjugated diphtheria toxin to an anti-lymphocyte antibody to target tumor cells, thereby creating the first immunotoxin.[26] With the development of monoclonal antibody technology and molecular cloning the development of this class of therapeutics rose dramatically as Figure 5 shows. Starting in the 1980s with the ability to create ITs, the number of publications per year rose until 1998 and kept a steady-state from the 2000s of about 60 publications per year. In contrast, ADC was first described in 1983, too, but it took another 27 years for these molecules to gain popularity, which is attributable to their decreased toxicity compared to standard

chemotherapy and their ineffectiveness against persistent tumors.[101] From 2010 the number of publications per year grew until a maximum of 206 publications in 2017. Although longer studied, not many ITs made it to the market. Only Denileukin diftitox, which targets the interleukin receptor 2 (IL-2R) with a conjugated DT moiety, was approved by the FDA in 1999. Its targeting unit was the ligand of the receptor, IL2 and no antibody fragment. Nevertheless, many efforts were made in the last years to improve IT properties that could open the way onto the market.

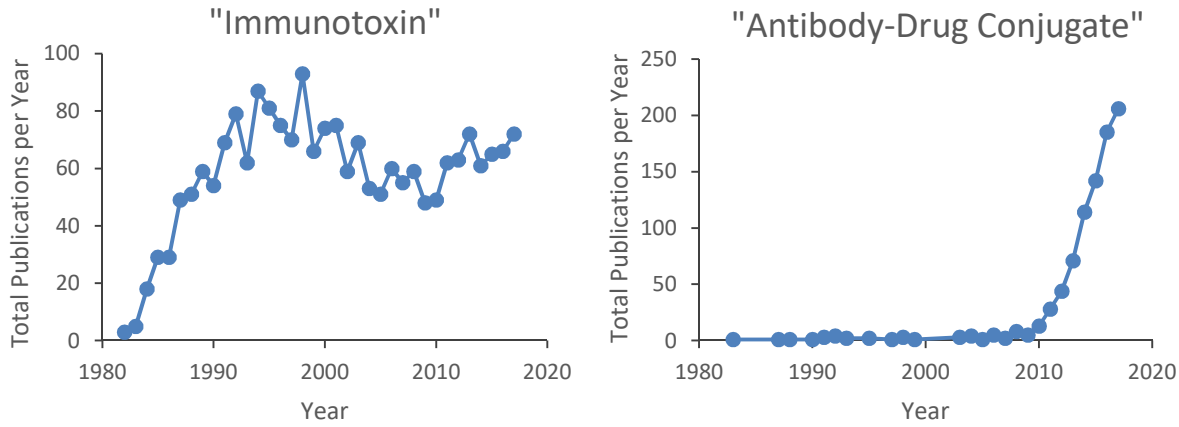

Figure 5: Statistic of publications per year concerning ADCs and ITs.
Publications on PubMed from 1980 – 2017 with the keywords "immunotoxin" and "antibody-drug conjugates" in titles and abstracts are represented. Data gathered from PubMed, accessed 02.03.2018.

1.4.2.1. Properties

Immunotoxins share one main property with ADCs which is the antibody moiety. It serves as targeting domain to specifically guide the toxin and reduce off-target toxicity. While ADCs are normally composed of full-length antibodies, ITs are mainly produced recombinantly as antibody fragment fusions, such as scFvs or Fabs, in *E. coli*. [102–104] The toxin and the antibody are linked by a peptide bond, making them less vulnerable to systemic release than ADCs with chemical linkers. IT linkers are often composed of sequences that are specifically cleaved by intracellular proteases, hence reducing off-target toxicity.[101] The toxin can be derived from plants or bacteria.

Most studied bacterial toxins in the context of ITs are diphtheria toxin (DT) and *Pseudomonas* Exotoxin A (PE). Plant-derived toxins are for example ricin, saporin and gelonin. All of these toxins differ in their cellular entry and intracellular escape mechanisms. They are separated in two classes regarding their mode of action. While some toxins naturally show active cellular binding through a binding domain (DT, PE, ricin), others are taken up by a cell by passive mechanisms and therefore constitute a low systemic toxicity (saporin, gelonin).[29,105] The similarity of all mentioned toxins is their ability to enzymatically inhibit the cellular protein translation in the cytosol. This is a main advantage over ADCs that target

microtubules in fast dividing tumor cells. With these bacterial or plant toxins, also resting cells like tumor stem cells are killed, which provides an ultimate benefit.

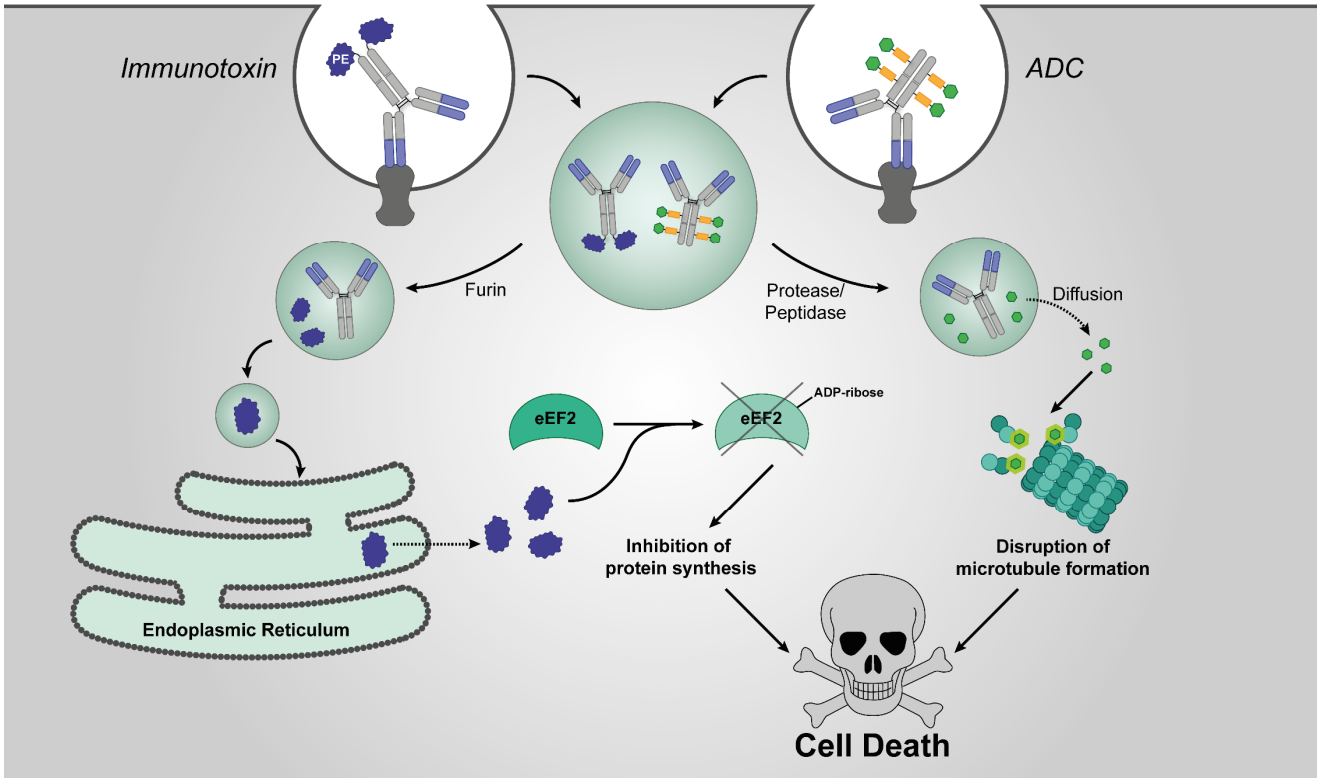

Figure 6: Mechanism of action of immunotoxins and ADCs in comparison.
ADCs and ITs bind to a receptor (e.g. HER2, EGFR or c-MET) on the cell surface and are internalized by receptor mediated endocytosis. The ADC traffics to lysosomes, where the cytotoxic payload (in this example a microtubule inhibitor) is released from upon degradation of the linker by proteases like cathepsin B, allowing drug penetration into the cytosol, disruption of microtubule dynamics, and cell death (right). In endosomes, the modified PE toxin is cleaved from the antibody by the furin protease (left). PE then undergoes retrograde transport through the Golgi to the endoplasmic reticulum (ER). The process of escape into the cytosol is unknown. The toxin then catalyzes irreversible ADP-ribosylation of eEF2, leading to global inhibition of protein synthesis and cell death. Figure and description modified from Alewine *et al.*[101]

One of the main problems is still the high immunogenicity and connected side-effects, although de-immunized variants have been developed to circumvent this issue.[30] Additionally, ITs have mainly been developed for hematological malignancies, since bad tumor penetration and anti-drug antibodies (ADAs) from the patients' immune response limited treatment of solid tumors.[106] Since only PE and gelonin were used in this study, the following chapters concentrate on their structure and mode of action.

1.4.2.2. *Pseudomonas* Exotoxin A and derivatives thereof

Pseudomonas Exotoxin A is one of the best characterized bacterial toxins, owed to its good producibility in *E. coli* and its effective translocation mechanisms into the cytosol of the target cell.[107] In 2015, three PE constructs were in clinical phase trials[101] and currently at least two next generation ITs are under clinical investigation[108,109]. As the name proposes, PE is one of the virulence factors of the Gram-negative

and potentially human pathogenic *Pseudomonas aeruginosa*. It was characterized as a mono-ADP-ribosyltransferase (ADPr) and further specified as NAD^+-diphthamide-ADP-ribosyltransferase.[110] PE belongs to the AB toxin family consisting of a domain A with enzymatic activity and a domain B for cell binding. PE is produced as a 638 aa precursor that is processed during excretion and host carboxypeptidases to a final 612 aa large protein.[111] It can be divided into three domains: domain Ia (aa 1–252) binds to alpha2-macroglobulin receptor/low- density lipoprotein receptor-related protein (α2MR/LRP/CD91) on the host cell and initiates the receptor mediated uptake of the toxin. It is followed by domain II (253–364) that enables translocation across cell membranes and includes a furin cleavage site that is flanked by a disulfide bridge. The last four residues of domain Ib (aa 365–404) together with domain III (aa 405–613) form the catalytic subunit of the toxin with ADP-ribosyltransferase activity.[112] Although PE can be taken up by a host cell by different mechanisms, the receptor-mediated uptake into clathrin-coated endosomes will be described below due to its importance for this work. After binding to CD91, clathrin-coated pits are formed and PE is transported to early endosomes. During the maturation from early to late endosomes, furin cleaves at a specific site between aa 279 and 280 in the sequence RHRQPR|G. Then chaperones and protein-disulfide-isomerases cleave the disulfide bond that is connecting both protein fragments. The C-terminal 37 kDa fragment is transported to the trans Golgi network by Rab9, where the KDEL receptor recognizes the last four amino acids (REDL) and PE is retrogradely transported to the endoplasmic reticulum (ER). Last, the toxin uses the cells ER-associated protein degradation pathway, specifically the Sec61p channel, to reach the cytosol.[111] This is probably because of a partially unfolded structure of PE. Once it has reached the cytosol it ADP-ribosylates the eukaryotic elongation factor 2 (eEF2) on ribosomes. This modification hinders eEF2 to translocate the mRNA from the ribosomal A- to P-site and therefore stops translation. It was suggested that this ultimately leads to a cell cycle arrest and subsequently to apoptosis.[111] The whole cycle from binding to the cell to cytosolic translocation takes only 50 to 180 minutes.[113]

To use PE in an immunotoxin setting, domain Ia that mediates binding to the host cell has to be replaced to reduce off-target toxicity. Antibody fragments were used for this purpose since the fusion proteins can directly be produced in *E. coli* with high yields and purities. [102–104] PE38KDEL was one of the first truncated versions where domain Ia (residues 1–252) and a portion of domain Ib (residues 365–380) have been deleted and the last aa of PE (REDLK) were replaced by KDEL.[107] In the immunotoxin HA22 (moxetumomab pasudotox) a targeting dsFv (disulfide-linked Fv fragment) towards the leukemia biomarker CD22 was fused to the N-terminus of PE38 yielding an effective treatment for leukemia.[114] Unfortunately these 1st generation ITs showed several side effects like the vascular leakage syndrome (VLS) and ADAs that diminished efficacy. Although domain II was termed translocation domain and facilitates endosomal escape when fused to other proteins[115,116], partial or complete deletion retains translocation activity of domain III into the cytosol.[117,118] This was exploited for the most recent de-

immunized variant, an only 24 kD large fragment of PE (PE24) that encompasses an improved furin cleavage site and the cytotoxic domain III.[119] This variant was additionally deimmunized by introduction of 8 point mutations found in a B-cell epitope mapping.[101,120–122] A mesothelin targeted IT with this PE24 fragment is the current state-of-the-art in immunotoxin research and is currently in clinical trials (as RG7787 or LMB-100).[109]

1.4.2.3. Gelonin

Besides bacterial toxins such as PE, some ribosome inactivating plant toxins were intensively studied to be used as immunotoxins. They belong to the family of ribosome inactivating proteins (RIPs) and are divided in class 1 and 2, depending whether or not they contain a cell targeting domain in addition to the ribosome inactivating domain. Class 1 RIPs like gelonin have the advantage of a very low off-target toxicity attributed to the lack of a cell recognition domain.[123] It is a glycoprotein with terminal mannose residues and is taken up by mannose receptor-mediated uptake or unspecific pinocytosis.[124] Gelonin is usually expressed in *E. coli* when used in biotechnological applications. In this setting no glycosylation is attached and although the function is not hindered, the uptake into the cytosol remains unclear.[125] Gelonin inhibits cellular protein translation in eukaryotes by hydrolyzing the *N*-glycosylic bond of adenine 4324 from the 28S rRNA of the 60S ribosomal subunit.[123] This prevents the recruitment of eukaryotic elongation translation factors eEF1 and 2 to the ribosomal subunit and translocation of the ribosome, thus inhibiting protein synthesis.[29] Additional studies showed that other mechanisms like DNA deadenylation may also contribute to apoptotic killing of cells through RIPs.[126,127] Similar to PE this is a catalytic process where only few molecules are needed to kill a cell.[128] Nevertheless it has been observed for recombinantly expressed gelonin, that a certain threshold concentration has to be reached intracellularly for effective cell killing.[128] Transfer from the endosomal lumen into the cytosol is still a major obstacle since recombinant gelonin has no active translocation mechanism and alternative ways for efficient endosomal release have been investigated in the last years.[129–131]

The first IT with gelonin was reported in 1981 when an anti-Thy1.1 antibody was chemically conjugated to gelonin via a cysteine reactive linker. The conjugate showed IC_{50} values in the high picomolar range and showed in vivo activity in a xenograft model and prolonged the life of mice. Notably, these mice were immunologically-deprived so that side-effects by ADAs or other immune reactions could not be observed.[132] One of the main obstacles is the translocation from endosomes to the cytoplasm. Several strategies and endosomal escape enhancers (EEEs) have been investigated for their potential to improve drug efficacy. A relatively new technology is photochemical internalization, which utilizes photosensitizers that intercalate into endosomal and lysosomal membranes and produce highly reactive oxygen species upon site directed irradiation. These disrupt the membranes and release the payload

from inside the compartment into the cytoplasm. This principle has been used for saporin and gelonin delivery and showed increased potency of the toxins *in vitro* and *in vivo*.[130,133,134] Other EEEs already used for toxin release are glycosylated triterpenoids like saponin, endosomolytic peptides like penetratin or pore-forming proteins, called perforins, like listeriolysin.[131,135–137] Although clearly potentiating the toxicity of immunotoxins, these methods always imply a co-administration of often high doses of adjuvant. Systemic administration of highly toxic and immunogenic proteins like listeriolysin are major problems that need to be addressed. Another strategy is to directly link the EEE to gelonin and has been shown for cell-penetrating peptides (CPPs) and the membrane disrupting peptide melittin. Both methods showed increased uptake and up to 120-fold or 30-fold increased toxicity, respectively.[102,138] In both cases, however, no targeting moiety was included and especially CPP coupling would trigger unspecific uptake into cells.

Gelonin derived immunotoxins have already been investigated in pre-clinical and clinical studies. A phase I study of a CD33 targeting humanized monoclonal antibody chemically conjugated to recombinant gelonin, HuM-195/rGel, showed a desirable safety profile. Unfortunately, therapeutic efficacy was limited in this construct.[139] Another promising candidate in pre-clinical testing is hSGZ, an immunotoxin consisting of a humanized anti-Fn14 scFv fused to recombinantly modified gelonin for the treatment of different solid tumors.[140] This construct further showed delayed tumor progression in mouse xenograft models of melanoma and in HER2-positive breast cancer without major toxicities.[141,142]

1.5. Methods for protein-protein conjugations

As previously mentioned, many ITs are composed of an antibody fragment and the toxin, both producible in high yields in bacteria. The major obstacle of fusions to whole antibodies is that a genetically attached toxin would act on the eukaryotic host ribosomes directly after its production leading to cell death. If the benefits of a conventional antibody, e.g. dimeric format, receptor-mediated endocytosis and elongated serum half-life, shall be incorporated, other coupling strategies have to be used. Several ITs have been generated using chemical linkers but these are not site selective and yield a mixture, making batch-to-batch standardization difficult. There are different site specific methods available for the conjugation of proteins, so-called protein ligation. Some of them are described in the following chapter.

1.5.1. Sortase A

Sortases are transpeptidases (EC 3.4.22.70) that are crucial for the physiology and pathogenesis of many Gram-positive bacteria. They are located at the plasma membrane and are anchoring different proteins like protein A to the cell wall, thereby ‘sorting’ them.[143] Sortase A (SrtA) was isolated from *Staphylococcus aureus* and earned much attention in the last years because of its applicability in protein ligation and

specific tagging of proteins. Although the natural protein contains an *N*-terminal membrane-anchoring sequence, a functional truncated form can be produced in bacteria.[144] The calcium-dependent SrtA recognizes the pentapeptide LPXTG (X can be any amino acid) and cleaves the peptide bond between threonine and glycine with its catalytic cysteine residue. This acyl-enzyme intermediate is resolved by the attack of the α-amino group of an oligoglycine peptide (often G_3 - G_5) generating a new peptide bond. The utilizationof this transpeptidation reaction is sometimes referred to as 'sortagging'. Since the product is again a substrate recognized by the enzyme, it is an equilibrium reaction and an excess of peptide has to be used in order to drive the reaction to the desired product. Because of the ease to introduce a glycine tag into proteins of interest or even small molecules, SrtA has gained a lot of interest in the previous years. Responsible has been the evolution of the enzyme to a much faster variant bearing five mutations (eSrtA: P94R/D160N/D165A/K190E/K196T) that resulted in a 120-fold increase in $k_{cat}/K_{M\ LPETG}$ and a 20-fold higher $K_{M\ GGG}$ value compare to the wildtype.[145] In a follow-up publication from the same working group, two additional variants with an altered substrate specificity towards the peptide sequences LPXSG and LAXTG have been introduced.[146] This raised the possibility of a dual labelling of one protein with different target molecules. Various applications like labelling and cyclizing proteins/peptides or generating fusion proteins were tested. Even entire cells and artificial surfaces were labeled or used as platforms for protein immobilization *via* sortase A.[143,147–150] The enzyme was also used for the generation of an ADC with properties comparable to established conjugates.[100] Sortagging has some disadvantages. First, high excess of the glycine substrate is needed to drive the equilibrium reaction near to completion. Molar ratios of 20:1 of the oligoglycine substrate are often reported.[151–153] Additionally, high enzyme amounts are needed, with concentrations in the same micromolar range as the substrates.

1.5.2. Microbial transglutaminase (mTG)

Transglutaminases (TGs, EC 2.3.2.13) are γ-glutamyltransferases, which catalyze the transamidation between the γ-carboxamide of glutamine residues (donor) and the ε-amine group of lysine residues thereby forming an isopeptide bond.[98] A side reaction is the deamidation of glutamine to glutamic acid that occurs when no amine substrate is available and a water molecule acts as nucleophile. Naturally, these bonds strengthen tissues and protect them from degradation in multicellular organisms.[154] In humans, several transglutaminases can be found like factor XIIIa with implications in blood coagulation or transglutaminase 2, which shapes the extracellular matrix, promotes cell adhesion and motility, and is involved in pathogenesis of celiac disease.[98,155,156] Transglutaminases are further found in prokaryotes. These enzymes are typically independent of calcium ions and GTP and show less deamidation side reactions, making them versatile biotechnological tools.[157,158] The most prominent and best investigated microbial transglutaminase (mTG) is found in *Streptomyces mobaraensis*. It can be easily produced in

high amounts in *E. coli* and has many applications in the food industry to improve quality and texture of meat, whey and milk products.[159,160] For recombinant expression, mTG has to be expressed as a pro-enzyme, also called zymogen, that includes an *N*-terminal inhibitory pro-peptide.[161] This is processed by an endogenous metalloprotease and a tripeptidyl aminopeptidase in two steps to give the active enzyme.[162,163] The substrate specificity of mTG is hard to describe and is barely defined. It shows high promiscuity towards the acyl acceptor and thus makes coupling of bigger proteins with several superficial lysines a trial and error approach. Acyl acceptors carrying either the electron-rich nitrile, azide, or the alkyne groups required for click chemistry were highly reactive as acceptor substrates.[164] When α–amines from amino acids are used, a longer linker between amine and carboxyl group is preferred.[164] While promiscuity is undesired for protein ligations it opens up possibilities for small molecular substrates. Regarding the glutamine residue, it has no clearly defined primary sequence specificity but must be located within a defined amino acid sequence motif with a particular conformational flexibility.[165,166] MTG has been used for conjugations of different molecule classes. Protein-DNA[167,168], protein-polymer[169] and protein-protein[170] conjugates have successfully been prepared, although often not perfectly site specific. The generation of ADCs by mTG reactions was realized after the discovery that IgGs are no substrate for mTG and that either deglycosylation or introduction of a Gln tag enabled site specific conjugation.[99,171–173] In human growth hormone two of several available glutamines are addressed, resulting in a heterogenous mix of conjugates.[169,174] This shows that mTG-mediated protein ligation is not predictable and needs empirical testing for every substrate.

1.5.3. Inteins and split inteins

Inteins are self-excising proteins that are found in all domains of life (archaea, bacteria and eukaryotes).[175] They are naturally flanked by exteins, which are assembled through the splicing event. Because of their unique mechanism, inteins can be regarded as single turnover enzymes that do not rely on an energy source or cofactors.[176] From first *in vitro* splicing experiments some main characteristics were elucidated. Splicing occurs when the intein and the first *C*-extein (Ext^C) residue are placed in a heterologous host protein. Inefficient splicing can result in single splice site cleavage as side reactions and splicing proceeds through a migrating branched intermediate with two *N*-termini.[177] In a natural context this reaction occurs spontaneously and happens co- or post-translationally.[178] Although inteins are often found in important housekeeping genes like DNA or RNA polymerase subunits in different organisms, they don't seem to have a regulatory function and therefore don't play any biological role.[178] Many inteins additionally contain a homing endonuclease domain (ENDO, Figure 7B) that recognizes intein-free alleles in the host genome and initiate recombination events for the insertion of the intein sequence in another gene.[179] Despite their low sequence homology, inteins have a conserved reaction

mechanism and sequence motifs that are necessary for the splicing reaction. The initial *N-X* (X = S or O) acyl shift is a nucleophilic attack of the *N*-terminal intein aa (1), which is typically a cysteine or serine, to the carbonyl carbon of the *C*-terminal Ext^N (-1) residue resulting in a (thio)ester intermediate. Next the Ext^N is cleaved from the intein and transferred onto the side chain of the first Ext^C residue (+1), which is either Thr, Ser or Cys, in a trans-esterification reaction. Then, the intein is completely removed from this branched intermediate by attack of the last intein aa (typically an Asn) to the adjacent peptide bond forming a succinimide ring on the intein's *C*-terminus. In a last step, the peptide bond between the esterified exteins is formed by an enthalpy-driven *X–N* acyl shift (Figure 7C).[180]

Besides classical inteins, buried in a pre-protein, naturally occurring split inteins have been reported. They reassemble after mixing both *N*- and *C*-terminal intein parts (Int^N and Int^C) and perform the splicing reaction in *trans*.[181–183] Split inteins are translated from two separate transcripts and assemble non-covalently into the canonical intein structure.[178] Although their natural occurance and function remain to be elusive, they offer great protein engineering potential. Biophysical and structural analysis showed that electrostatic interactions are the main driving forces for the fast and strong association of split intein fragments and that they adopt the highly entangled topology seen in canonical inteins.[178]

Protein *trans*-splicing (PTS) by natural or designed artificial split inteins further opened new possibilities for protein ligation.[184–186] Expressed protein ligation (EPL) is used to ligate peptides or other tags to the *C*-terminus of recombinant proteins. In this method, the Ext^N is fused to a modified intein lacking the ability to perform *trans*-thioesterification. Cleavage of the α-thioester intermediate is achieved by addition of an exogenously added thiol. The newly formed thioester is rapidly and irreversibly rearranged to form a native peptide bond.[187,188] Limitations are especially the requirements of high protein and peptide concentrations in the micro- to millimolar range and preparation of thioesters is not trivial.[189]

Therefore, PTS has several advantages for protein-protein or semisynthetic protein ligations. In contrast to EPL, the native peptide bond is formed directly during the PTS reaction with lower concentrations of both reaction partners needed.[189] Especially if chemical entities should be attached by a synthetic peptide, the short part of the split intein should not be longer than 40 aa, which can be routinely achieved using optimized synthesis protocols.[190]

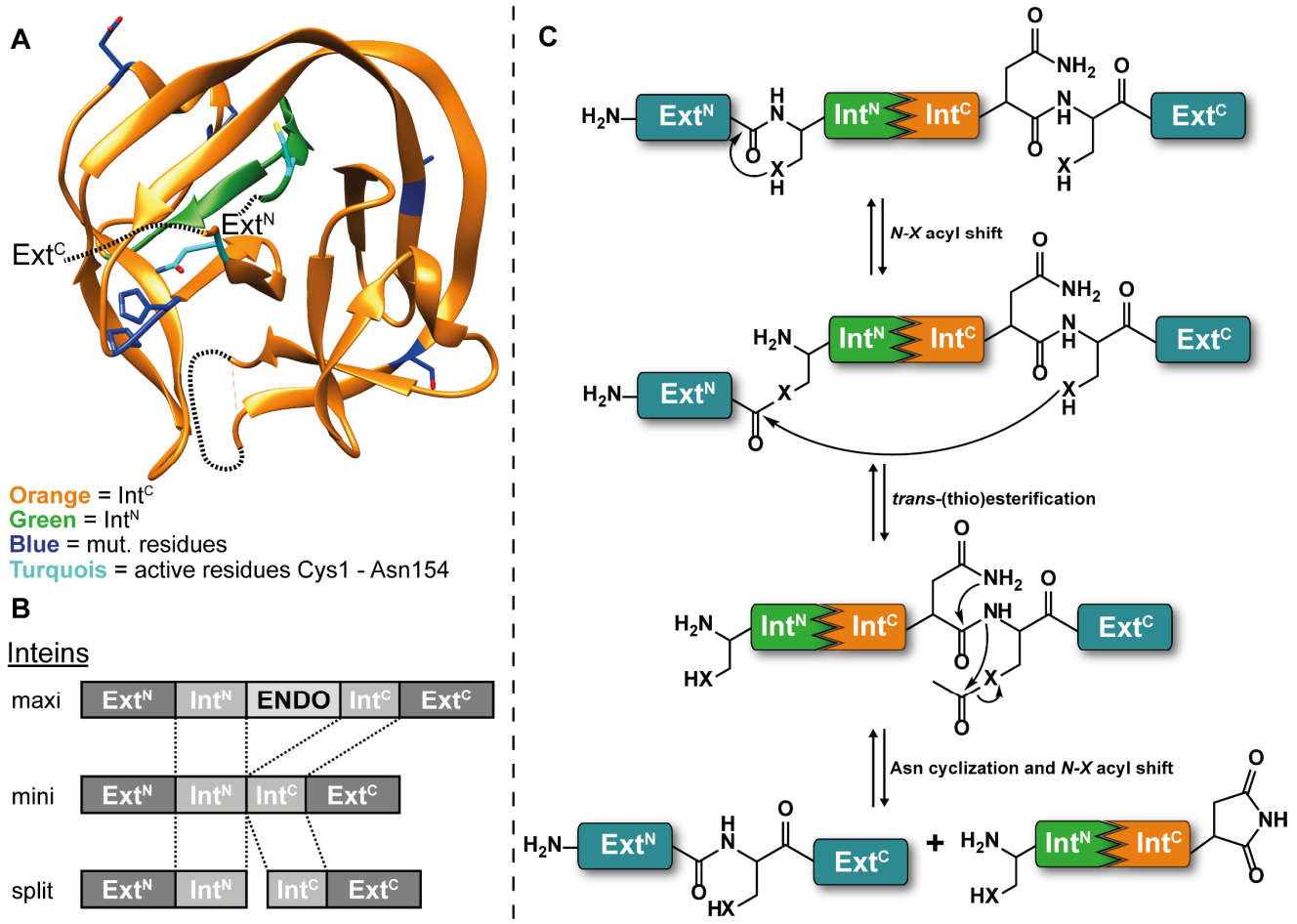

Figure 7: Split inteins structure and mechanism.
A) 3D structure of the mini intein *Ssp* DnaB created with UCSF chimera software (PDB: 1MI8). Mutations leading to the evolved variant M86 are depicted in blue, the Int^N fragment in the split version is shown in green and the Int^C fragment is represented in orange. Adjacent extein sequences are denoted as Ext^C and Ext^N. Active residues in the active site are colored turquois. *B)* Different formats of inteins are presented with their domain structure. Maxi inteins include a homing endonuclease (ENDO) domain in between the intein sequences. This domain is missing in mini inteins. Split inteins are characterized by a break in the intein domain. *C)* Intein splicing mechanism *in trans*. After assembly and folding of the active intein complex (colors as defined in *A)*) the bond between Ext^N and Int^N is activated to a linear (thio)ester intermediate by an *N-O* or *N-S* acyl rearrangement. Next, this bond is attacked by the hydroxyl or thiol group of the first amino acid of the Ext^C, resulting in a branched intermediate. By cyclization of the conserved C-terminal asparagine residue of the intein, a succinimide derivative is formed and the liberated free α-amino group spontaneously rearranges by another *O-N* or *S-N* acyl transfer to the native peptide bond between the exteins.

Natural split inteins with Int^N parts between 102 and 123 aa and Int^C parts of 36 aa are described. Even shorter fragments were achieved by design and yielded a 11-aa long Int^N and a 6-aa long Int^C part.[191] With this toolbox, a validation of which split intein is most suitable for a specific application is possible. This technology has been used to immobilize proteins to glass surfaces[192], to tag proteins in mammalian cells[193] or to generate bispecific antibodies even in culture medium[186]. An artificially evolved split intein with an unusual short *N*-terminal part of only 11 aa showed very good splicing yields in a previous study.[194] It is based on the *Ssp* DnaB mini intein from the cyanobacterium *Synechocystis* sp.. The screening process led to a very promiscuous intein related to surrounding extein sequences. It was able to splice at 9 of 10 tested insertion sites in different proteins. This feature makes the M86 variant a perfect candidate for the combination with a multitude of toxins and antibodies for exploratory studies. The kinetic

parameters of the split version improved dramatically. The K_D value of the two intein fragments was reduced by a factor of 9 and the rate of protein splicing was increased 60-fold. In total 8 mutations were introduced compared to the WT that all are located in the Int^C part and only some of them are in proximity of the active site. The most striking mutation is the H143R mutation. His-143 is a highly conserved residue thought to be part of a charge-relay system catalyzing the Asn cyclization during splicing. The M86 variant could splice a small Ext^N peptide to a thioredoxin Ext^C protein with conversion levels of >95 % of which 90 % were already achieved after 30 min with negligible amounts of side products.[194]

1.6. Objective

The aim of this work was the generation of novel immunotoxins that combine beneficial properties of full-length antibodies with the high potency of bacterial and plant toxins. This should be achieved by using split inteins, which enable separate protein production in mammalian and prokaryotic cells. Immunotoxins are produced as fusion proteins, including antibody fragments, in bacteria. This is, however, not possible for conventional antibodies. To this end, several fusion proteins containing toxic and non-toxic proteins or domains from bacterial or plant origin were cloned and optimized for expression yield and purity. Beside the well characterized antibody trastuzumab, a new single-chain antibody consisting of two tandem VHH domains should be developed, produced and characterized. In a next step intein *trans* splicing should be analyzed and optimized to yield immunotoxins with a high toxin/antibody ratio (TAR). Biochemical parameters like stability and hydrophobicity as well as biological functions like *in vitro* activity and target specificity should then be analyzed. This should be achieved by applying different biochemical and cell culture based methods. Ultimately the cytotoxicity of the constructs should be tested and compared in various cell lines. This could be seen as a proof-of-concept study for the development of next generation biological drugs for cancer treatment.

2. Materials

2.1. Bacterial strains

Escherichia coli strains with the following genotype were used:

DH5α F– Φ80*lac*ZΔM15 Δ(*lac*ZYA-*arg*F) U169 *rec*A1 *end*A1 *hsd*R17 (rK–, mK+) *pho*A *sup*E44 λ– *thi*-1 *gyr*A96 *rel*A1

BL21(DE3) F– *omp*T *hsd*SB(rB–, mB–) *gal dcm* (DE3)

T7 Shuffle F´ *lac*, *pro*, *lacI*^{q} / Δ(*ara-leu*)7697 *ara*D139 *fhu*A2 *lac*Z::T7 gene1 Δ(*pho*A)*Pvu*II *pho*R *ahp*C* *gal*E (or U) *gal*K λ*att*::pNEB3-r1-cDsbC (Spec^{R}, *lac*I^{q}) Δ*trx*B *rps*L150(Str^{R}) Δ*gor* Δ(*mal*F)3

2.2. Eukaryotic cell lines

Cell line	Culture medium
A549 Human lung carcinoma	DMEM with 4 mM L-glutamine, 10 % (v/v) fetal bovine serum (FBS)
CHO-KI Chinese hamster ovary	DMEM/Ham's F-12, 10 % (v/v) fetal bovine serum (FBS)
MDA-MB-468 Mammary gland adenocarcinoma	RPMI 1640 with 2 mM L-glutamine, 10 % (v/v) FBS, 1 mM sodium pyruvate
SK-BR-3 Mammary gland adenocarcinoma	DMEM with 4 mM L-glutamine, 10 % (v/v) fetal bovine serum (FBS)
Expi293F Human embryonic kidney cells optimized for antibody production	Expi293™ Expression Medium with 4 mM L-glutamine Cultivation as suspension cultures with 110 rpm orbital shaking

2.3. Plasmids

pEXPR_TEV-AldC-H20C-Fc-Srt

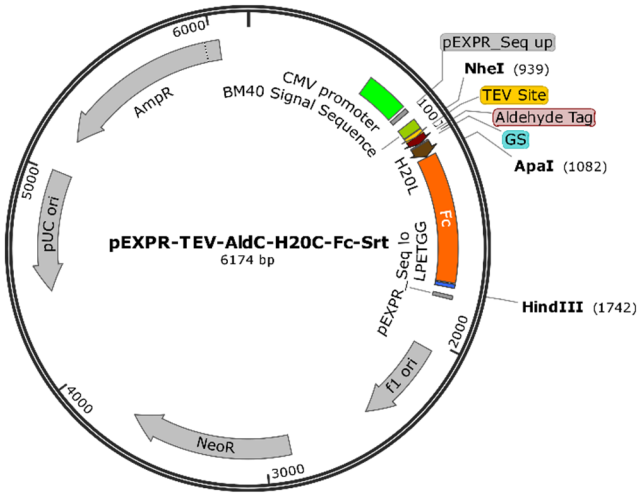

Figure 8: Plasmid map of pEXPR_TEV-AldC-H20C-Fc-Srt.
Most important features and restriction sites are annotated. **AmpR**: beta-lactamase as selection marker for ampicillin resistance; **pUC ori**: origin of replication for prokaryotes; **NeoR**: aminoglycoside phosphotransferase from Tn5 as selection marker for stable insertions; **f1 ori**: origin of replication of f1 phage; **CMV promoter**: cytomegalovirus promoter for high level expression in eukaryotes; **BM40 Signal Sequence**: excretion signal for expression into cell culture medium; **TEV Site**: ENLYFQS protease cleavage site; **Aldehyde Tag:** recognition site of formylglycine –generating enzyme; **GS**: glycine serine linker; **H20L**: 20 aa long IgG1 hinge region; **Fc**: CDS of IgG1 Fc domain; **LPETGS**: sortase A recognition sequence; **pEXPR_Seq up and lo:** binding sites of sequencing primers.

pEXPR_7D12-9G8_Fc_GGGGS3_IntN

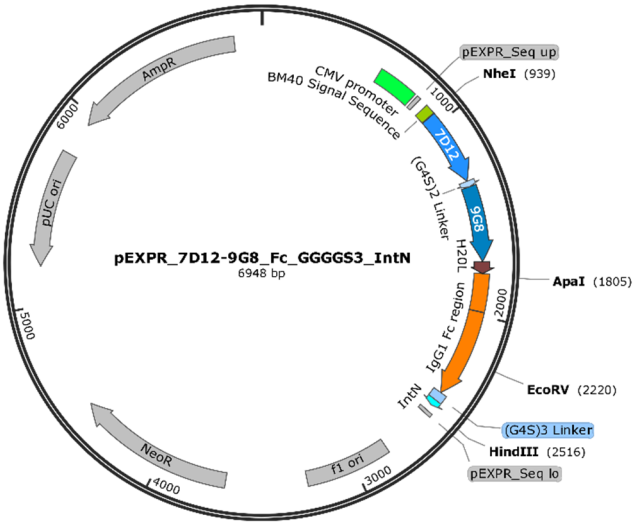

Figure 9: Plasmid map of pEXPR_7D12-9G8_Fc_GGGGS3_IntN.
Most important features and restriction sites are annotated in Figure 8. **7D12**: coding sequence (CDS) of 7D12 VHH; **(G4S)2 linker**: CDS of a 10 aa long glycine serine linker; **9G8**: CDS of 9G8 VHH; **IgG1 Fc region**: CDS of Fc domain; **(G4S)3 linker**: 15 aa linker; **IntN**: CDS of *N*-terminal intein fragment.

pTT5-Trastu-LC-(GGGGS)3-IntN

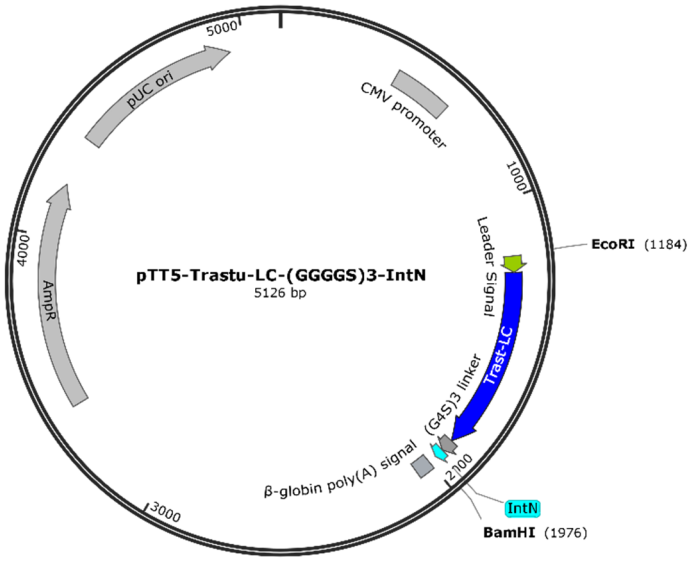

Figure 10: Plasmid map of pTT5-Trastu-LC-(GGGGS)3-IntN.
Most important features and restriction sites are annotated. **AmpR**: beta-lactamase as selection marker for ampicillin resistance; **pUC ori**: origin of replication for prokaryotes; **CMV promoter**: cytomegalovirus promoter for high level expression in eukaryotes; **Leader Signal**: excretion signal for expression into cell culture medium; **Trast-LC**: CDS of the light chain of Trastuzumab; **(G4S)3 linker**: 15 aa linker; **IntN**: CDS of *N*-terminal intein fragment. β-globulin poly(A) signal: eukaryotic transcription termination signal.

pTT5-Trastu-HC-IntN

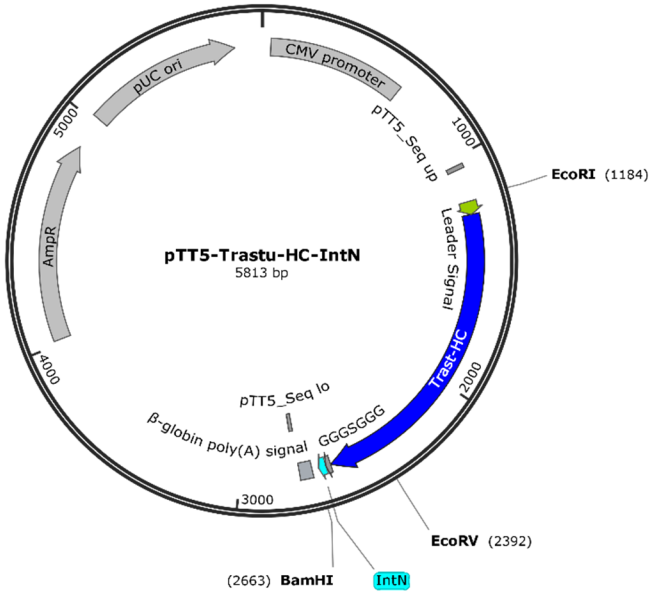

Figure 11: Plasmid map of pTT5-Trastu-HC-IntN.
Most important features and restriction sites are annotated. **Trast-HC**: CDS of the heavy chain of Trastuzumab; **GGGSGGG**: 7 aa linker; **pTT5_Seq up and lo**: sequencing primer binding sites. For all other annotations see Figure 10.

pTT5-Trastu-HC-WT

The sequence and map is identical to pTT5-Trastu-HC-IntN except for the lack of the GGGSGGG linker and the Int^N sequence.

pTT5-Trastu-LC-WT

The sequence and map is identical to pTT5-Trastu-LC-(GGGGS)3-IntN except for the lack of the (G4S)3 linker and the Int^N sequence.

pET-22b(+)_IntC-Gelonin

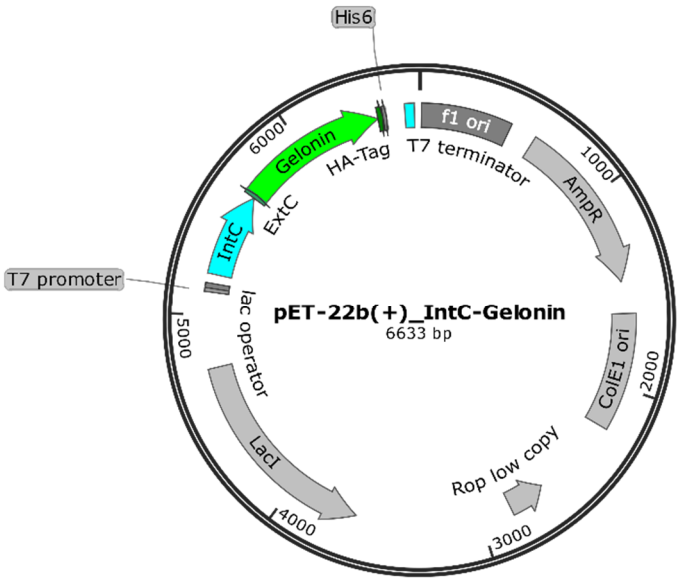

Figure 12: Plasmid map of pET-22b(+)_IntC-Gelonin.
Most important features and restriction sites are annotated. **AmpR**: beta-lactamase as selection marker for ampicillin resistance; **ColE1 ori**: origin of replication for prokaryotes; **T7 promoter**: promoter for high level expression in *E. coli*; **LacI**: CDS of lac inhibitor; **lac operator**: binding site for lacI; **IntC**: CDS of *C*-terminal intein fragment; **ExtC**: short sequence of the natural extein; **Gelonin**: CDS of gelonin; **HA-Tag**: specificity tag from hemagglutinin; **His6**: tag for IMAC purification.

pMal_IntC-Furin-Gelonin-LPETGS

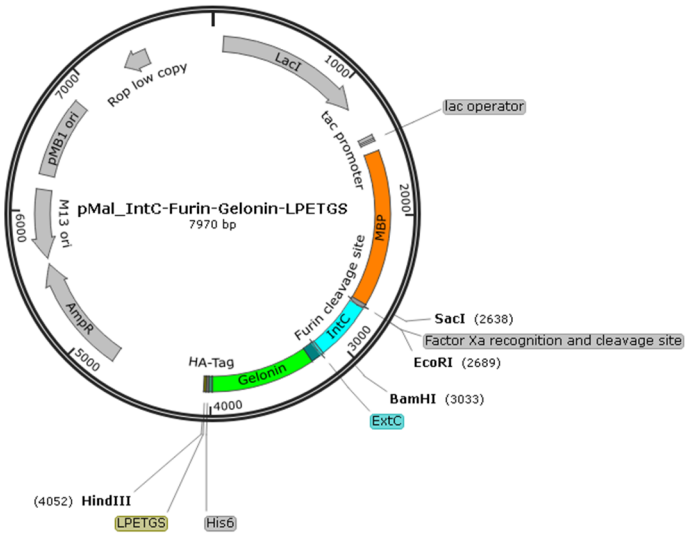

Figure 13: Plasmid map of pMal_IntC-Furin-Gelonin-LPETGS.
Most important features and restriction sites are annotated. **AmpR**: beta-lactamase as selection marker for ampicillin resistance; **pMB1 ori**: origin of replication for prokaryotes (about 20 copies); **M13 ori**: origin of replication of M13 phage; **tac promoter**: combination of trp and lac promoters for high level expression in *E. coli*; **LacI**: CDS of lac inhibitor; **lac operator**: binding site for lacI; **MBP**: CDS of maltose binding protein; **Factor Xa recognition and cleavage site**: cleavage site for MBP removal; **IntC**: CDS of *C*-terminal intein fragment; **ExtC**: short sequence of the natural extein; **Furin cleavage site**: cleavage site for lysosomal protease furin; **Gelonin**: CDS of gelonin; **HA-Tag**: specificity tag from hemagglutinin; **His6**: tag for IMAC purification; **LPETGS:** sortase A tag.

pIT021

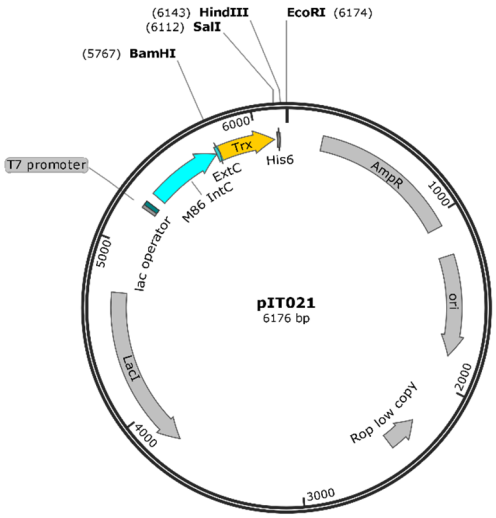

Figure 14: Plasmid map of pIT021.
Most important features and restriction sites are annotated. **AmpR**: beta-lactamase as selection marker for ampicillin resistance; **ori**: origin of replication for prokaryotes; T**7 promoter**: promoter for T7 RNA polymerase; **LacI**: CDS of lac inhibitor; **lac operator**: binding site for lacI; **Trx**: CDS of bacterial thioredoxin; **His6**: tag for IMAC purification.

pMal_TEV-PE24-HA-His6-KDEL

The sequence and map is identical to pMal_IntC-Furin-Gelonin-LPETGS except for some small changes: the furin cleavage site and gelonin CDS were exchanged to the PE24 CDS. The Factor Xa cleavage site was replaced by a tobacco etch virus (TEV) protease cleavage site.

pET32a-Trx-Int^{C}-Gelonin

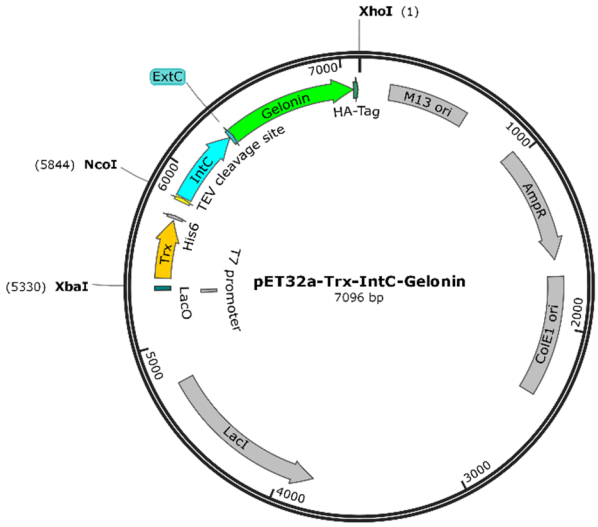

Figure 15: Plasmid map of pET32a-Trx-Int^{C}-Gelonin.
Most important features and restriction sites are annotated. **AmpR**: beta-lactamase as selection marker for ampicillin resistance; **M13 ori**: origin of replication of M13 phage; **ColE1 ori**: origin of replication for prokaryotes; T**7 promoter**: promoter for T7 RNA polymerase; **LacI**: CDS of lac inhibitor; **lacO**: binding site for lacI; **Trx**: CDS of bacterial thioredoxin; TEV **cleavage site**: cleavage site for the TEV protease; For all other annotations see Figure 13.

2.4. Oligonucleotides

Oligonucleotides were synthesized and (those exceeding 80 bp) HPLC purified by Sigma-Aldrich.

2.4.1. Sequencing primers

Name	Sequence (5' – 3')
pEXPR Seq lo	TAGAAGGCACAGTCGAGG
pEXPR Seq up	GAGAACCCACTGCTTACTGGC
pTT5 Seq lo	CCATATGTCCTTCCGAGTG
pTT5 Seq up	CTGCGCTAAGATTGTCAGT
T7 promotor up	TAATACGACTCACTATAGGG
T7 terminator lo	GCTAGTTATTGCTCAGCGG

pKB Seq lo	GGGATGTGCTGCAAGGCGA
pIT21 Seq lo	AAATAGGCGTATCACGAGGCC

2.4.2. Cloning primers

Name	Sequence (5' – 3')
7D12-9G8-IntN1 lo	GCTGATGCAGCCGCCGCCGCTGCCGCCGCCGCCGGGGCTCAGGCTCAG
7D12-9G8-IntN2 lo	TCATCAGGATCCGGCCAGGCTGATCAGGCTGTCGCCGCTGATGCAGCCG CCGCC
7D12-9G8-TEVdel-NheI up	AAGGGCGCTAGCCGCCCA
Fc-A297N-SDM lo	GTACTGTTCCTCCCGGGGCTTGGT
Fc-A297N-SDM up	AACAGCACCTACCGGGTGGTGTCC
Gelonin-SOE lo	AAAGCTCACGGTATCCAGGCCGCTACCGCTACCTTCAATGCT
Gelonin-SOE up	AGCATTGAAGGTAGCGGTAGCGGCCTGGATACCGTGAGCTTT
pTT5 SOE up	CTCCGATATCGCCGTGGAATGGGAG
TEV-SEED-SDM-fwd	GGAACACAAGTGACAGTGTCCTCCGGCAGCGAGCCCAAGAGC
TEV-SEED-SDM-rev	GCTCTTGGGCTCGCTGCCGGAGGACACTGTCACTTGTGTTCC
Trast-HC-IntN lo	AATGCGGATCCTCAGGCCAGGCTGATCAGGCTGTCGCCGCTGATGCAGC CGCCGCCGCTGCCGCCGCCCTTGCCGGGGCTCAGGCTC
Trastu-LC-EcoRI up	AATGCGGAATTCGCCACCATGAAGCTGCC
Trastu-LC-IntN lo	AATGCGGGATCCTCAGGCCAGGCTGATCAGGCTGTCGCCGCTGATGCAA GATCCCCCTCCGCCACTTCC

2.5. Chemicals

Chemical	Supplier
2-Mercaptoethanol	Carl Roth GmbH, Karlsruhe, Germany
Acetic acid	Carl Roth GmbH, Karlsruhe, Germany
Acetonitrile	Carl Roth GmbH, Karlsruhe, Germany
Acrylamide/Bisacrylamide (37,5:1)	Carl Roth GmbH, Karlsruhe, Germany
Agar-agar	Carl Roth GmbH, Karlsruhe, Germany
Agarose	Carl Roth GmbH, Karlsruhe, Germany
Ammonium acetate	Carl Roth GmbH, Karlsruhe, Germany

Ammonium hydrogene carbonate	Carl Roth GmbH, Karlsruhe, Germany
Ammonium persulfate (APS)	Carl Roth GmbH, Karlsruhe, Germany
Ampicillin, sodiumsalt	Carl Roth GmbH, Karlsruhe, Germany
Bromophenol blue	Carl Roth GmbH, Karlsruhe, Germany
Citric acid	Carl Roth GmbH, Karlsruhe, Germany
Coomassie Brilliant Blue-G250	Carl Roth GmbH, Karlsruhe, Germany
Coomassie Brilliant Blue-R250	Carl Roth GmbH, Karlsruhe, Germany
Dimethyl sulfoxide (DMSO)	Carl Roth GmbH, Karlsruhe, Germany
Disodium hydrogen phosphate	Carl Roth GmbH, Karlsruhe, Germany
Dithiotreitol (DTT)	Carl Roth GmbH, Karlsruhe, Germany
Ethanol	Fisher Scientific, Hampton, USA
Ethylenediaminetetraacetic acid disodium salt (EDTA)	Carl Roth GmbH, Karlsruhe, Germany
Glycine	Carl Roth GmbH, Karlsruhe, Germany
HDGreen™ Plus	Intas-Science-Imaging Instruments GmbH, Göttingen, Germany
Hydrochloric acid (HCl)	Carl Roth GmbH, Karlsruhe, Germany
Imidazole	Carl Roth GmbH, Karlsruhe, Germany
Isopropanol	Carl Roth GmbH, Karlsruhe, Germany
Isopropyl β-D-1 thiogalactopyranoside (IPTG)	Carbolution Chemicals GmbH, St. Ingbert, Germany
Magnesium chloride	Carl Roth GmbH, Karlsruhe, Germany
Meliseptol	B. Braun Melsungen AG, Melsungen
N,N-Dimethylformamid (DMF)	Carl Roth GmbH, Karlsruhe, Germany
Nickel chloride	Carl Roth GmbH, Karlsruhe, Germany
Polyethylenimine, 25 kDa, linear (PEI)	Polysciences, Eppelheim, Germany
Potassium chloride	Carl Roth GmbH, Karlsruhe, Germany
Potassium dihydrogen phosphate	Carl Roth GmbH, Karlsruhe, Germany
Potassium hydrogen phosphate	Carl Roth GmbH, Karlsruhe, Germany
Sodium chloride	Carl Roth GmbH, Karlsruhe, Germany
Sodium dihydrogen phosphate dihydrate	Carl Roth GmbH, Karlsruhe, Germany
Sodium dodecyl sulfate (SDS)	Carl Roth GmbH, Karlsruhe, Germany
Sodium hydroxide	Carl Roth GmbH, Karlsruhe, Germany
Sypro Orange Gel Protein Stain	Sigma-Aldrich, St. Louis, USA
Tetramethylethylenediamine (TEMED)	Sigma-Aldrich, St. Louis, USA
Trifluoressigsäure (TFA)	Carl Roth GmbH, Karlsruhe, Germany

Tris(hydroxymethyl)aminomethan (Tris)	Carl Roth GmbH, Karlsruhe, Germany
Trisodium citrate	Carl Roth GmbH, Karlsruhe, Germany
Tryptone/Peptone	Carl Roth GmbH, Karlsruhe, Germany
TWEEN-20	Carl Roth GmbH, Karlsruhe, Germany
Yeast extract	Carl Roth GmbH, Karlsruhe, Germany

2.6. Cell culture media and reagents

Component	Supplier
Dulbecco's Modified Eagle's Medium high glucose (DMEM, D6429)	Sigma-Aldrich, St. Louis, USA
Dulbecco's Modified Eagle's Medium/Nutrient Mixture F-12 Ham (DMEM/F-12, D6421)	Sigma-Aldrich, St. Louis, USA
Expi293™ Expression Medium	Thermo Fisher Scientific Inc., Waltham, USA
Fetal bovine serum superior (FBS)	Biochrom GmbH, Berlin, Germany
L-Glutamine 200 mM	Sigma-Aldrich, St. Louis, USA
Penicillin/Streptomycin (100x)	Thermo Fisher Scientific Inc., Waltham, USA
Polyethylenimine, 25 kDa, linear (PEI)	Polysciences, Eppelheim, Germany
RPMI-1640 Medium (D8785)	Sigma-Aldrich, St. Louis, USA
Sodium pyruvate	EMD Millipore, Darmstadt, Germany
Trypan Blue Solution, 0.4 %	Thermo Fisher Scientific Inc., Waltham, USA
Trypsin-EDTA solution	Sigma-Aldrich, St. Louis, USA

2.7. Solutions and buffers

Buffers and solutions were prepared with deionized water if not stated otherwise.

Buffer/solution	Composition
4 % paraformaldehyde solution	4 % (w/v) paraformaldehyde in PBS Dissolve with NaOH addition at 60 °C pH 6.9, adjust with HCl
Ampicillin stock solution	100 mg/mL Ampicillin
AP buffer	100 mM Tris/HCl pH 9.1 50 mM $MgCl_2$ 100 mM NaCl
APS stock solution	10 % APS

BLI kinetics buffer	0.1 % (w/v) BSA 0.02 % (v/v) Tween-20 in PBS
Coomassie destaining solution 1	10 % (v/v) Acetic acid 25 % (v/v) Isopropanol
Coomassie destaining solution 2	10 % (v/v) Acetic acid
Coomassie staining solution	0.2 % (w/v) Coomassie Brilliant Blue R-250 0.2 % (w/v) Coomassie Brilliant Blue G-250 30 % (v/v) Isopropanol 7.5 % (v/v) Acetic acid
dYT	1 % (w/v) Yeast extract, 1.6 % (w/v) Tryptone 0.5 % (w/v) NaCl 1.5 % (w/v) Agar-agar (for agar plates)
HIC buffer A	25 mM Tris-HCl pH 7.5 1.5 M $(NH_4)_2SO_2$
HIC buffer B	25 mM Tris-HCl pH 7.5
IMAC elution buffer	50 mM Tris-HCl pH 7.5 600 mM NaCl 500 mM Imidazole
IMAC lysis/running buffer	50 mM Tris-HCl pH 7.5 600 mM NaCl 20 mM Imidazole
Immunostaining (IS) glycine buffer, low pH	200 mM glycine, 150 mM NaCl pH 2.5, adjusted with HCl
Intein splicing buffer (ISB)	50 mM Tris-HCl pH 7.5 300 mM NaCl 1 mM EDTA
PBS-B	1 % (w/v) BSA in PBS, sterile-filtered
PBS-T	0.05 % (v/v) Tween-20 in PBS
PBS-TM	5% (w/v) milk powder in 1x PBS-T
PEI stock	1 mg/mL Polyethylenimine (Linear 25 kDa) pH 7.5 adjusted with HCl
Phosphate buffer saline (PBS)	137 mM NaCl 2.7 mM KCl 10 mM Na_2HPO_4 1.8 mM KH_2PO_4 pH 7.4
Protein A elution buffer	0.1 M Citric acid pH 3.0
Protein A neutralizing buffer	1 M Tris-HCl pH 9.0
Protein A running buffer	20 mM Sodium phosphate pH 7.0
SDS-PAGE 4 × running gel buffer	3 M Tris-HCl pH 8.85 4 g/L SDS

SDS-PAGE 4 × stacking gel buffer	0.5 M Tris-HCl pH 6.8 4 g/L SDS
SDS-PAGE 5 × sample buffer	0.25 M Tris-HCl pH 8 7.5 % (w/v) SDS 25 % (v/v) Glycerin 0.25 mg/ml Bromphenol blue 12.5 % (v/v) 2-mercaptoethanol
SDS-PAGE running buffer	50 mM Tris-HCl pH 8.8 190 mM Glycine 1 g/L SDS
SEC running buffer (analytical)	100 mM sodium phosphate pH 7.0 100 mM sodium chloride
Stripping buffer, low pH	50 mM Glycine 150 mM NaCl pH 2.7
TAE buffer (50 ×)	2 M Tris 1 M Acetic acid 0.1M EDTA
Western blot transfer buffer	25 mM Tris 192 mM Glycin 20 % Methanol

2.8. Protein solutions and standards

Protein/standard	Supplier
10 × T4 DNA ligase buffer	New England Biolabs, Ipswich, USA
10x CutSmartBuffer	New England Biolabs, Ipswich, USA
2-log DNA ladder	New England Biolabs, Ipswich, USA
5 × Q5 reaction buffer	New England Biolabs, Ipswich, USA
6x-His Tag Monoclonal Antibody (4E3D10H2/E3), Alexa Fluor 647	Thermo Fisher Scientific, Waltham, USA
Albumin fraction V (BSA)	Carl Roth GmbH, Karlsruhe, Germany
Alexa Fluor 488 Polyclonal Antibody (quenching)	Thermo Fisher Scientific, Waltham, USA
Alexa Fluor 488-conjugated AffiniPure Fab Fragment Goat Anti-Human IgG	Jackson ImmunoResearch, West Grove, USA
Anti-Human Polyvalent Immunoglobulins (α, γ and μ-chain specific)−Alkaline Phosphatase antibody (goat)	Sigma-Aldrich, St. Louis, USA

Anti-Mouse IgG (whole molecule)−Alkaline Phosphatase antibody (goat)	Sigma-Aldrich, St. Louis, USA
***Apa*I**	New England Biolabs, Ipswich, USA
***Bam*HI-HF**	New England Biolabs, Ipswich, USA
Blue prestained protein standard, broad range	New England Biolabs, Ipswich, USA
EGFR_ECD	Merck KGaA, Darmstadt, Germany
Gel loading dye (6x)	New England Biolabs, Ipswich, USA
***Hind*III-HF**	New England Biolabs, Ipswich, USA
***Nhe*I-HF**	New England Biolabs, Ipswich, USA
Penta·His Antibody, BSA-free (mouse)	QIAGEN, Hilden, Germany
Q5® High-Fidelity DNA Polymerase	New England Biolabs, Ipswich, USA
Taq DNA Polymerase	New England Biolabs, Ipswich, USA

2.9. Columns, consumables and kits

Consumable	Supplier
CellTiter96 AQueous One Solution Cell Proliferation Assay	Promega, Fitchburg, USA
Corning cell culture flasks (25 or 75 cm2)	Sigma-Aldrich, St. Louis, USA
Corning Erlenmeyer cell culture flasks	Sigma-Aldrich, St. Louis, USA
Dip and Read Anti-hIgG Fc Capture (AHC) Biosensors	FortéBio, Menlo Park, USA
HisTrap HP, 1 mL column	GE Healthcare, Little Chalfont, UK
HisTrap HP, 5 mL column	GE Healthcare, Little Chalfont, UK
HiTrap Protein A HP, 1 mL column	GE Healthcare, Little Chalfont, UK
Nunc™ Lab-Tek™ II Chamber Slide™	Thermo Fisher Scientific, Waltham, USA
Pierce Polyacrylamide Spin Desalting Columns	Thermo Fisher Scientific, Waltham, USA
Protein A HP SpinTrap	GE Healthcare, Little Chalfont, UK
PureYield Plasmid Midiprep System	Promega, Fitchburg, USA
Rabbit reticulocyte lysate system, nuclease treated	Promega, Fitchburg, USA

Superdex 200 16/60 pg, SEC column	GE Healthcare, Little Chalfont, UK
TSKgel Butyl-NPR column (4.6 mm x 3.5 cm, 2.5 μm)	Tosoh Bioscience, Griesheim, Germany
TSKgel® SuperSW3000	Tosoh Bioscience, Griesheim, Germany
Wizard Plus SV Minipreps DNA Purification System	Promega, Fitchburg, USA

2.10. Instruments

Instrument	Supplier
Accuri C6 flow cytometer	Becton Dickinson, New Jersey, USA
Äkta Purifier UPC-900 P900 Frac-920, Unicorn 5 software	GE Healthcare, Little Chalfont, UK
Äkta Start, Unicon start software	GE Healthcare, Little Chalfont, UK
BioRad 96CFX RT-PCR detection system	Bio-Rad, München, Germany
BioSpec-nano Micro-volume UV-Vis Spectrophotometer	Shimadzu, Kyoto, Japan
Cell Disrupter	Constant Systems Ltd, Northant, UK
Fluoroskan Ascent FL	Thermo Fisher Scientific, Waltham, USA
FortéBio Octet Red	FortéBio, Menlo Park, USA
GelDoc-It 2 Imaging System	UVP, LLC, Upland, USA
Gene Pulser und pulse controller	Bio-Rad Laboratories, Hercules, USA
Infinite M1000	Tecan, Männedorf, Switzerland
LC 1100 HPLC	Agilent Technologies, Santa Clara, USA
Leica TCS SP8 with LAS AF software	Leica Microsystems, Wetzlar, Germany
MCO-19AICUV CO2 incubator	Panasonic, Kadoma, Japan
New BrunsWick S41i	Eppendorf, Hamburg, Germany
PCR Cycler Eppendorf Mastercycler	Eppendorf, Hamburg, Germany
Puranity PU 20 Basic Water purification system	VWR, Radnor, USA
Shimadzu LCMS-2020 with Phenomenex Jupiter 5u C4 LC Column	Shimadzu, Kyoto, Japan
Shimadzu UV-2102 PC spectrophotometer	Shimadzu, Kyoto, Japan

Further instruments comprised common laboratory equipment.

3. Methods

3.1. Cell culture

3.1.1. Culturing adherent cell lines

All adherent cell lines were incubated under standard conditions at 37 °C in a humidified atmosphere with 5 % CO_2 in T75 cell culture flasks. The A549 and SK-BR-3 cells were maintained in DMEM culture medium with the addition of 10 % FBS. MDA-MB-468 cells were cultured in RPMI-1640 medium with addition of 10 % FBS, 2 mM L-glutamine and 1 mM sodium pyruvate. CHO-KI cells were maintained in DMEM/F-12 HAM with addition of 10 % FBS and 4 mM L-glutamine.

For passaging the cells the old medium was removed and the cells were washed with 5 ml sterile PBS. Next, 1 ml Trypsin/EDTA was added and incubated for 4 - 8 min at 37 °C. The complete detachment of cells was controlled using microscopy. To stop the trypsin reaction 4 - 6 ml medium was added and the cell suspension was transferred to a new flask at a dilution factor between ½ and 1/10 depending on the growth rate of the cell line. The flask was filled up to 5 ml (T25) or 10 ml (T75) with fresh medium.

3.1.2. Culturing suspension cultures

The non-adherent cell line Expi293F™ was obtained from Thermo Fisher Scientific and was cultivated in serum-free Expi293™ Expression Medium on an orbital shaker at 110 rpm with 8 % CO_2. Every 3 – 4 days the cell density was determined using a Neubauer improved hemocytometer. Therefore 5 – 10 μl of cell suspension were mixed with trypan blue solution for the discrimination of dead cells and added to the counting chamber. Routinely the cell density reached 4 – 7 x 10^6 cells/ml after 3 – 4 days. Cells were seeded at a density of 0.5 x 10^6 cells/ml in fresh, pre-warmed medium.

3.1.3. Cryopreservation of cell lines

Eukaryotic cells were stored in the vapor phase of liquid nitrogen. For cryopreservation, adherent cells were, first detached using Trypsin/EDTA. Then, cells were counted (viability >95 %), centrifuged and resuspended to a concentration of at least 5×10^6 vc/mL (viable cells per ml) in chilled growth medium supplemented with 10 % DMSO (v/v) (without antibiotics). 1 mL aliquots were dispensed into cryogenic storage vials, transferred into a Mr. Frosty isopropanol freezing container and stored at –80 °C. The following day, stocks were transferred to the gas phase of liquid nitrogen.

3.1.4. Recovering frozen cells

Cryopreserved cells were thawed in a 37 °C water bath and directly transferred to 5 ml of pre-warmed culture medium. After centrifugation for 5 min at 100 x g the cells were resuspended in fresh medium and transferred to a culture flask (T25 or T75) for adherent cells or directly to an Erlenmeyer flask for suspension cells.

3.2. Cell-based assays

3.2.1. Cytotoxicity assay

Cell viability after addition of immunotoxins was assessed with the CellTiter 96® AQueous One Solution Cell Proliferation Assay. 5,000 cells were seeded per well in a 96-well plate in the 90 μl of the corresponding medium with additional pen/strep solution and incubated for 24 h. The cells were then treated in triplicate with 10 μl of varying concentrations of antibodies, toxins or immunotoxins that were pre-diluted in DMEM +10 % FBS. After 72 h, 20 μl of the MTS solution were added per well and the plates were incubated for 0.5 – 3 h under standard conditions. Last, the absorption was measured at 485 nm in a Tecan reader. Cell viability of reference wells with untreated cells was set to 100 %.

3.2.2. Immunostainings and confocal microscopy

To follow the fate of antibodies and toxins after incubation with target cells, immunostainings were performed and analyzed by confocal microscopy. Cells were seeded in 8-chamber microscopy slides (Nunc™ Lab-Tek™ II Chamber Slide™) with 12,000 cells per well. Two days later, cells were treated with analytes for 1 h and washed two times for 30 s with low pH IS glycine buffer. After a PBS wash, half of the wells were stained directly while the other half were incubated for another 3 h in growth medium. Cells were then washed three times with PBS and fixed with 4 % paraformaldehyde for 30 min. After permeabilization with 0.2 % (v/v) Triton X-100 in PBS, slides were blocked with 1 % (w/v) BSA in PBS for 30 min. Stainings with primary antibodies were performed overnight at 4 °C. Anti-hIgG Fab-Alexa 488 was used in 1:500 dilution, anti-His6 Alexa 647 antibody in 1:1000 dilution. Microscopy was performed directly on the 8-chamber slide with a Leica TCS SP8 confocal microscope (Leica Microsystems). The intensity for all channels was checked for positive and negative controls and not changed throughout the experiment. All pictures were captured at a resolution 2048 x 2048 pixel and an averaging of 4 pictures.

3.2.3. Characterization of cell binding

Trypsinized cells were counted and 1 – 2 x 10^5 cells were seeded in 96-well round well plates. Between washing and staining steps cells were pelleted by centrifugation at 1,000 x g for 5 min at 4 °C. Then, they were incubated with varying concentrations of parental antibodies or ITs in 1x PBS + 1 % (w/v) BSA on ice for 45 min. After washing three times with ice-cold buffer, a 1:100 dilution of αhIgG Fab-Alexa 488 antibody was added for 30 min on ice. After another washing cycle cells were diluted in 100 μl buffer an analyzed with a BD Accuri C6 flow cytometer. The mean fluorescence intensities were normalized and plotted against antibody/IT concentration.

3.2.4. Internalization studies using flow cytometry

Another method for the confirmation of antibody internalization is the use of flow cytometry. In this case cell surface receptors need to be discriminated from internalized ones. This is achieved by washing off antibodies on the outside of the cell or by quenching the fluorophore of the detection antibody. Cells were first detached by trypsin/EDTA and incubated in 96-well round well plates with the antibody or IT for 1 h at 4 °C in PBS-B. Between washing and staining steps cells were pelleted by centrifugation at 1,000 x g for 5 min at 4 °C. After the binding step cells were washed twice with cold PBS-B and incubated for another 30 min at 4 °C with the α-hIgG-Fab-Alexa488 detection antibody (1:100 dilution). After another two washing steps plates were separated and either incubated for 1 h at 37 °C or 4 °C, respectively, and washed again twice. Non-internalized antibodies were either quenched by the addition of an α–Alexa488 quenching antibody (1:20) for 1 h or an incubation for 1 min in stripping buffer with a pH of 2.7. Cells were analyzed by flow cytometry after another two washing steps.

3.3. Molecular biology methods

3.3.1. Polymerase chain reaction (PCR)

Polymerase chain reaction (PCR) was used for assembly and amplification of gene fragments and to screen for *E. coli* colonies transformed with desired plasmids (colony PCR).

A typical PCR mixture is shown in the table below:

Component	Volume (µl)
oligonucleotide primer up (10 µM)	1
oligonucleotide primer lo (10 µM)	1
Template (plasmid DNA)	0.5
5x Q5 reaction buffer	10
dNTPs (10 mM each)	1
Q5 High-Fidelity DNA Polymerase	0.25
ddH_2O	Ad 50 µl

PCR reactions with an extension of the desired sequence with two reverse primers, 10 cycles were performed with the first primer pair. After that, the second outer primer was added and another 30 cycles were performed. Single and small mutations were introduced by splicing by overlap extension (SOE) PCR. Two individual PCRs were performed and the mutation was inserted in one of the primers. The second PCR included a primer that was complementary to a great part of the mutational primer. A third PCR ligates both fragments together with only the outer primer pair used. Colony PCR was performed using a small sample from *E. coli* colonies that was boiled in 15 µl of H_2O for 10 min at 98 °C and 1 µl of this was used as template for the PCR reaction. If possible, 10 × Thermopol Reaction Buffer and TAQ DNA polymerase were used for colony PCRs.

A typical PCR procedure included an initial denaturation step for 2 min at 98 °C followed by 30 cycles with consecutive steps for denaturation (30 s at 98 °C), primer annealing (30 s at 52-57 °C) and elongation (30-90 s at 72 °C) as well as a final elongation step for 2 min at 72 °C.

3.3.2. Restriction digest

Restriction digests of PCR products and DNA plasmids were typically performed using 18 µL purified PCR product or 2 µg purified plasmids with 2 µL of 10× CutSmart buffer and 1 µL of each restriction enzyme. H_2O was used to fill up to the final reaction volume of 20 µL. Reactions were usually incubated for at least 1 h at the recommended temperature. Samples including *Apa*I were first incubated for 1 h at 25 °C followed by the addition of further enzymes and another incubation step for 1 h at 37 °C.

3.3.3. DNA Ligation

After restriction digest of PCR fragments and plasmids with the appropriate enzymes, both fragments were ligated using T4 DNA ligase. Therefore 5 – 8 µl digested plasmid backbone and 30 – 40 µl of insert were mixed with the appropriate volume of 10x T4 DNA ligase buffer to a final 1x concentration and 1

μl of T4 DNA ligase. After a reaction at RT for at least 30 min the ligation was precipitated using ethanol-ammonium acetate precipitation (3.3.5) and used for transformation of *E. coli* DH5α.

3.3.4. Agarose gel electrophoresis

PCR reactions, restriction digests and plasmids were analyzed for their proper sizes using agarose gel electrophoresis. Therefore 1 % (w/v) agarose was dissolved in 1x TAE buffer by boiling the mixture shortly using a microwave oven with open lid. The liquid agarose was stored in a 60 °C chamber. Directly before running a gel, 5 ml HDGreen were added to 25 ml of agarose gel solution and poured into the appropriate chamber. Samples were prepared with 6x loading dye and transferred to the gel with an additional 2-log DNA ladder as length standard. The gel was run at 110 V for 20 – 40 min in 1x TAE buffer. Afterwards the gel was irradiated with UV light and analyzed on a GelDoc-It2 device with the 535 nm emission filter. When fragments needed to be cut out from a gel, it was placed on a UV-transilluminator and UV irradiation was strictly limited to define the edges of the fragments to minimize UV-mediated DNA damages like thymine dimers.

3.3.5. DNA purification

DNA from digestions and SOE PCR fragments were cut from agarose gels and isolated using Wizard SV Gel and PCR Clean-up System. Digested PCR products were directly purified via the same system without prior gel electrophoresis.

DNA from ligation mixtures was prepared for transformation by ethanol-ammonium acetate precipitation. Therefore, 1/10 vol. 7 M ammonium acetate solution and 3 vol. 99 % ethanol were added and the resulting mixture incubated for at least 1 h at -20 °C. After centrifugation for 30 min at 14,000 × g the supernatant was discarded and resulting DNA precipitate dried at 37 °C. Finally, DNA was dissolved in 20 μL H2O.

3.3.6. Plasmid DNA isolation

Plasmid DNA was isolated in small scales from *E. coli* overnight cultures using Wizard Plus SV Minipreps DNA Purification System according to the manufacturer's instructions. For larger scales and transfection of mammalian cells, PureYield Plasmid Midiprep System was applied.

3.3.7. Generation of electrocompetent *E. coli*

Transformation of *E. coli* was performed by electroporation. To make the bacteria electrocompetent all salts had to be removed. Therefore 50 ml dYT were inoculated with 500 µl of an O/N culture of DH5α or BL21 (DE3) and grown at 37 °C until an optical density at 600 nm (OD_{600}) of 0.5–0.7 was reached. The cells were centrifuged at 4000 rpm and 4 °C for 12 min. The supernatant was removed and the pellet was dissolved in 30 ml ice-cold ddH_2O, followed by another centrifugation step. This washing step was repeated with 20 ml and 10 ml water. The remaining cell pellet was dissolved in 500 µl ddH_2O for direct use or in 10 % DMSO in ddH_2O for cryocompetent cells for later use. Cryostocks were divided in aliquots of 100 µl and stored at –80 °C.

3.3.8. Transformation of *E. coli* by electroporation

Before electroporation took place, cuvettes with a gap of 2 mm were pre-cooled on ice. Electrocompetent cells were either used directly after generation or thawed from a cryostock on ice. For retransformations, typically 1 µl of plasmid solution was added to 100 µl of competent *E. coli*. When bacteria were transformed with ligated plasmids, the complete volume was added. The mixture was added to the cooled electroporation cuvette and incubated for 2 – 5 min. A pulse of 2.5 kV, 25 µF and a resistance of 200 Ω was applied to achieve uptake of plasmids. Directly after the pulse 1 ml of warm medium was added to the cells followed by a regeneration at 37 °C for 1 h. Afterwards 50 µl (retransformations) or the whole volume (cloning) were plated on an agar plate with ampicillin.

3.3.9. DNA sequencing

Cloned plasmids were verified by DNA sequencing performed by SEQLAB sequence laboratories (Göttingen). Samples with 12 µL of purified plasmid (700 – 1200 ng) were mixed with 3 µL primer stock solution (10 µM).

3.4. Protein expression

3.4.1. Protein expression in *Escherichia coli*

Toxins and Int^C-Trx were produced in *E. coli* BL21 (DE3). Cells were transfected with the corresponding expression plasmids by electroporation and seeded on agar plates with ampicillin. The next day a single colony was used to inoculate 50 ml of dYT medium. After an overnight incubation at 37 °C shaking at 180 rpm, 1 l of medium was inoculated with the pre-culture and induced with 0.5 mM IPTG when an OD_{600} of 0.6–0.8 was reached. After 4 – 20 h at 30 °C the cells were harvested by centrifugation,

resuspended in IMAC lysis buffer, frozen O/N or lyzed directly in a cell disruptor. After removing the cell debris by centrifugation (13,000 x g, 4 °C, 30 min), the supernatant was sterile filtered with a 0.45 μm filter and applied directly to IMAC chromatography.

3.4.2. Mammalian protein expression

For production of antibodies, Expi293F™ cells were transiently transfected with the corresponding pTT5 and pEXPR plasmids using polyethylenimine (PEI). Cells were seeded to $1x10^6$ c/ml the day before transfection. The next day cell density should have reached about $2.5x10^6$ cells/ml which is optimal for transfection. For mammalian production, 30 μg of plasmid DNA were mixed with 90 μg of linear PEI in expression medium and incubated for 15 min at RT. Afterwards the pre-complexed mixture was added dropwise to 30 ml of the cells. 24h later, the cells were fed with 0.5 % (w/v) tryptone. The supernatant was collected 120 h after transfection and purified by protein A affinity chromatography.

3.5. Biochemical and biophysical methods

3.5.1. Sodium dodecyl sulfate polyacrylamide gel electrophoresis (SDS-PAGE)

Protein samples were analyzed by protein size under reducing conditions in a SDS-PAGE. For the separation 10 or 15 % (w/v) polyacrylamide gels were prepared by pouring separation gel solution between two electrophoresis plates which was overlaid with isopropanol and polymerized for 30 min. Afterwards the isopropanol was decanted and residual solvent was removed by washing with dH_2O. The stacking gel solution was then poured on top of the separation gel and a comb was inserted. After another 30 min the gels were ready for electrophoresis or stored in wet paper towels at 4 °C for a maximum of two weeks.

Component	Separation Gel (10 %)	Stacking Gel (4 %)
Acrylamide-bisacrylamide	10.4 ml	2.9 ml
SDS-PAGE 4 × running gel buffer	7.8 ml	
SDS-PAGE 4 × stacking gel buffer		4.3 ml
ddH_2O	13 ml	10.1 ml
10 % APS	234 μl	156 μl
TEMED	11.7 μl	13 μl

The composition of stacking and separation gels is shown in the table above. Before electrophoresis, protein samples were denatured by addition of 5x sample buffer and boiling at 98 °C for 5 min. For non-reducing gels, samples were loaded in sample buffer lacking β–mercaptoethanol. Gels were prepared by

covering them with running buffer in a gel chamber and rinsing the pockets with buffer. After a short centrifugation the samples were loaded onto the gel together with a prestained protein marker and separated at 40 mA and max. voltage for 40 min. Proteins conjugated with fluorescent dyes were visualized under UV-light using the GelDoc-It2 imaging system device with the appropriate emission filter. Protein bands were stained with Coomassie staining solution for 20 min followed by removal of background staining by successive incubation in destaining solutions 1 and 2.

3.5.2. Western Blot (WB)

Western blot analysis is used to visualize specific proteins after SDS-PAGE separation by transferring the proteins onto a membrane and detection of the protein by a specific antibody. If the primary antibody is unconjugated, a secondary antibody linked to an enzyme or a fluorescent tag is used to visualize the protein band on the membrane. In this case, antibody-alkaline phosphatase (AP) conjugates were utilized. A mixture of Nitro-blue tetrazolium (NBT) and 5-bromo-4-chloro-3'-indolyphosphate (BCIP) were used as substrates for the enzyme, yielding an insoluble black-purple precipitate.

Altogether 12 Whatman filter papers and 1 nitrocellulose membrane were cut out in the exact size of the SDS gel. After pre-wetting all papers, the membrane and the SDS gel in WB transfer buffer for 5 min, a semidry blot was arranged as follows (from bottom to top) in a semidry blotting chamber: 6x Whatman paper, nitrocellulose membrane, SDS gel, 6x Whatman paper. The blot was run for 45 min at 12 V and 300 mA. The membrane was shortly rinsed in dH_2O, stained with Ponceau S solution to control successful transfer, destained with PBS-T and blocked with PBS-TM for 1 h at RT or O/N at 4 °C. Primary antibodies were diluted in PBS-T and incubated with the membrane while constantly shaking for 1h at RT. The membrane was washed three times 10 min with PBS-T and optionally incubated with a secondary antibody for 1 h at RT. After another three washing steps, the membrane was equilibrated in AP buffer. Then 50 μl NBT and 75 μl BCIP were added in AP buffer and incubated under constant shaking until the desired color intensity was reached. The membrane was then washed with dH_2O and PBS several times to remove the substrates and stop the reaction.

3.5.3. *In vitro* protein translation assay

Inhibition of protein translation was analyzed using rabbit reticulocyte lysate (RRL) and measurement of luciferase activity. In this assay an eukaryotic translation machinery from a cell lysate is used together with a mRNA encoding firefly luciferase to visualize protein translation. The assay was performed as suggested by the manufacturer in a total volume of 25 μl. Briefly, RRL was mixed with firefly luciferase mRNA and the protein of interest (Ab, toxin or IT) and incubated for 90 min at 30 °C. Then 5 μl of each

reaction were transferred to a black 96-well plate. To start the luciferase reaction, 50 μl luciferase assay reagent was added and luminescence was directly measured in a Fluoroskan Ascent FL luminometer. A control without any protein added served as positive control and was set as relative protein translation of 100 %.

3.5.4. Determination of protein concentration

Protein concentrations were estimated by UV-spectroscopy at 280 nm using calculated extinction coefficients and a BioSpec-nano Spectrophotometer. Protein samples were diluted prior to measurement to reduce lost material. For each measurement 4.5 μl sample were used with a path length of 0.7 mm. The given OD_{280} depicts the quotient of absorption and path length. The Lambert-Beer law was used for the calculation of the protein concentration.

$$A = \varepsilon \cdot c \cdot d$$

$$c = \frac{A}{\varepsilon \cdot d}$$

$$c = \frac{OD_{280}}{\varepsilon}$$

A = absorption

ε = molar extinction coefficient (M^{-1} cm^{-1}) at 280 nm

c = concentration (M)

d = path length (cm)

3.5.5. Thermal shift assay

Melting temperatures (T_m) were determined *via* thermal shift assay. 36 μl 100 – 200 μg/mL protein solution supplemented with 4 μl SYPRO Orange (diluted 1:100) were subjected to measurements using a BioRad 96CFX RT-PCR detection system with 0.5 °C/30 s to 99 °C. T_m values were calculated using BioRad analysis software.

3.5.6. Biolayer interferometry (BLI)

Binding parameters of VHH-Fc fusions were determined using biolayer interferometry. All protein dilutions were performed in 1x kinetics buffer. Prior to the experiment anti-human Fc (AHC) biosensors were pre-wet in PBS for 20 min followed by loading with 70 μ/ml of the desired VHH-Fc for 600 s. A baseline was obtained subsequently by incubation in kinetics buffer for 60 s. The following association was performed with hEGFR-ECD for 600 s followed by the dissociation in kinetics buffer for 900 s. All

steps were performed in 200 μL at 25 °C and 1000 rpm sensor agitation. Sensorgrams were fitted using 2:1 or 1:1 Langmuir binding model (analysis software version 9.0) after subtraction of control curve data (without binding ligand).

3.6. Protein purification and chromatographic methods

All buffers used for chromatographic purifications were sterile-filtered before use to prevent clogging of the columns. After finishing, all columns were stored in 20 % EtOH unless otherwise stated.

3.6.1. Immobilized metal affinity chromatography (IMAC)

Toxins produced in *E. coli* BL21 (DE3) and PTS products were conducted to IMAC purification. HisTrap HP (GE Healthcare) columns packed with Ni Sepharose High Performance were equilibrated with IMAC running buffer before sample application. *E. coli* lysate was applied in IMAC A buffer while PTS reactions were applied in PBS. Loosely bound impurities were washed from the column with 10 ml at 8 % IMAC elution buffer. Bound proteins were eluted with a gradient from 8 to 100 % IMAC elution buffer over 15 min. The eluted proteins were dialyzed against the buffer of choice and concentrated in Amicon Ultra centrifugal filters. The column was recovered by subsequent washing steps with 100 mM EDTA, 0.1 M NaOH and 30 % isopropanol with water washes in between with 3 column volumes (CV) each. Before the next sample was loaded the column was loaded with 100 mM $NiCl_2$ for 3 – 5 column volumes and primed with 5 CV if IMAC running buffer.

3.6.2. Protein A affinity chromatography

Antibodies were purified by protein A affinity chromatography with HiTrap Protein A HP columns. Supernatants of antibody productions were diluted 1:1.5 in protein A running buffer and applied to the pre-equilibrated column. Antibodies were eluted with 10 ml protein A elution buffer into 1.5 ml vials filled with 200 μl protein A neutralizing buffer. Purified antibodies were dialyzed or directly concentrated and buffer-exchanged in Amicon Ultra centrifugation filters.

3.6.3. Size exclusion chromatography (SEC)

3.6.3.1. Preparative SEC

Toxins still contained several impurities after the initial IMAC purification and showed only partially PTS performance. To improve the splicing efficiency MBP-Gelonin and MBP-PE24 were further purified by preparative SEC. A Superdex 200 10/60 pg column with a column volume of 120 ml was used on an

ÄKTA purifier system. The sample was pre-concentrated and a maximum volume of 4 ml was injected. The column was operated at 1 ml/min flow over 120 min and the absorption at 280 nm was analyzed. Afterwards another run could be conducted. For smaller scales a Superdex 200 10/300 column with 24 ml bed volume was used and run at 0.5 ml/min. A maximum sample volume of 0.4 ml was loaded here. Fractions were analyzed on a reducing SD-PAGE and concentrated using Amicon Ultra centrifugation filters.

3.6.3.2. Analytical SEC

Antibodies were analyzed for aggregation with an analytical SEC. A TSKgel SuperSW3000 (4.6 mm ID x 30.0 cm L) column was used on a Agilent LC 1100 HPLC. The running buffer was composed of 0.1 M sodium phosphate (pH 7.0) and 0.1 mM sodium chloride. An amount of 30 μg in a max. volume of 50 μl were injected and analyzed in a 20 min run at 0.35 ml min^{-1}. The absorption at 280 nm was analyzed.

3.6.4. Hydrophobic interaction chromatography (HIC)

Antibodies and ITs were analyzed for a change in hydrophobicity by hydrophobic interaction chromatography on a TSKgel Butyl-NPR column using an Agilent LC 1100 HPLC. The HIC method was applied using a high-salt mobile phase (HIC buffer A) and a low-salt elution buffer (HIC buffer B). Proteins of interest (30 - 50 μg) in 0.75 M $(NH_4)_2SO_2$ were loaded and eluted with a linear gradient to 100% buffer B over 20 or 35 min with a flow rate of 0.9 ml/min.

3.6.5. Protein *trans*-splicing

3.6.5.1. In solution

For the initial assessment of splicing conditions and testing different antibody and toxin formats PTS reactions were carried out in a small scale in solution. The reaction mixture contained 4 – 6 μM antibody-IntN, 2 – 8 eq. IntC-partner and TCEP at varying concentrations in intein splicing buffer (ISB). Temperatures from 4 – 37 °C were tested in a maximum timeframe of 26 h. Samples were subsequently denatured by heating them for 5 min at 98 °C in reducing 5x sample buffer and conducted to SDS-PAGE.

3.6.5.2. On protein A agarose beads

Preparative protein splicing reactions were performed on a solid support as described previously for coupling cytotoxic agents to reduced cysteines of antibodies.[195] The whole procedure is depicted in Figure 28. Abs were first incubated with protein A agarose (protein A HP SpinTrap) for 30 min under shaking in ISB. The supernatant was removed by centrifugation and the slurry washed 2x with ISB. Toxin

at a defined molar excess (typically 4 – 8 fold) towards the antibody was then added together with a TCEP excess of at least 169-fold, relative to the antibody. Incubation with the beads occurred for 18 – 24 h at 25 °C under continuous shaking. Unreacted toxin was removed by centrifugation and residual reducing agent was removed by washing 3x with PBS. Immunotoxins had to be re-oxidized in PBS with 100 eq. of dehydroascorbic acid for 2 h at 37 °C to close the interchain disulfide bridges of the antibody (Figure 28). ITs were eluted after 2 washing steps with 300 μl elution buffer in 1.5 ml reaction vials pre-loaded with 60 μl protein A neutralizing buffer, diluted in IMAC running buffer and subjected to IMAC.

4. Results and Discussion

4.1. Generation of antibodies for intein splicing

The main goal of this work to generate specific and potent immunotoxins for potential cancer treatment. The first requirement is to find targets that are commonly overexpressed on tumors and that can be addressed with antibodies. Two receptor tyrosine kinases that meet this requirement belong to the epidermal growth factor receptor (EGFR) family. The human epidermal growth factor receptors (HER) 1 and 2 are found on several solid tumors[196–198] and monoclonal antibodies like cetuximab (Erbitux®) and the ADC trastuzumab-emtansin (Kadcyla®) have already been risen against HER1 and HER2, respectively. Choosing those receptors and antibodies as models was obvious because both are well characterized in different studies. Since cetixumab has some disadvantages like bad expression yields in mammalian cells and known side effects during treatment like skin rash, another antibody format for targeting HER1 was chosen. Two camelid VHH domains (7D12 and 9G8) were screened for EGFR binding and antagonistic properties by phage display in 2007 and well characterized in the following years.[80,199–201] They bind to different epitopes on domain II and III of the extracellular domain of HER1 with dissociation constants in the double digit nanomolar range.[80] For the targeting of HER2 the commercially available trastuzumab antibody was used since it is well characterized, too, and many conjugates and ADCs have already been constructed on its basis, thus making it a good reference.

4.1.1. Cloning and productions

4.1.1.1. 7D9G-Fc-Int^N

The sequences for the VHH domains were derived from Schmitz *et al.* in 2013 and were ordered as genes inserted into a standard vector at GeneArt® (Thermo Fisher Scientific). All antibody sequences were entered as amino acids and the corresponding DNA sequence was optimized towards mammalian expression on the GeneArt® platform. Both domains were separated by a 10 amino acid glycine serine linker that was previously optimized for the biparatopic 7D12-9G8 orientation, in short 7D9G.

All cloning steps were performed using standard molecular biology methods (3.3). The ordered gene strings contained N-terminal *Nhe*I and C-terminal *Apa*I restriction sites for cloning into a pEXPR backbone with a pre-existing IgG1 Fc fragment.[152] TEV protease cleavage sites were deleted after insertion into the plasmid by site-directed mutagenesis (SDM) and splicing by overlap extension polymerase chain reaction (SOE PCR). Additionally, a sortase A recognition site (LPETGG) was included at the *C*-terminus for a possible dual application of the antibody. All cloning steps were confirmed by sequencing. The final construct encoded the 7D12-9G8 domains followed by a hinge region, a glycosylated Fc fragment, a $(G_4S)_3$ linker, the Int^N sequence, a GS linker and the LPETGG tag (

Figure 16). Additionally, the single VHH domains were constructed as Fc fusions and tested in initial binding analysis. Parts of this have already been published.[202]

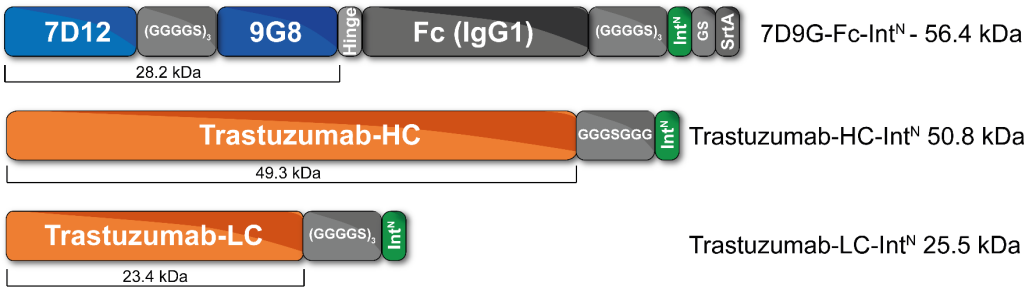

Figure 16: Schematic depiction of antibodies used for the generation of ITs.
The top shows the VHH domains linked by a glycine serine linker attached to an IgG scaffold and the *C*-terminal intein and SrtA tags. With 56.4 kDa for the monomer, it is slightly larger than the trastuzumab heavy chain but smaller in the final dimeric format than the full trastuzumab antibody. Below both trastuzumab chains with different GS linkers and the Int^N tag are shown with corresponding molecular weights. Detailed sequence information can be found in 7.1.2.

The antibody was produced in Expi293F cells with a different protocol than recommended that included linear polyethylenimin (PEI) as transfection agent (3.4.2). After purification by protein A affinity chromatography (Figure 17A), the antibody was dialyzed to intein splicing buffer (ISB) and concentrated by centrifugation in Amicon® Ultra centrifugal filters. Generally, 120 – 150 mg/l of purified antibody were yielded. Proteins were analyzed by sodium dodecyl sulfate polyacrylamide gel electrophoresis (SDS-PAGE) that confirmed a size of 58 kDa under reducing conditions and approximately double the size without addition of β–mercaptoethanol (Figure 17B). Size exclusion chromatography (SEC) further confirmed a low percentage of aggregates (<3 %) and the protein were then stored at 4 °C.

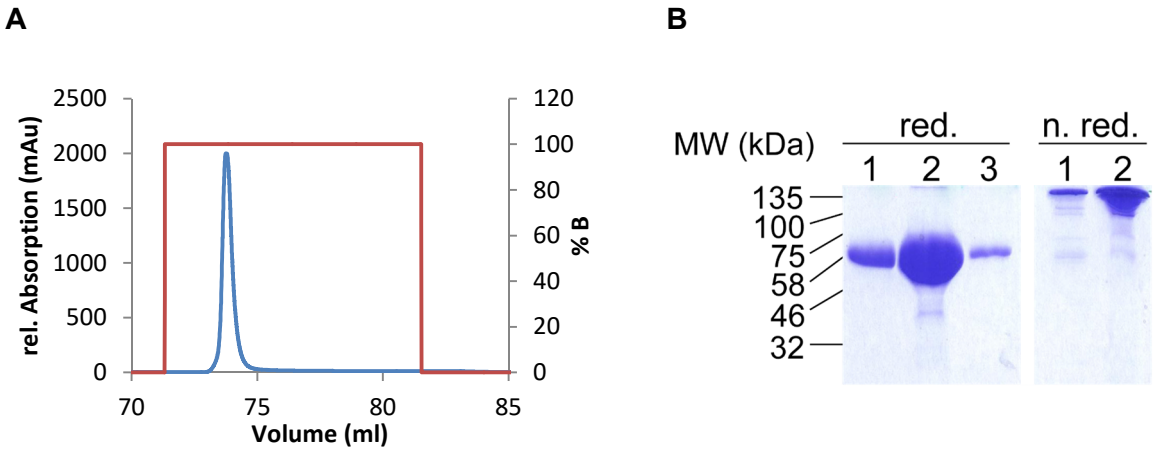

Figure 17: Production and purification of 7D9G-Fc-Int^N in Expi293F cells.
A) Chromatogram of the protein A purification. The absorption was measured at 280 nm. Blue = absorption at 280 nm. Red = gradient concentration of protein A elution buffer. *B)* SDS-PAGE of the elution fractions. A single band could be observed as expected. On the right side, fractions 1 and 2 were also analyzed under non-reducing conditions.

4.1.1.2. Trast-Int^N

The basis for cloning of different trastuzumab variants with the Int^N sequence on the *C*-terminus of either heavy or light chain were pTT5 plasmids for mammalian expression with the wildtype of trastuzumab or trastuzumab with a LPETGS sequence attached after a linker. These plasmids were kindly provided by Marcel Rieker (Merck KGaA). From this starting point the intein sequences were inserted by PCR with reverse primers including the additional sequences. As for all cloning works the resulting plasmids were confirmed by sequencing.

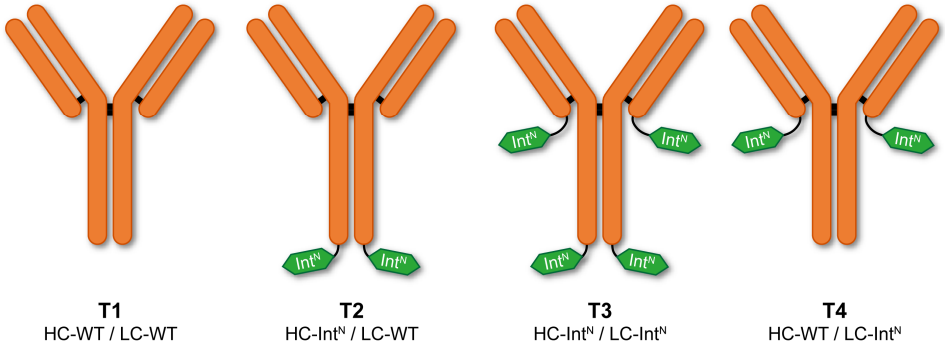

Figure 18: Overview of trastuzumab variants.

Trastuzumab variants were produced the same way as the VHH construct with expression yields of 80 – 120 mg/l of purified antibody. The purity was analyzed by SDS-PAGE and SEC analysis showed low amounts of aggregates of <3 % (Figure 20). Four different variants were expressed that contained either the WT or the intein sequence on the heavy and/or light chain. The resulting variants were named according to Figure 18.

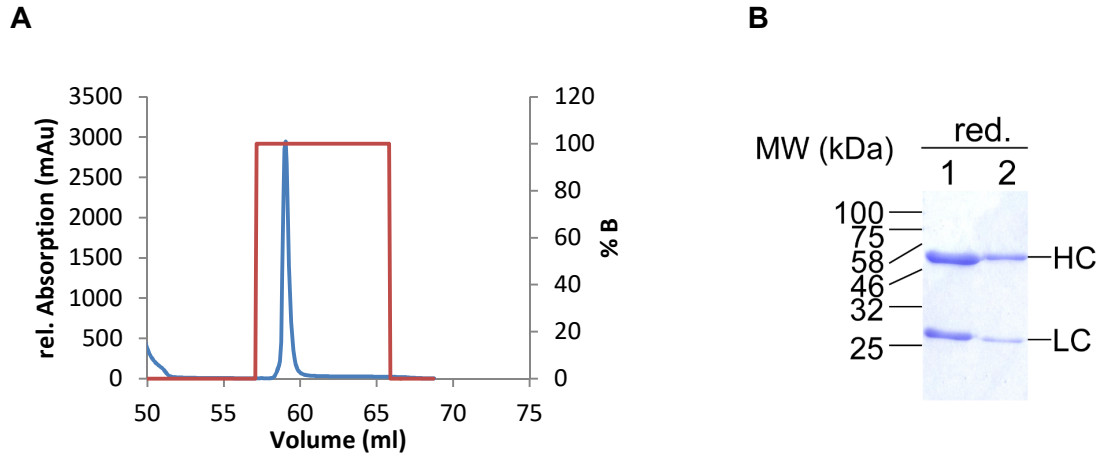

Figure 19: Production and purification of Trast-Int^N in Expi293F cells.
A) Chromatogram of the protein A purification. The absorption was analyzed at 280 nm. Blue = absorption at 280 nm. Red = gradient concentration of protein A elution buffer. *B)* SDS-PAGE of the elution fractions. Protein bands corresponding to HC and LC were found as expected.

Figure 19A shows the chromatogram exemplarily for all purifications and B shows a reducing SDS-PAGE of variants T2 and 4, respectively. Although the molecular weight of HC and LC are different for both constructs, they cannot be discriminated on the SDS gel.

The 7D9G-Fc-Int^N variant and the T2 construct were used throughout the whole thesis as they were best suited for comparisons because of the *C*-terminal intein sequence. Therefore, combined and concentrated probes were directly compared by SDS-PAGE and analytical SEC analysis (Figure 20). A HPLC system was used for a high resolution separation. Aggregates can be detected by this method, since they are at least double the size of a monomeric antibody and travel a lot faster through the column, resulting in a timeframe of about 0.7 min between monomeric and aggregate peaks in a 20 min run.

The area under the peaks was used to calculate the percentage of aggregated proteins in each sample. For the VHH construct, aggregates represented a minor fraction of only 2.4 %. In the trastuzumab sample the high-molecular weight fraction was 5.1 %.

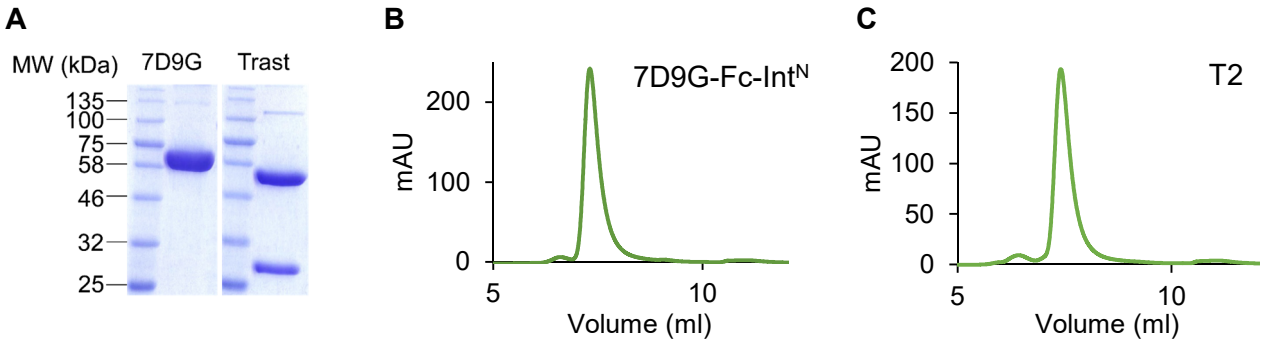

Figure 20: SDS-PAGE and SEC analysis of produced antibodies.
A) Reducing SDS-PAGE of combined and concentrated antibodies. 7D9G = 7D9G-Fc-Int^N; Trast = T2. *B – C)* Analytical SEC of both antibodies analyzed on an Agilent HPLC system using a TSKgel SuperSW3000 column. Parts of this have already been published.[202]

4.1.2. Binding characteristics on sensor tips and on cells

While binding and functionality was proven in several studies for trastuzumab, the de novo constructed VHH-Fc construct needed to be tested for correct antigen binding. In previous studies the camelid domains were either used alone or in dimeric or trimeric fusions but without a Fc domain.[80,201] One way to measure the binding kinetics and thereby also the affinity towards an antigen is biolayer interferometry (BLI). In this method an analyte is attached to a pre-functionalized sensor tip. In this case the antibody is bound to anti-human Fc tips and the antigen, the extracellular domain of EGFR/HER1 is titrated in a concentration row in solution. The BLI measurement gives a real-time response of the growing biolayer on the tip and thus measures the rate of association (k_{on}) and subsequently also the rate constant of dissociation (k_{off}) when dipped into a buffer solution. This enables the calculation of the equilibrium dissociation constant K_D as parameter of affinity to the antigen.[203]

At the equilibrium of a molecular binding event, the following is given:

$$\mathbf{A + B \leftrightarrows AB}$$

This means for the calculation of the equilibrium dissociation constant K_D:

$$\mathbf{[A] \cdot [B] \cdot k_{on} = [AB] \cdot k_{off}} \quad (1)$$

$$\mathbf{K_D = \frac{k_{off}}{k_{on}} = \frac{[A] \cdot [B]}{[AB]}} \quad (2)$$

[A] and [B] are the concentrations of molecule A and B, respectively. The following units are defined:

Concentrations:	M
k_{off}:	s^{-1}
k_{on}:	$M^{-1}\ s^{-1}$
K_D:	M

Off and on rates were then fitted by software-based algorithms in a global mode, which includes all samples available.

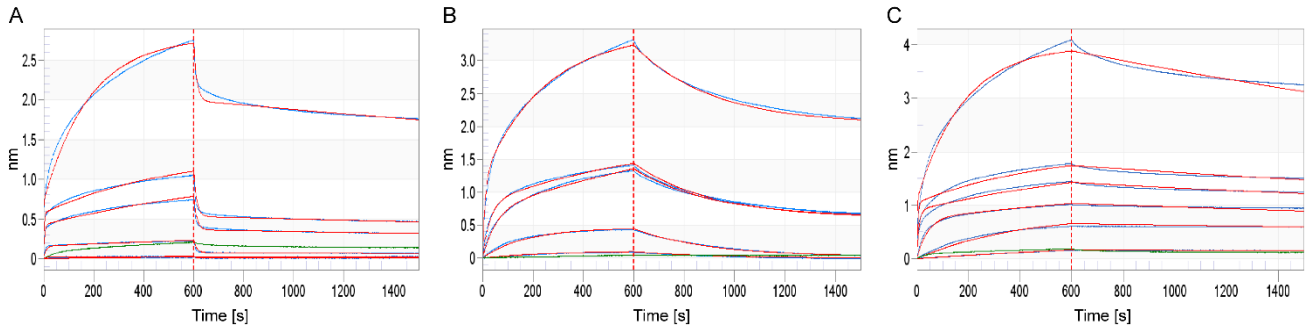

Figure 21: BLI analysis of HER1 binding of VHH-Fc constructs.
Antibodies were captured on biosensor tips and EGFR ectodomain was titrated at 3000, 1000, 500, 100, 10 and 1 nM. The graphs show measurements and fittings of *A)* 7D12-Fc, *B)* 9G8-Fc and *C)* 7D12-9G8-Fc. A 2:1 fit for heterogeneous ligands (antibody) was used for all three constructs.

All VHH constructs including the single 7D12 and 9G8 domains were fitted using a 2:1 global fit (Figure 21). This is normally used if the immobilized protein fraction is heterogeneous or has impurities that also bind to the analyte in solution. While a 2:1 fit for the double VHH variant would be plausible because it has two different binding domains, both single domain constructs should be represented by a 1:1 fit. Since these showed the same responses, this leads to the presumption that the experimental settings were not ideal or that impurities were included in the antibody solutions. A hint towards the solution of this problem is shown for the 9G8-Fc measurement. As shown in Figure 22 the 1:1 global fit matches the concentrations of 10 and 100 nM almost perfectly, while the deviation for the same fit is enormous when applied to the complete set of concentrations.

The K_D values of all formats could thus only be estimated to be in the low to mid nanomolar range and the bivalent construct shows probably due to avidity effects the highest affinity towards the antigen. A literature value of 5.4 nM is reported for the 7D12 VHH and measured with surface plasmon resonance (SPR), which is a comparable label-free method.[204] This fits to the observed affinity of the BLI measurement. The physical principles between both methods differ which might account for some of the difference. Another unrelated protein, C4bp, was included in the analysis as negative control. As expected, no binding of this protein was observed to the antibody-loaded sensor tips (Figure 21, green lines), thus confirming specific binding to HER1.

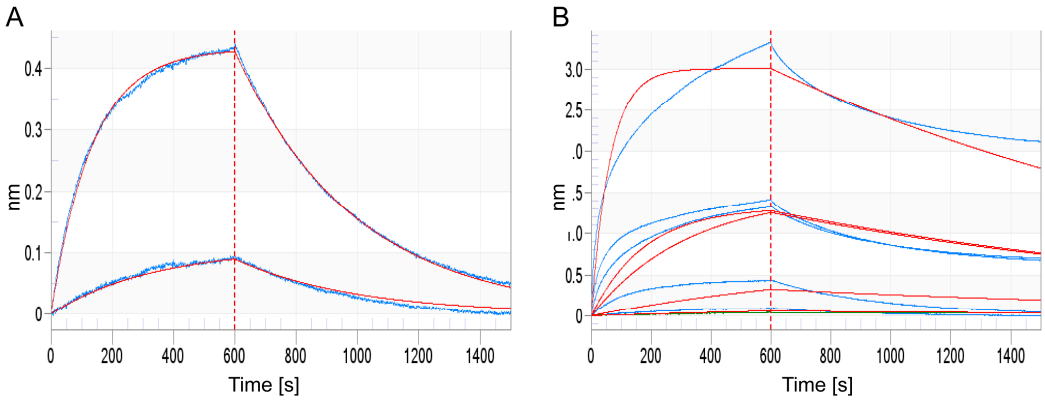

Figure 22: Comparison of different fitting models for different concentrations of the 9G8-Fc antibody.
A) 1:1 global fit only for the lowest HER1 concentrations, 10 and 100 nM. An almost perfect fitting is achieved here. *B)* 1:1 global fit for the complete concentration range shows large deviations, which proposes variations in the measurement of high analyte concentrations.

Another way to measure the affinity to the antigen is by direct binding to receptor overexpressing cells. This method may also be more suited because it resembles the *in vivo* situation much better. Another argument for the cell binding analysis was that the ectodomain of HER2 was not available for analysis of trastuzumab. 7D9G-Fc-Int^N was included in this assay to verify binding of HER1 in the more natural environment of the cell surface. For this purpose MDA-MB-469 cells overexpressing HER1 and SK-BR-3 cells overexpressing HER2 were incubated with the antibodies at 4 °C to prevent internalization. The bound antibodies were then stained with a α–hIgG Fab-488 conjugate and the cells were analyzed using flow cytometry. The mean fluorescence intensities were plotted against the antibody concentration on a logarithmic scale yielding a typical sigmoidal curve (Figure 23). Fitting of this with a 4-parameter function resulted in K_D values of 4.48 and 8.17 nM for the 7D9G and the trastuzumab construct, respectively. These values are in good correlation to literature values. Roovers *et al.* determined a K_D for the 7D9G fusion on cells with 3.1 – 5.4 nM which exactly the observed range.[80] The K_D of trastuzumab is reported to be 5 nM on SK-BR-3 cells which is also in agreement with the results.[205]

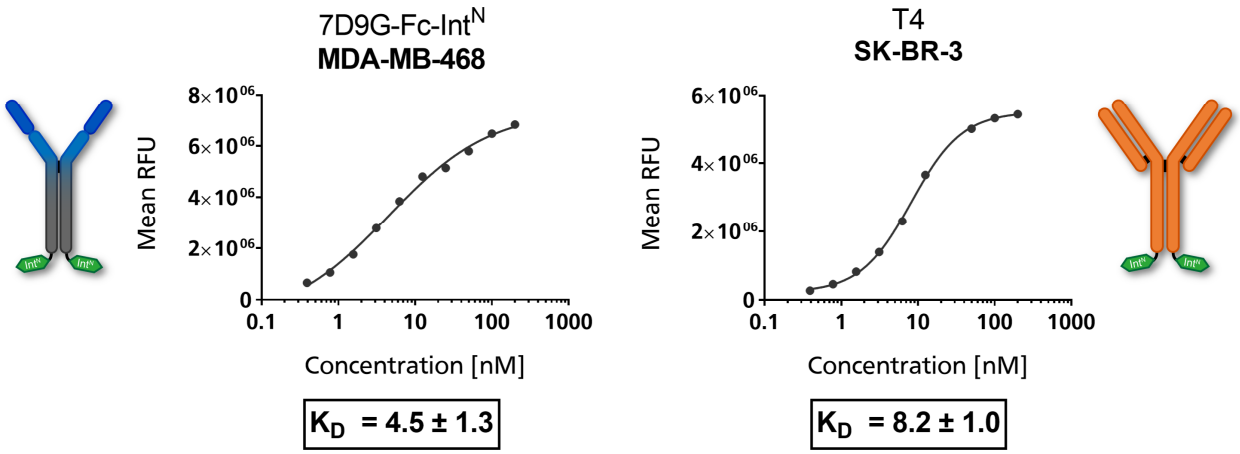

Figure 23: Binding characteristics of HER1 and 2 targeting antibody constructs on cells.
MDA-MB-468 cells (HER1$^+$) and SK-BR-3 cells (HER2$^+$) cells were titrated with the 7D9G and the T4 construct, respectively. Affinities were calculated by sigmoidal curve fitting using GraphPad Prism software (GraphPad Software, Inc.).

4.2. Selection of highly potent toxins for the generation of effective immunotoxins

4.2.1. Selection and cloning

Toxins had to be found that could be safely produced under S1 safety levels but retained a biological effect. On the one hand gelonin was found to meet both requirements because it has no cellular uptake mechanism and is almost non-toxic to humans but retains protein translation inhibition upon targeted delivery into the cytoplasm. On the other hand, the second domain of Pseudomonas Exotoxin A (ETA/PE) comprising residues 253 – 364 (Figure 24) was reported to facilitate cytoplasmic uptake of different cargoes and is inherently non-toxic.[206–208] It was used as an endosomal escaper and could be functionalized in a later step with a traceable fluorescent dye or a cytotoxic agent *via* a second enzymatic reaction with mTG. In a later section of the thesis, the next generation toxin PE24 based on the cytotoxic domain III of PE was used because of its high clinical relevance. It was determined to be safe for S1 production because of a lacking cell binding domain when produced in *E. coli*, making it unable to penetrate human cells. The chosen toxins or toxin domains were fused to the *C*-terminus of the Int^C fragment of the M86 mutant of the *Ssp* DnaB mini intein.

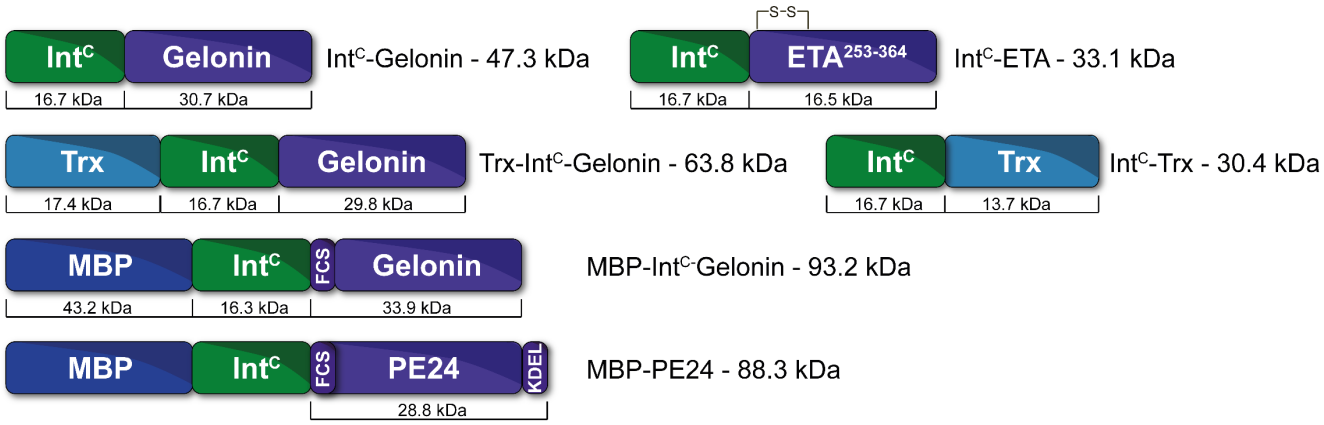

Figure 24: Schematic representation of toxin fusion proteins.
Different variations of fusions were analyzed for expression and splicing properties. All fusions contain the obligatory Int^C sequence (green). Gelonin, domain II of ETA and a variant of the cytotoxic domain of ETA (PE24) served as toxic cargoes (purple). The intramolecular disulfide bridge in ETA$^{253-364}$ is depicted. Maltose binding protein (MBP, dark blue) and thioredoxin (Trx, light blue) were used to increase solubility and expression yields. In the Int^C-Trx construct, thioredoxin also serves as splicing cargo. FCS = furin cleavage site. KDEL = amino acid sequence for ER retention. All molecular weights of domains and complete constructs are given. Note that small tags like HA or His6 tags are not depicted. Please refer to the plasmid section for more details (2.3).

Since many proteins show higher expression yields when fused to bacterial thioredoxin (Trx) or maltose binding protein (MBP) because of increased solubility, *C*-terminal fusions with these proteins were tested as well. The plasmid backbones pET22b (+), pMal and pET32 were used for the expression of toxins without fusion partner, toxins as MBP and Trx fusions, respectively. All tested constructs are summarized in Figure 24. Gene strings encoding each Int^C-toxin were inserted into donor plasmids at suitable restriction sites using standard molecular biology methods (3.3). Additionally, some protein constructs contained small *C*-terminal tags like HA (YPYDVPDYA), mTG (TTGTLQSVSYT) and/or SrtA (LPETGS) tags for functionalization. These may not be denoted in Figure 24 but can be found in the plasmid maps in 2.3.

4.2.2. Optimization of expression host

The first step in the expression of toxins in *E. coli* is the choice of the correct expression strain. The 'standard' expression strain yielding high protein amounts is BL21 (DE3). It is deficient in proteases and contains the gene for the T7 RNA polymerase under the control of a lac promoter on the λDE3 lysogen. Protein expression is initiated by the addition of IPTG.[209] The strain T7 shuffle has the ability to produce oxidized proteins in the normally reducing cytoplasm.[210] The disufide bond isomerase DsbC helps to correct mis-oxidized proteins and acts as a chaperone on protein that don't contain a disulfide bridge.[211] The Int^C-ETA fusion contains a disulfide bridge and was tested for expression in both strains.

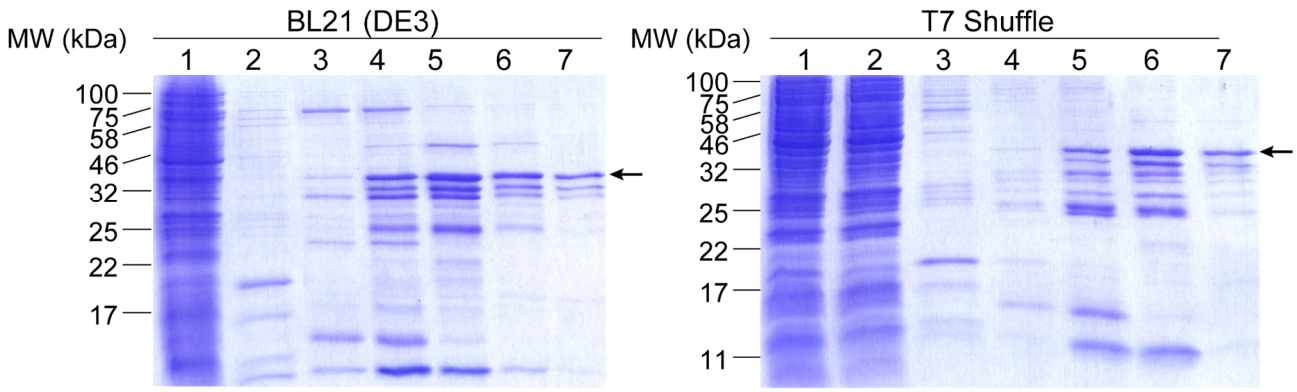

Figure 25: Expression of Int^{C}-ETA in the *E. coli* strains BL21 (DE3) and T7 Shuffle.
IMAC fractions of BL21 (DE3) (left) and T7 Shuffle (right) expressions were analyzed by SDS-PAGE. Left: 1 = FT; 2 = Wash; 3 – 7 = elution fractions F9 – F13. Right: 1 = Lysate; 2 = FT; 3 = Wash; 4 – 7 = elution fractions F9 – F12.

Expression was initiated with 1 mM IPTG and expression was performed at 37 °C for 5 h. Afterwards, cells were subjected to lysis and purified using IMAC. Figure 25 shows that the desired product could be detected at approximately 32 kDa but many impurities diminished the yield. About 1 mg protein per liter of production volume were reached. Considering the amount of impurities, this would not be satisfying for later splicing reactions in a higher scale. Comparing both strains, BL21 (DE3) showed slightly higher expression yields but also showed some more impurities. Several sequential productions showed the same picture, hence, other factors like temperature and quantity of IPTG were anylzed in a next step.

4.2.3. Optimization of temperature and IPTG concentration

For the optimization of expression temperature and IPTG concentration productions were carried out in a small scale in reaction tubes in a total of 10 ml. After induction with varying IPTG concentrations from 0.1 to 1 mM samples were incubated O/N at 20, 25 or 37 °C. The next day, a defined amount of cells was extracted from each tube and lyzed directly by adding 5x SDS sample buffer and boiling samples for 10 min at 98 °C. 10 μl were loaded per lane on a polyacrylamide gel and analyzed by western blot. The ponceau red S staining of the membranes showed that the proteins were successfully transferred onto the nitrocellulose membrane (Figure 25 top). Staining the membrane with an α–His5-AP antibody (Figure 25 bottom) showed no differences in the expression levels for the ETA construct. Notably, too much protein was loaded per lane because the desired protein band is overexposed and several other proteins were stained unspecifically. Nevertheless, even the ponceau S staining showed that a high amount of fusion protein was produced at all tested conditions. It was unclear, however, why this could not be reproduced at a 1 l scale. Potentially, also the IMAC purification was inefficient, leading to a high loss of desired protein.

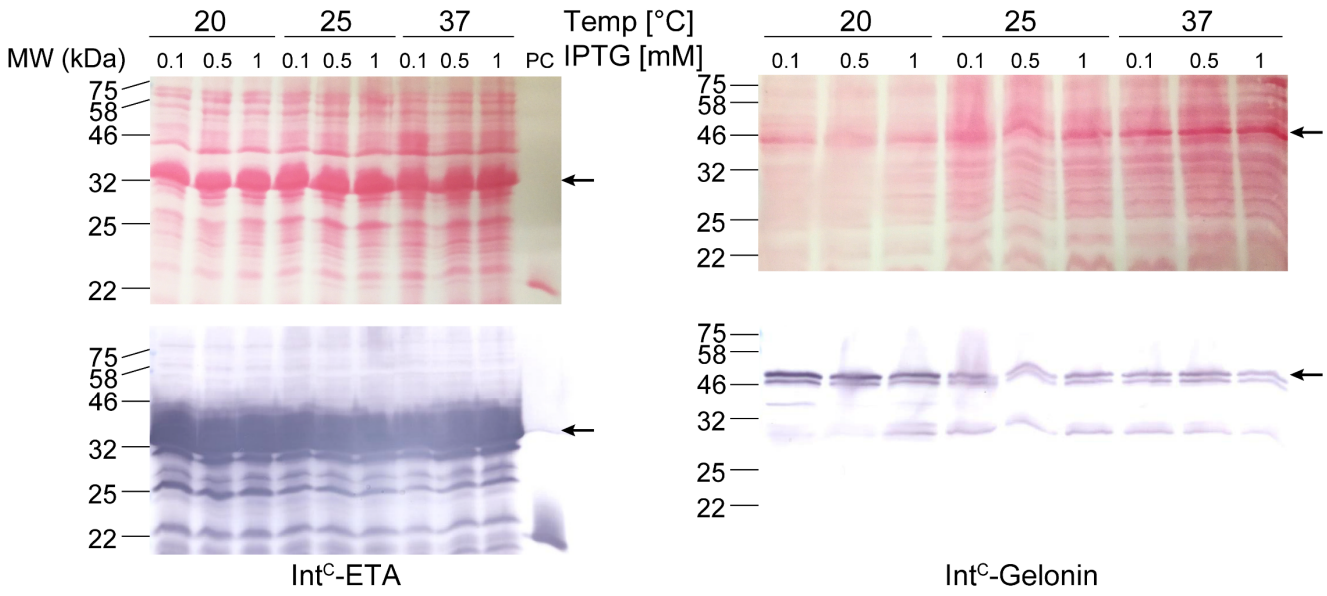

Figure 26: Optimization of temperature and IPTG concentration for the production of Int^{C}-constructs.
Expressions in a 50 ml scale were analyzed by western blot. A constant cell number was lyzed by boiling in SDS loading dye and subjected to SDS-PAGE followed by WB analysis. Top: Ponceau S red staining of transferred proteins on a nitrocellulose membrane. Bottom: WB showing the toxin fusions visualized by an α–His6 (mouse) antibody (1:5000) and a secondary α–mouse-AP antibody (1:10,000). Left: Int^{C}-ETA expression. Right: Int^{C}-Gelonin expression. Different temperatures and IPTG concentrations were tested as depicted above the lanes. SrtA was loaded as positive control (PC) for the antibody.

IntC-Gelonin showed an increased production with lower temperatures and minimal IPTG concentrations. Obviously, production yield in general was much lower compared to ETA. Although the same cell number should have been lyzed, also the background signals in the gelonin WB are much weaker than on the ETA blot. This could be explained if production of the external protein slowed down the expression machinery in a fashion that also production housekeeping proteins was inhibited. Unfortunately, subsequent production of both proteins in a liter scale with the optimized parameters (20 °C and 0.1 mM IPTG) did not lead to an increased yield, although purity was much higher this time (data not shown). Since these results were not satisfying, fusions with solubilizing proteins like thioredoxin and maltose binding protein were generated and tested for beneficial production properties.

4.2.4. Optimization of protein format and fusions

The different fusion proteins are depicted in Figure 24. A comparison of the three proteins Int^{C}-Gelonin, Trx-Int^{C}-Gelonin and MBP-Int^{C}-Gelonin was performed. While the gelonin construct without fusion partner was expressed in a 2 l scale O/N, both Trx and MBP fusions were produced in 1 l and incubated only 4 h at 30 °C after induction of gene expression. Figure 27 shows the striking differences in production yields. These were strongly increased for both new fusions. In the case of the Trx fusion a total of 7 mg purified protein were available after IMAC. With 12 mg, even more protein was produced as MBP fusion.

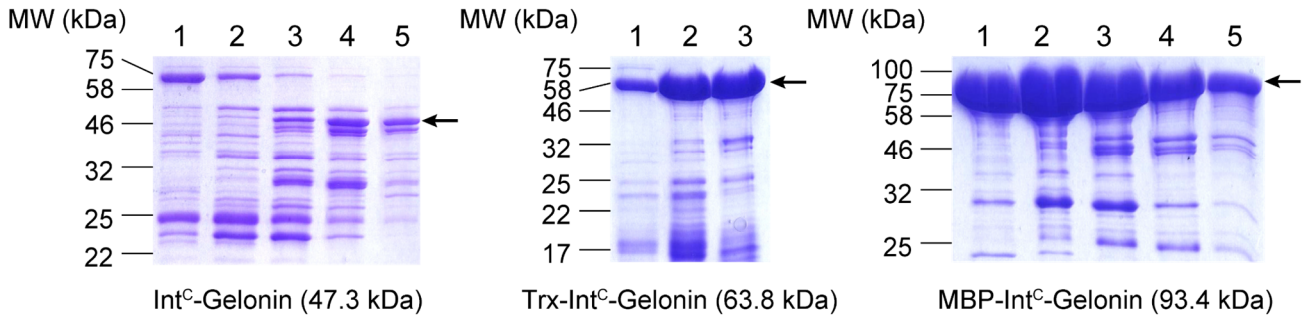

Figure 27: Comparison of production yields of different gelonin fusion constructs with Trx and MBP.
IMAC fractions of Int^{C}-Gelonin (left), Trx-Int^{C}-Gelonin (middle) and MBP-Int^{C}-Gelonin (right) expressions were analyzed by SDS-PAGE. Left: 1 – 5 = elution fractions F9 – F13. Middle: 1 – 3 = elution fractions F10 – F12. Right: 1 – 5 = elution fractions F11 – F15. Arrows indicate desired protein bands.

Both Trx and MBP constructs still contain impurities. These results showed that the MBP-Int^{C} fusions were best suited for the expression and all subsequent proteins were constructed this way. Following expressions confirmed reproducible productions for both gelonin and later PE24 fusions in acceptable yields ranging from 6 to 17 mg/l. Expressions were all carried out at 30 °C for 4 – 16 h.

4.3. Protein *trans*-splicing in solution and on solid support

Both antibody and toxin parts were expressed successfully and could be conjugated in a next step using protein *trans*-splicing. Since the active residues during this process is a cysteine, a reducing agent had to be added to make sure that none of the Int^{N} cysteines was oxidized. This may be a problem for antibodies since they contain several inter- and intramolecular disulfide bridges that are broken upon reduction. Nevertheless, other intermolecular forces like hydrophobic interactions stabilize the antibody under normal conditions. If the IT shall be purified after a PTS reaction and used for secondary analysis, the reducing agent has to be removed and an oxidizing agent needs to be added to close the opened disulfide bridges again. This can be achieved by adding dehydroascorbic acid, the oxidized form of vitamin C.[195]

While initial tests for the optimization of the reaction were carried out in solution, larger scaled productions of ITs were conducted using a solid support. This process is depicted in Figure 28. For this purpose, protein A beads were used to capture the antibody. PTS reactions could be performed directly using this slurry.[195] After finishing the reaction, side-products and reducing agents could simply be washed off and reoxidation could be performed. By eluting the ITs with a low pH buffer, a pre-purified IT is yielded. The same process in solution would need several more steps including dialyses that increases the risk of contaminations and loss of protein.

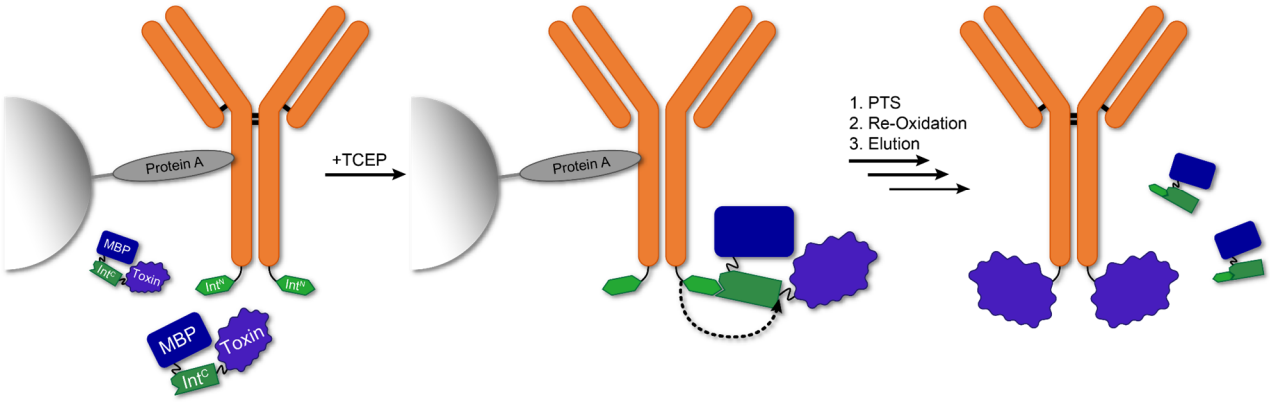

Figure 28: PTS on solid support.
Schematic representation of the splicing and purification process on protein A beads. Antibodies were first bound to protein A agarose. Afterwards the reducing agent TCEP and the toxin splicing partner were added and incubated O/N at 25 °C under constant shaking (1. PTS). After the unreacted toxin had been washed away, the antibody was oxidized using DHAA in PBS for 3 h at 25 °C (2. Re-Oxidation). Last, the formed IT was eluted from the beads using protein A elution buffer (3. Elution). The product was then dialyzed in the desired buffer and concentrated before further analyses.[202]

4.3.1. Evaluation of important parameters for efficient PTS

As already pointed out in the introduction, intein splicing is a very specific reaction. It has already been shown to work in crude extracts and even in living cells.[193] The toxin preparations still contained some impurities which makes analysis by SDS-PAGE more difficult but does not interfere with the splicing reaction. The most important parameters for a PTS reaction are temperature, time and the concentration of the reducing agent. Analysis of a pH range from pH 6.5 to 8 did not show altered splicing efficiency in the utilized M86 *Ssp* DnaB mini intein (data not shown).

A time-dependent assay was performed with the 7D9G-Fc-Int^{N} antibody and Int^{C}-ETA at 25 °C over a period of 20 h. After 1, 2, 4 and 20 h a sample was taken from the reaction mixture and denatured in SDS sample buffer. SDS-PAGE revealed that a product band already showed up at about 75 kDa after 1 h which steadily increases up to 20 h. The protein bands of the Ab and the toxin bands at 58 and 33 kDa, respectively, decrease at a similar rate. The same trend could be seen if less toxin was added. Notably, the OD280 measurement suggested that the applied volume of toxin should have resulted in a 3 eq. excess of toxin over Ab. The first five lanes of Figure 29A showed that, however, substoichiometric levels of toxin versus antibody were used. Nevertheless, splicing was observed and the time course indicated that reaction times of >20 h are preferable.

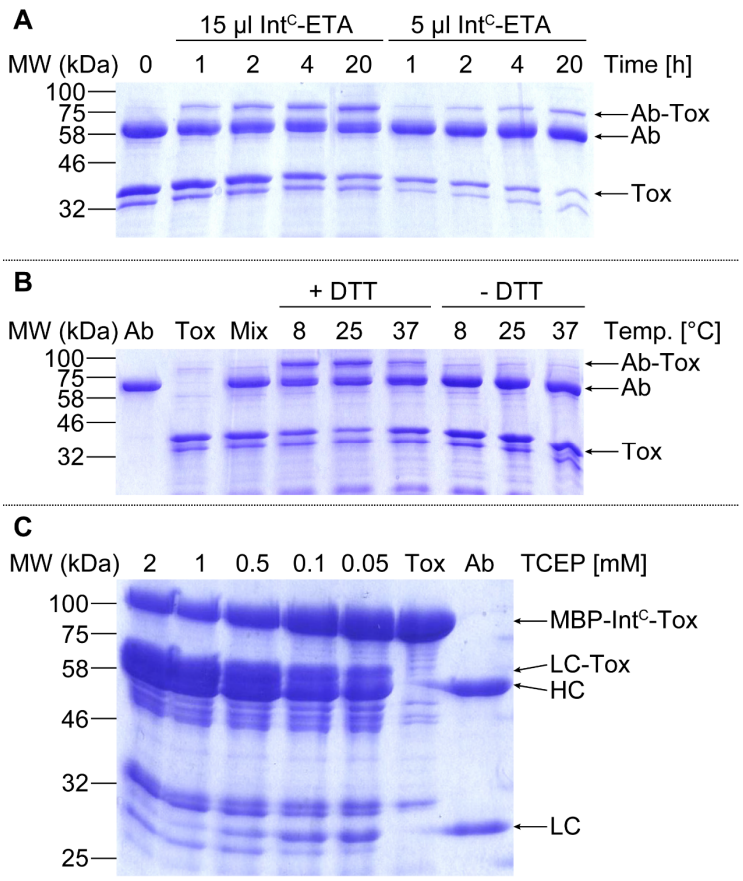

Figure 29: Influence of time, temperature and reductant on PTS efficiency.
A) 7D9G-Fc-Int^N was incubated with Int^C-ETA for up to 20 h at 25 °C. After 1, 2, 4 and 20 h a sample was taken and analyzed by SDS-PAGE. Additionally, different amounts of Int^C splicing partner were added. *B)* 7D9G-Fc-Int^N was mixed with Int^C-ETA at different temperatures and in the presence or absence of reductant as depicted above the gel image. The antibody (Ab), the toxin (Tox) and the mixture of both at 0 h (Mix) was loaded as controls. *C)* T2 was incubated with MBP-Int^C-Gelonin O/N at 25 °C with different TCEP concentrations from 0.05 to 2 mM. Toxin and antibody served as controls. All relevant proteins and fragments are marked with arrows.

Next, the influence of the temperature on splicing efficacy was analyzed. Therefore, 0.9 μM 7D9G-Fc-Int^N was mixed with 14 μM Int^C-ETA (theoretical) with 2 mM DTT or without DTT at 8, 25 and 37 °C O/N (Figure 29B). The first conspicuity is that the toxin was again available substoichiometrically compared to the antibody. The realistic stock concentration of Int^C-ETA was thus much lower than expected. Protein splicing worked nonetheless and showed a maximum of desired product at 25 °C (Figure 29B). Splicing was still quite efficient at 8 °C but showed a strong decrease already at 37 °C. Additionally, the samples without reductant verify that it is a necessity to include it in each reaction. In conclusion, reactions were all carried out at 25 °C.

Third, the dependence on a reducing agent was analyzed. As already shown in Figure 29B, the complete lack of DTT or a comparable reagent prevents splicing. DTT is commonly used for several biochemical assays but has disadvantages since is volatile that would result in decreasing amounts over a period of 20 – 24 h at 25 °C. Additionally, reduction with DTT is a reversible reaction. To circumvent this, tris(2-carboxyethyl)phosphine (TCEP) was used on exchange which is an irreversible and non-volatile reducing agent. A concentration row ranging from 2 – 0.05 mM TCEP was tested for the reaction of MBP-Int^C-Gelonin with T2. Figure 29C shows the decrease in free LC-Int^N at about 25 kDa and the decrease of MBP-Int^C-Gelonin as markers for reaction progression. The additional band of the splicing product at about 56 kDa is not clearly distinguishable from the HC band. Nevertheless, the experiment shows that 1 and 2 mM TCEP are required for a complete reaction, while reaction efficacy decreases already at 0.5 mM. The concentration of the Ab-Int^N in the reaction was 3 μM, resulting in a minimum excess of 166–fold of the reducing agent over the Int^N containing protein.

4.3.2. Comparison of different antibody constructs for PTS

After the best conditions for performing PTs reactions were identified, different antibody constructs were tested for their capability to conjugate to toxins. In contrast to ADCs, the conjugation partner in ITs is bigger by a factor of 20 – 30, which raises the question if toxins can be attached to both heavy and light chain. Especially for the latter a steric hindrance between a 150 kDa antibody and a 90 kDa toxin fusion protein is quite likely. In the MBP fusions, the active intein sequence is in the middle of the molecule, further complicating the situation.

Three different trasuzumab variants were produced together with the WT, as already shown in 4.1.1.2, which had the IntN sequence attached *C*-terminally of the LC and/or the HC. In a first reaction, Int^C-Trx was used as a model protein that was suitable because of the small size and the resulting products that could be easily separated by SDS-PAGE. Abs were applied at 1.5 μM together with 2 mM TCEP and almost equimolar Int^C-Trx. As Figure 30 depicts, WT trastuzumab (T1) does not react with the Trx protein as expected. T2 and T4 that had the intein sequence attached to the LC and HC, respectively, both display an additional product band and confirm their ability to splice to an intein partner. The splicing efficacy seems to be slightly higher for the HC but differences are minimal. Interestingly, the variant with Int^N on both LC and HC (T3) shows efficient splicing at both sites. The overall coupling efficiency is limited to the amount of Int^C-Trx in the reaction, which is consumed to about 70 – 80 %. Increasing the IntC concentration would most likely increase the ratio of conjugated to unconjugated Ab chains.

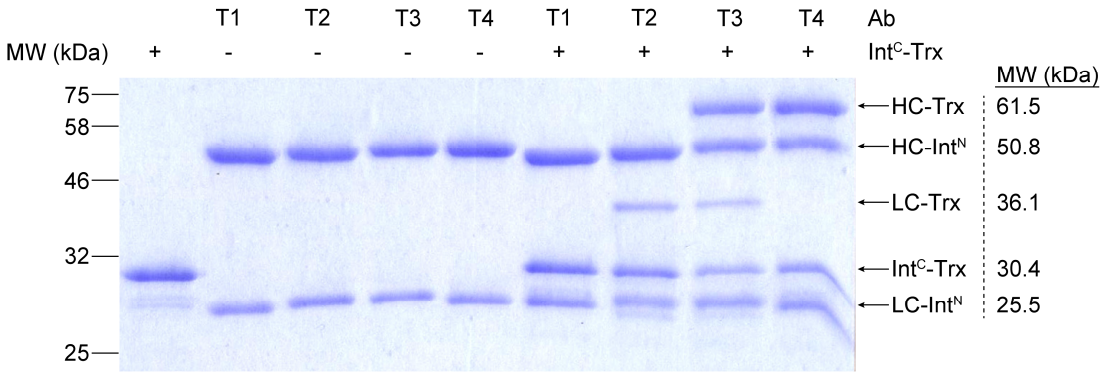

Figure 30: PTS of trastuzumab variants with Int^C-Trx.
The ability of the Int^N fragment to splice either on the HC and/or on the LC was tested with the Int^C-Trx fusion. Splicing reactions were carried out O/N at 25 °C. The first 5 lanes show the splicing partners alone, followed by 4 lanes with the splicing reactions. All protein fractions, educts and products are marked with arrows and their corresponding molecular weights on the right.

The same experiment was then performed with MBP-Int^C-Gelonin, all trastuzumab variants and 7D9G-Fc-Int^N. In this case it was difficult to discriminate between the different species because the area between 50 and 60 kDa and the region between 80 and 93 kDa contained several proteins and fragments. Reaction progression can nevertheless always be visualized by the difference in protein band intensities

between controls and reactions because the same amounts of Ab and toxins have been loaded in all lanes. Strangely, the VHH construct didn't react with the toxin at all (Figure 31) although it showed splicing activity in tests before (Figure 29 A and B). Trastuzumab WT again didn't show splicing activity as expected. Although gelonin has a size of 30 kDa, compared to 14 kDa of Trx, good splicing yields to both LC and HC were reached. Strikingly the LC reacted to almost 100 % in the case of T2 and to about 80 % in the T3 variant and showed better splicing efficacy than the HC. For T3 the conjugation might have even be pushed to completion if more toxin would have been available. Almost the complete toxin was consumed in this reaction. Since educts and products are in such proximity, efficacies cannot be determined in more detail for the HC conjugates. However, at least 50 % reacted to the desired product that could be enhanced by increasing the amount of toxin educt.

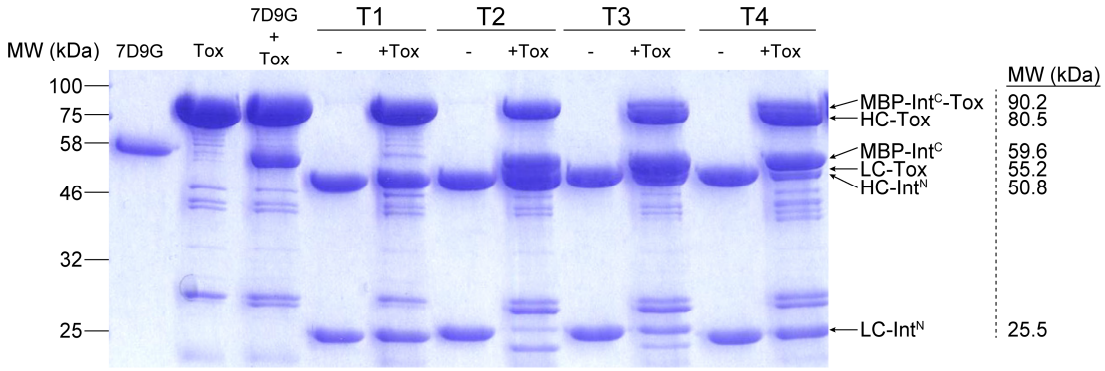

Figure 31: Toxins can be coupled to the heavy and the light chain of trastuzumab.
7D9G-Fc-Int^N and all trastuzumab variants were tested for splicing efficiency with MBP-Int^C-Gelonin under standard conditions. The first three lanes show the VHH construct, the toxin alone and their mixture, respectively. The other lanes contain T1-T4 variants either alone or their PTS reaction with the toxin. All protein fractions, educts and products are marked with arrows and their corresponding molecular weights on the right.

4.3.3. Conjugation of gelonin and PE24 to trastuzumab and 7D9G-Fc on solid support

Chapter 4.3.2 showed that it is possible to couple toxins as a MBP fusion to trastuzumab's LC and HC. The VHH construct had also already shown to work in PTS reactions (Figure 29 A and B), so the next step was the preparative coupling of two cytotoxic proteins to yield ITs with biological function. The latter should be as comparable as possible, so only the T4 variant was used representative for all trastuzumab ITs because both T4 and the VHH construct contained an Int^N sequence located on the *C*-terminus. The reactions were performed on protein A beads as already stated in 4.3 and as described in 3.6.5.2. All intermediate steps were stored and analyzed by SDS-PAGE. In Figure 32 the coupling of both MBP-Int^C-Gelonin and MBP-Int^C-PE24 to 7D9G-Fc-Int^N and T4 are shown. The FT-Ab lane shows that the protein A slurry was highly effective in capturing the complete amount of antibody. In this reaction 3 nmol antibody was loaded, corresponding to 0.34 and 0.44 mg for the VHH and the T4 constructs, respectively. A 6-fold excess of toxin (3-fold relative to each HC) was then added together with 1 mM

TCEP in a total volume of 300 µl and incubated for 20 h with the slurry. The comparison between the toxin load and the toxin flow-through after the reaction clearly exhibited an increase in the side product MBP-Int^{C}/Int^{N} at a size of about 60 kDa. Still, there was a lot of toxin that had not reacted. Both elution fractions depicted a successful PTS reaction and an additional band appeared at 91 and 83 kDa for the gelonin ITs and at 87 and 79 kDa for the PE24 ITs, respectively.

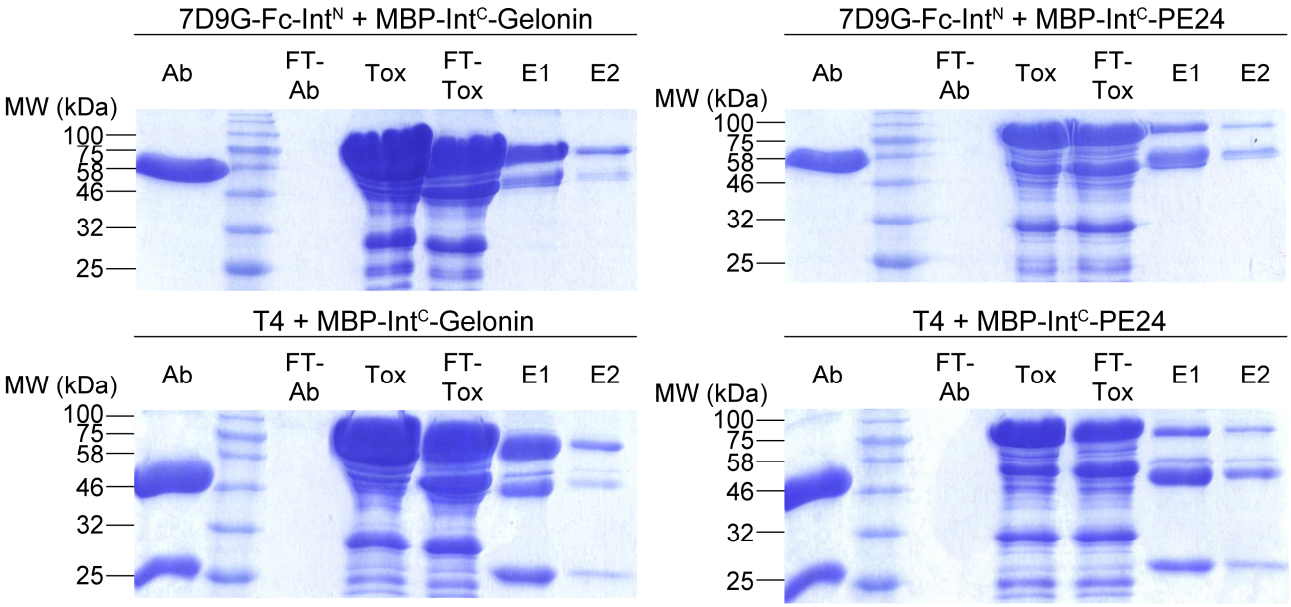

Figure 32: Semi-preparative PTS on protein A beads.
Antibodies were bound to protein A agarose and reacted with MBP-Int^{C}-Gelonin and MBP-Int^{C}-PE24 as depicted in Figure 28. The antibody load (Ab), FT that did not bind to the beads (FT-Ab), toxin load (Tox), unreacted toxin (FT-Tox) and both elution fractions are presented on each gel. Elutions still contained small amounts of unspecifically bound MBP-Int^{C}-Toxins. MBP-Int^{C}-Gelonin (left) generally showed better splicing efficacy than MBP-Int^{C}-PE24 (right).

Additionally, a small fraction of the MBP-Int^{C}/Int^{N} side product was co-purified and represents a small impurity without biological function. Noticeably, the PTS efficacy was a lot higher with the gelonin toxin than with the PE24 fusion. A toxin/antibody ratio (TAR) of 1.4 was reached for both 7D9G-Fc-Gelonin and T4-Gelonin. The TAR of the PE24 ITs was much lower and only 0.8 and 0.7 was reached for 7D9G-Fc-PE24 and T4-PE24, respectively. A possible cause of for the diminished reactivity could be aggregation, since accessibility of the Int^{C} intein domain is necessary for a successful reaction. Thus, in a next step the aggregation of the toxins was assessed and the influence on PTS efficacy was tested.

4.3.4. SEC purification of MBP toxins increases PTS efficiency

Protein aggregation can occur if part of the protein is mis-folded or if the storage buffer is too close to the pI of the protein which leads to bad solubility and hydrophobic interactions.[212] The Int^{C} sequence is naturally unstructured and folds into the correct shape when the Int^{N} counterpart is present. This may affect aggregation, depending on the fusion partner in the protein. After production of both gelonin and

PE24 as MBP fusions and purification by IMAC, both proteins were concentrated and subjected to preparative SEC. For this purpose, a Superdex 200 10/300 column with 24 ml bed volume was used. In total 17.5 mg MBP-Int^{C}-Gelonin and 10 mg MBP-Int^{C}-PE24 were purified by SEC. Figure 33 shows the chromatograms and the corresponding fractions analyzed by SDS-PAGE. For both proteins there are four peaks visible. The first three from 7 – 14 min all contain the desired toxin as visualized by the reducing gels below. There are still some impurities visible, though. The fourth peak clearly corresponds to smaller impurities that could successfully be cleaned-off with this method. Nevertheless, the question remained why there were so many different species of protein with the same molecular weight. Apparently, the first peak at about 7 min shows aggregates. These are much more prominent in the PE24 samples than in the gelonin sample. In fact, aggregates make up the largest fraction in the PE24 sample. This observation fits with the bad splicing data presented in 4.3.3 for the PE24 construct. It seems that gelonin has a lower tendency to aggregate. The different fractions were conducted to a PTS reaction to verify that aggregates could not perform splicing reactions any more.

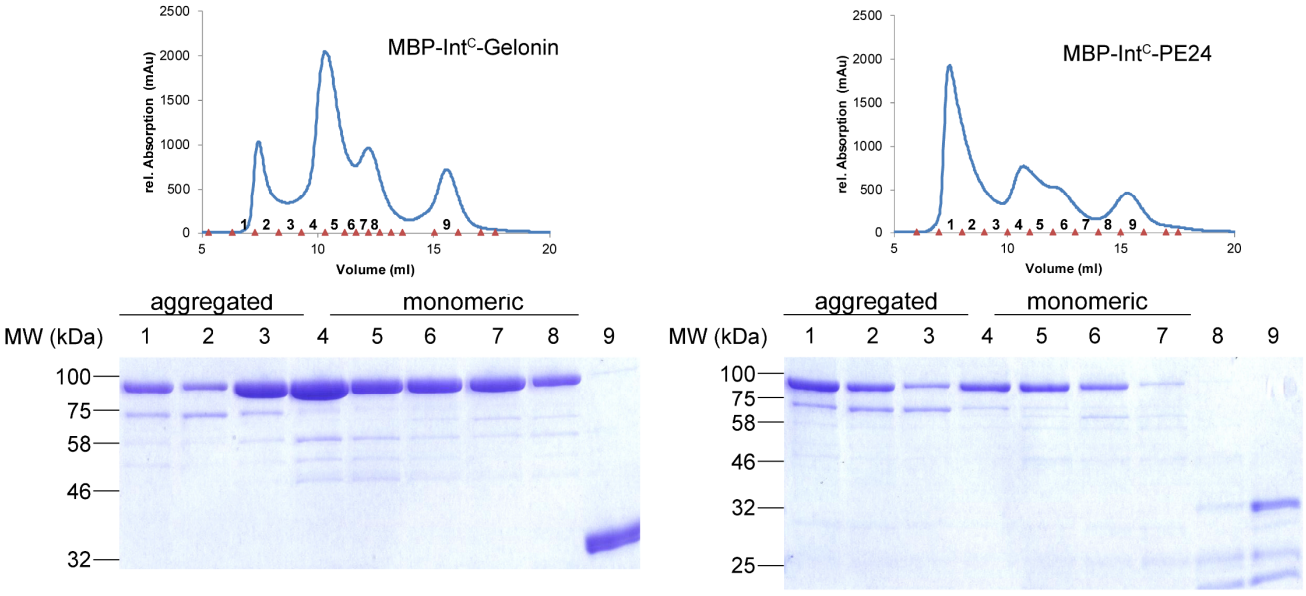

Figure 33: SEC purification of monomeric toxins for enhanced reactivity.
SEC revealed several aggregation states of MBP-Int^{C}-Gelonin and –PE24. SEC chromatograms (top) recorded at 280 nm with respective fractions that were analyzed by reducing SDS-PAGE (bottom). The toxin is spread over a broad range that is resembled by three distinct peaks in the chromatogram. This indicates different aggregation states, from high-molecular weight aggregates to dimers or trimers and the desired monomers. The last peak at 16 min clearly shows small molecular weight impurities from IMAC purification.

Fractions 2, 4, 8 or 1, 2, 4 and 6 were tested in analytical PTS reactions of the gelonin and PE24 constructs, respectively. They were incubated with 7D9G-Fc-Int^{N} O/N and analyzed by SDS-PAGE. The gel revealed (Figure 34) that no splicing activity could be observed for the aggregated fractions 1 and 2 but could be observed for fractions 4 and 8 of the gelonin construct and fractions 4 and 6 of the PE24

construct. This confirms that aggregated Int^C containing proteins are not able to combine with their counterpart and conduct protein splicing.

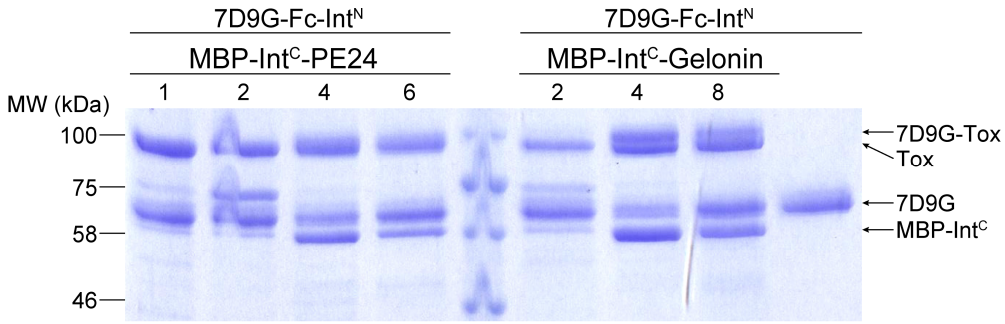

Figure 34: Differential reactivity of SEC fractions in protein splicing.
Fractions from SEC purification (Figure 33) are numbered correspondingly and were tested for PTS efficacy with 7D9G-Fc-Int^N. Most important protein fractions, educts and products are marked with arrows on the right.

The soluble fractions from 9 – 14 min were pooled and concentrated for preparative PTS reactions. For MBP-Int^C-Gelonin a total of 9.3 mg were obtained, which corresponds to a yield of 53 %. A total of 5.9 mg were purified for MBP-Int^C-PE24, corresponding to a yield of 59 %. It is possible though that both proteins could aggregate again during concentration process since osmolarity and hydration behavior may change. This could be assessed by another SEC but was not performed because of the limited amount of available toxins.

Another possibility to increase splicing efficacy is the *N*-terminal cleavage of the solubility tag MBP, thus reaching better accessibility of the Int^C domain. A TEV site was introduced into the MBP-Int^C-PE24 construct and the protein was cleaved in a standard TEV cleavage reaction at RT O/N. A white precipitate formed and both solid and soluble fractions were analyzed by SDS-PAGE (Figure S 2). The precipitate was composed of the Int^C-PE24 fragment, while the soluble fraction mainly contained the MBP tag. This showed that the large MBP is essential for solubility of the fusion protein and that its presence is mandatory in PTS reactions.

4.3.5. Purification of immunotoxins

New ITs were produced in PTS reactions on protein A beads with the freshly purified 'monomeric' toxins. This time 1 mg of antibody was coupled to protein A beads and 4 eq. of toxin together with 1 mM TCEP (69-fold excess) were added in 600 μl. SDS-PAGE analysis revealed increased PE24 splicing efficacies and TARs of 0.9 and 0.8 for 7D9G and T4, respectively (Figure 35). This shows that SEC purification led to an improvement in reactivity.

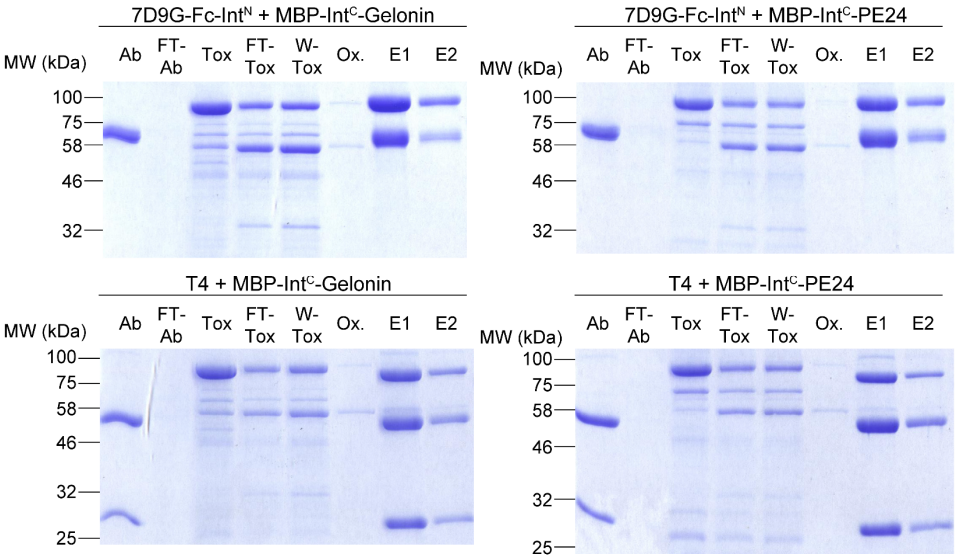

Figure 35: Preparative PTS on protein A beads with SEC purified toxins.
Antibodies and toxins used for PTS as already shown in 4.3.3. Denotation of SDS-PAGE lanes is the same as in Figure 32. A sample of the oxidation FT (Ox.) was included and showed that only a small amount of antibody is release from the beads during this process. Splicing efficacy of MBP-Int^C-PE24 was increased compared to the previous test because of SEC purification, while splicing efficacy of MBP-Int^C-Gelonin was slightly decreased. This may be attributed to the decreased toxin and TCEP equivalents.

As expected, the PTS efficacy of MBP-Int^C-Gelonin was a bit lower in this reaction and TARs of 1.1 and 1.0 could be achieved for the VHH Ab and T4, respectively. Although there was still potential for improvement of reaction conditions, these ITs depicted a very good starting point for further analysis. A TAR of 1 means that in average every Ab molecule had one toxin molecule attached. This is composed, however, of a distribution of molecules with 0, 1 or 2 toxins. An easy way to increase the TAR is to remove unreacted antibodies from the ITs by exploiting the His_6 tag of the toxin domains. An IMAC was performed and the flow-through contained free antibody as expected (Figure 36). The elution fractions included the ITs with an increased TAR. Although a gradient elution was applied, the different TAR species of 1 and 2 could not be resolved. The final ITs (Figure 36 bottom) all had a TAR of approximately 1.3 that was determined by densitometry from the SDS gel. These conjugates were used for biochemical and biological characterizations. An optimized protocol for IT generation that includes all optimization parameters is included in 3.6.5.2.

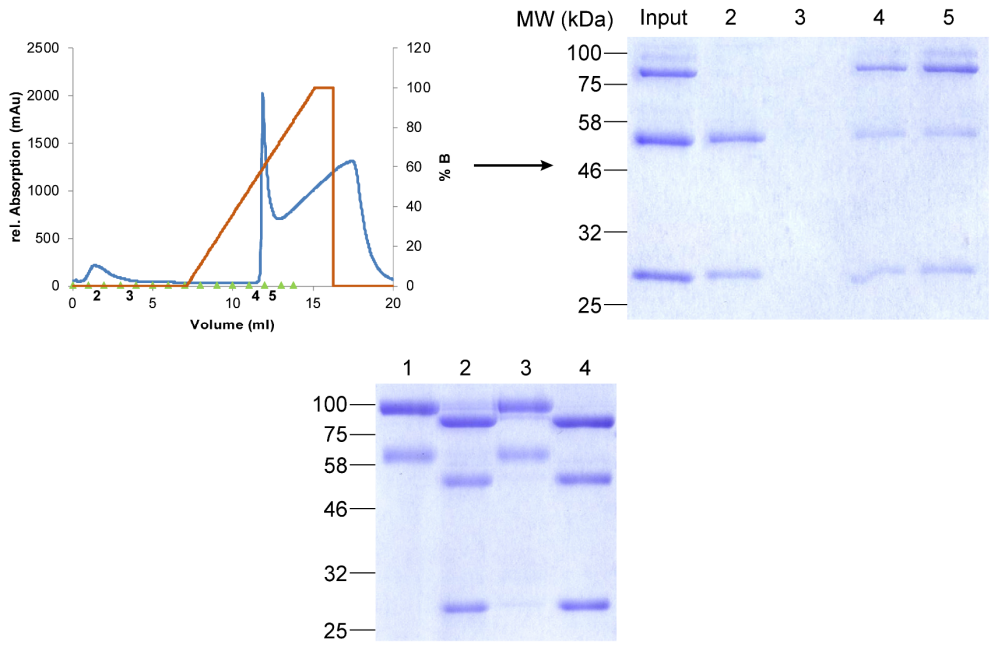

Figure 36: IMAC purification of ITs.
Residual antibody without conjugated toxin was removed by IMAC. Only ITs with 1 or 2 toxins per Ab contained a His_6 tag and were bound by the Ni sepharose column. A gradient over 10 min to 100 % elution buffer was used to elute bound ITs. The chromatogram is shown on the top left. The absorption at 280 nm is depicted in blue, the gradient in red and fractions in green. The latter were analyzed by SDS-PAGE. Input = protein solution prior to IMAC; 2 – 5 = fractions as depicted in IMAC chromatogram. The bottom gel summarizes the purified and concentrated IT preparations. 1 = 7D9G-Gelonin; 2 = T4-Gelonin; 3 = 7D9G-PE24; 4 = T4-PE24.

4.4. Characterization of immunotoxins

4.4.1. Hydrophobicity

ITs with gelonin were subjected to hydrophobic interaction chromatography (HIC) to investigate the change in hydrophobicity. ADCs often suffer from a strong increase in hydrophobicity that influences their pharmakokinetic properties and was linked to the development of drug resistence.[213,214] 30 μg samples were injected with an Agilent LC 1100 device and separated over 30 or 45 min for trastuzumab or 7D9G samples, respectively. The running buffer contains high ammonium sulfate concentrations that reduces solvation of the protein and thus exposes hydrophobic surface regions, which in turn interact with the column material. Proteins are eluted with a low-salt buffer without ammonium sulfate that resolvates the antibodies and washes them from the column. The more hydrophobic a protein, the later it elutes. All trastuzumab variants that were analyzed are characterized by a similar hydrophobicity (Figure 37A). The T2 variant showed a double peak that was hard to explain because SDS-PAGE analysis confirmed a homogeneous molecule. The T4 variant was the most hydrophobic variant. Interestingly, when gelonin was conjugated this contributed to hydrophilicity.

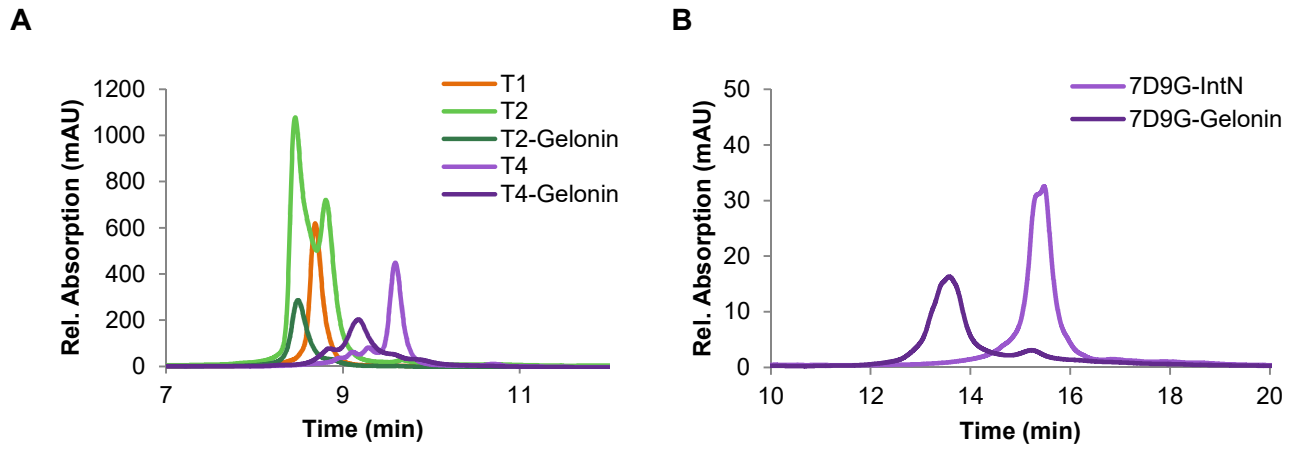

Figure 37: HIC analysis of gelonin ITs.
A) Trastuzumab variants and gelonin ITs were separated on a TSKgel Butyl-NPR column with a gradient from 0 – 100 % buffer B over 20 min at 0.9 ml/min. The absorption was measured at 220 nm resulting in higher absorptions. *B)* For the separation of the VHH samples, the gradient was applied over 35 min. Retention times are therefore not comparable. The absorption was measured at 280 nm.

This is a reversal of the phenomenon observed with extremely hydrophobic payloads for ADC development like MMAE that shift the anitbody signal to higher elution times. The same effect was observed for the VHH antibody that eluted earlier when conjugated with gelonin. This effect makes ITs valuable molecules in drug research.

4.4.2. Thermal stability

Another property important for stability of the molecule and its pharmacokinetics is the thermal stability. It is a direct measure for molecular stability and susceptibility to aggregation during long term storage at elevated temperatures. It can be measured by a fluorescent probe that undergoes dramatic increases in quantum yield when bound to hydrophobic regions in denatured proteins. Protein samples are incrementally heated up from 25 to 100 °C and fluorescence is measured at each step. The change is monitored and the melting point can be determined at the inflection point of the first derivative of the fluorescence emission as a function of temperature ($-dF/dT$).[215] The VHH ITs didn't show any differences in thermal stability and showed a consistent melting point at 60 °C, although signal to noise ratio in the experiment was unsatisfying (Figure 38 left). This was confirmed in a another experiment only comprising 7D9G-Fc-Int^{N}, MBP-Int^{C}-Gelonin, and 7D9G-Gelonin which was performed in triplicate (Figure S 1). Both parental toxins show a melting point at 50 °C, which most probably corresponds to the MBP domain because this is the predominant domain available in both constructs.

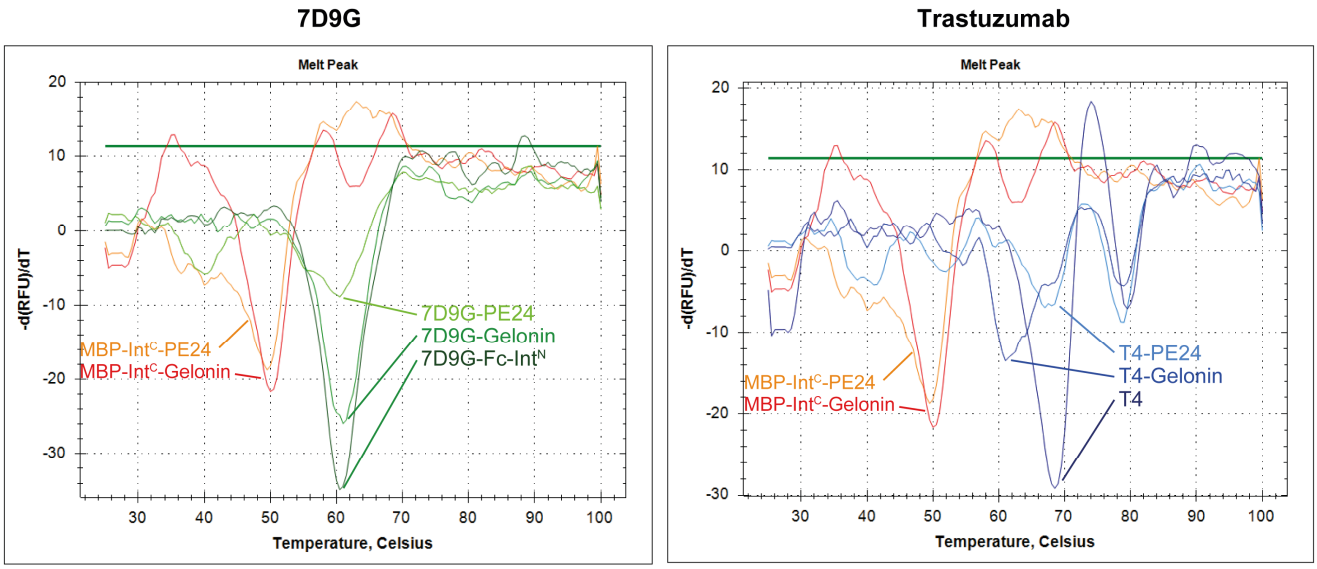

Figure 38: Melting curve determination by thermal shift assay.
Antibodies, ITs and MBP-Toxins were diluted to 150 µg/ml in PBS and SyproOrange was added to a final dilution of 1:1000. The left analysis shows the differences in thermal stability of VHH constructs. 7D9G-PE24 was characterized by an additional melting point at 40 °C, while the gelonin conjugate did not display differences to the parental Ab. On the right side the trastuzumab conjugates are compared. Here, the PE24 IT displayed the same additional melting point around 40 °C like for the VHH construct. The T4-Gelonin IT was characterized by a reduced melting point from 69 to 61 °C. All proteins are labelled with the corresponding colors of the graphs.

The trastuzumab-based ITs show a divergent behavior in melting temperatures (Figure 38). Here, the unconjugated antibody has two melting points at 69 and 80 °C, consistent with the reported differences in domain stability of Fab and Fc, respectively.[216] Literature reports melting temperatures of 61 and 71 for Fab and Fc fragments, respectively. Notably, these values were measured with differential scanning calorimetry (DSC) that might explain the difference. Interestingly, the first melting point is lowered after gelonin conjugation, which would mean that its presence destabilizes the Fab fragment. Although the signal is much lower for the PE24 conjugate it does not show a decreased stability. Another melting area was visible around 40 °C that also exists in MBP-Int^C-PE24. This suggests that PE24 might diminish the biophysical stability of immunotoxins and should be investigated in more detail. The measurements of all ITs were fuzzier compared to the parental antibodies leading to a bad signal/noise ratio, which made the determination of T_M values difficult. The protein concentration was already raised from 100 to 150 μg/ml but no improvement in signal quality was achieved. Overall results show, however, that thermal stability of ITs is not reduced and emphasizes the suitability of intein-ligated antibody-toxin conjugates.

4.5. Biological effects of immunotoxins

4.5.1. Inhibition of protein translation *in vitro*

Since elution from protein A includes a low pH step that might harm the structural and functional integrity of the respective toxin protein, the activity of ITs was assessed in a protein translation assay *in vitro* using rabbit reticulocyte lysate. These mammalian cell lysates can be used to perform analysis in an almost native environment. An mRNA that is translated into a reporter protein is added together with different sample concentrations and controls. In this case firefly luciferase was used and translation rate visualized by adding the substrate luciferin and measuring bioluminescence. The amount of translated luciferase is proportional with the emitted photons. While gelonin showed inhibition in the picomolar range (IC_{50} = 251 pM) as reported before (Figure 39), PE24 did not show inhibition of rabbit ribosomal protein synthesis in this assay (data not shown). This is probably due to the fact that NAD^+ is needed for activity of PE24 and not enough of this co-factor may be included in the rabbit lysate.[217] Both trastuzumab and 7D9G conjugates to gelonin showed IC_{50} values in the same range compared to the parental toxin with half maximal inhibitions at 183 pM and 84 pM, respectively. The IC_{50} values of ITs were expected to be slightly lower than for the parental toxins because of a stoichiometry of 1–2 toxins per antibody. Parts of this have already been published.[202]

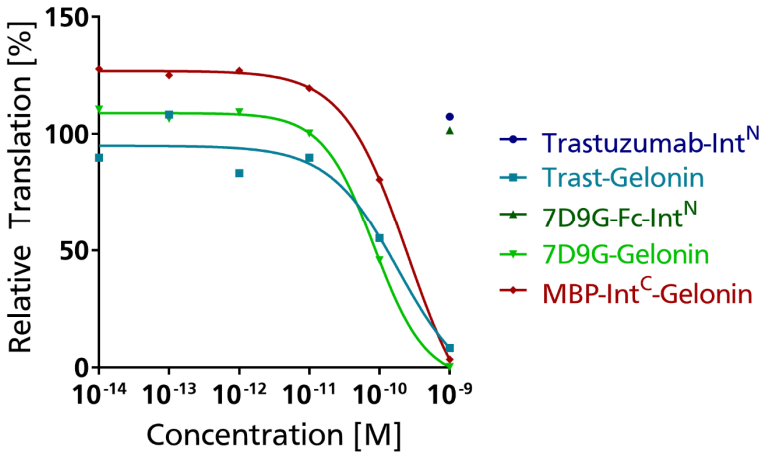

Figure 39: Protein translation is inhibited by gelonin and its ITs *in vitro*.
Rabbit reticulocyte lysate was mixed with various concentrations of analyte and the mRNA of the reporter enzyme luciferase. A control without analyte was set as a relative translation of 100 %. Gelonin conjugates showed similar inhibition compared to the unconjugated toxin with IC_{50} values around 100 pM. This assay was performed qualitatively with single measurements per sample. Sigmoidal curve fitting was performed using GraphPad Prism software (GraphPad Software, Inc.).[202]

4.5.2. Binding characteristics on cells

An additional load of about 30 – 60 kDa at the C-terminus of the antibodies could influence their binding characteristics for their antigen. To test the influence of the toxins on binding, MDA-MB-468 and SK-BR-

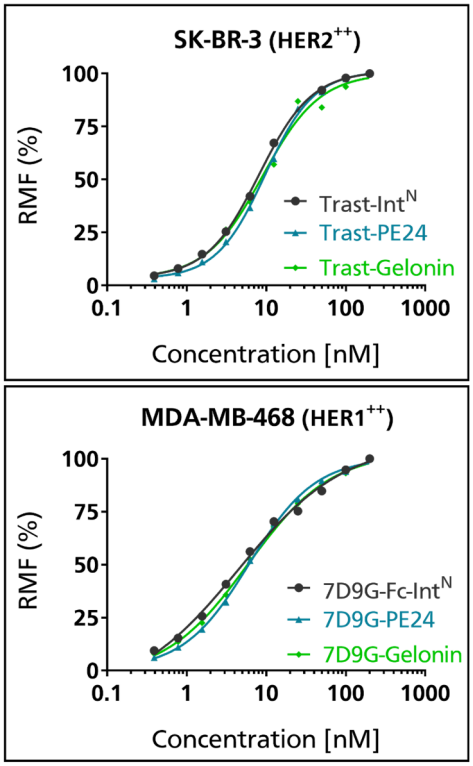

Figure 40: Binding of ITs to receptor overexpressing cells is not altered compared to the parental Abs.
MDA-MB-468 cells (HER1$^+$) and SK-BR-3 cells (HER2$^+$) cells were titrated with the 7D9G and the T4 based ITs, respectively. Binding characteristic and strength were not altered when toxins were attached. Affinities were calculated by sigmoidal curve fitting using GraphPad Prism software (GraphPad Software, Inc.).[202]

3 cells were titrated with both the parental antibodies and their respective ITs and analyzed by flow cytometry. The binding curves (Figure 40) displayed no significant deviations in K_D values compared to the parental antibodies. 7D9G binding to MDA-MB-468 cells showed an expected high affinity binding with a K_D of 4.5 ± 1.0 nM. The gelonin and PE24 conjugates had slightly decreased binding affinities of 5.9 ± 0.6 nM and 6.1 ± 0.4 nM, respectively. The same was observed for trastuzumab. While the parental antibody bound to HER2 overexpressing SK-BR-3 cells with a K_D of 8.2 ± 0.3 nM, the gelonin and PE24 conjugates showed dissociation constants of 9.1 ± 1.3 and 9.7 ± 0.4, respectively. Thus, the attachment of such bulky additives at the C-terminus of both antibodies does not impair their binding properties.[202]

4.5.3. Internalization

After binding to the cell surface of a target cell, ADCs or ITs have to be internalized to release their cytotoxic payload and kill the cell. The internalization has already been shown for trastuzumab upon HER2 binding and is well documented.[218] However, no data are available for the bivalent VHH-Fc fusion. Therefore, A549 cells also overexpressing HER1 were treated with 100 nM 7D9G-Fc-Int^N and 7D9G-Gelonin and incubated for 1 h at either 4 °C or 37 °C. At low temperatures the membrane dynamics are inhibited and antibodies are not internalized but bind only to the surface. The staining antibody was later quenched with an α–Alexa488 antibody. A549 cells incubated at 4 °C show a significantly reduced fluorescence when the surface bound antibodies were quenched, while no reduction was observed for cells incubated at 37 °C (Figure 41 top). Notice that only the quenched samples are presented for A549 at 37 °C although the colors are depicted for not quenched samples. This clearly shows that the 7D9G antibody shows very good internalization characteristics and confirms the suitability for IT treatment.

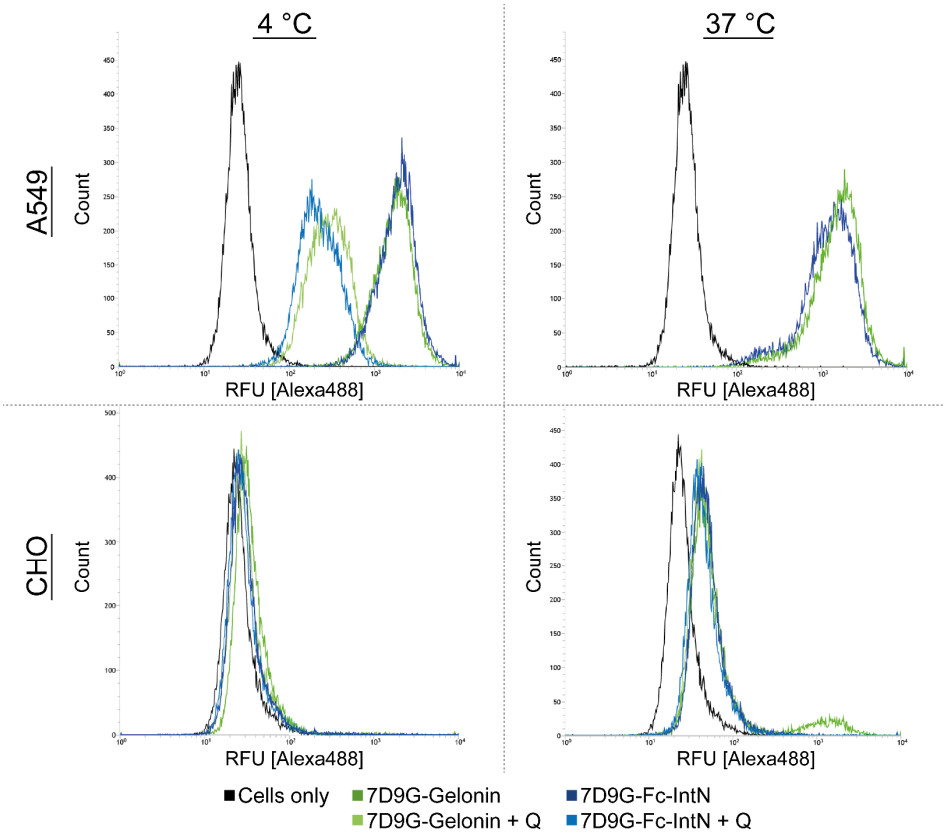

Figure 41: Internalization of 7D9G-Gelonin in A549 cells.
Cells displaying the HER1 receptor on their cell surface (A549) and control cells without HER1 (CHO) were incubated with 7D9G-Gelonin and 7D9G-Fc-Int^N at 4 °C and 37 °C, stained with α–hIgG-Fab Alexa488 secondary antibody and analyzed by flow cytometry. Histograms show the relative fluorescence units (RFU) of the detection antibody as measure of receptor binding on a logarithmic scale. In some samples (light colors), surface bound antibodies were quenched with an α–Alexa488 antibody. Note that the green and blue curves in the 37 °C A549 histogram display the quenched samples.

CHO control cells not displaying EGFR on their surface confirmed specific binding to the receptor. Only a slight shift was observed in the 37 °C samples which could also account for unspecific adherence of the secondary antibody to the cell surface.

To investigate the internalization and the time-dependent release of the toxins inside the cell, confocal microscopy was applied. Cells were treated with ITs for one or four hours and the respective route of the IgG and the toxin were followed by staining them with specific antibodies. All surface bound antibodies were removed by stripping them with a low pH washing step. This made sure that the signals obtained during microscopy accounts only for internalized antibodies. The latter were visualized using the Alexa488 labeled α-hIgG Fab fragment and the toxins were stained with an Alexa647 labelled α-His_6 antibody. HER1 positive MDA-MB-468 cells showed endocytic uptake of 7D9G-Gelonin and 7D9G-PE24 after 1h of incubation, marked by a punctate pattern in the 488-channel inside the cell (Figure 42). Additionally, after 1 h, signals for the antibody and the toxin colocalize for both the gelonin and PE24 IT. After four hours, however, the toxin fluorescence of the PE24 IT is clearly reduced in the vesicles. Gelonin still seems to be attached to the antibody at this time point as a high degree of colocalization of

antibody and gelonin is observed. This may be explained by the retrograde transport mechanism of PE24[219] that may result in a more efficient and faster transport to the cytosol than gelonin. CHO cells confirmed that the VHH did not bind unspecifically and no fluorescence could be detected for both antibody and toxin.

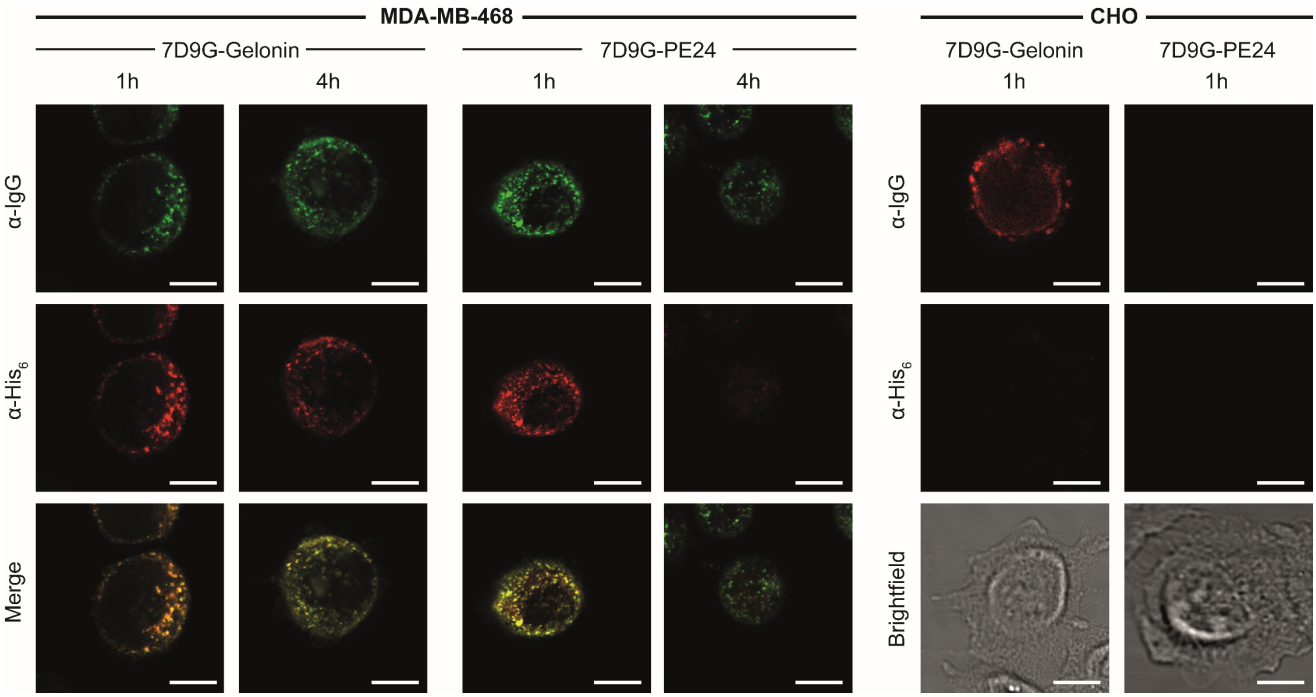

Figure 42: Internalization of 7D9G-ITs and endosomal release of toxins.
MDA-MB-468 (HER1 overexpressing) cells were treated for 1h with 7D9G ITs, washed with low pH glycine buffer to remove surface bound conjugates and stained directly or incubated for another 3h before staining. CHO cells were used as negative cell line. Anti-hIgG Fab-Alexa 488 (1:500) and anti-His6 Alexa 647 antibody (1:1000) were used to specifically visualize the antibody fraction and the toxin fraction of the ITs, respectively. Scale bar = 10 µm.[202]

Internalization was also confirmed for the trastuzumab ITs on SK-BR-3 cells (Figure 43). The overall staining intensitites for the Alexa488 and Alexa647 signals were strongly decreased compared those of MDA-MB-469 stained with the VHH ITs. A possible explanation was a different permeabilization of SK-BR-3 cells by triton X-100 which could lead to a decreased penetration and binding of the secondary antibodies. The signal/noise ratio was thus strongly decreased. Binding and internalization could nevertheless be observed and was characterized by a punctuate pattern. Colocalization of toxin and Ab was observed for both 1 and 4 h timepoints. No cytosolic delivery of PE24 could be verified in this cell line with trastuzumab. Since every tumor cell line has different characteristics that also affect organelle dynamics it is possible that maturation of endosomes to late endosomes and lysosomes is slower and also lysosomal proteases like furin occur at a later timepoint. Longer monitoring of the trafficking and specific staining of furin could elucidate if this was the case in SK-BR-3 compared to MDA-MB-468 cells.

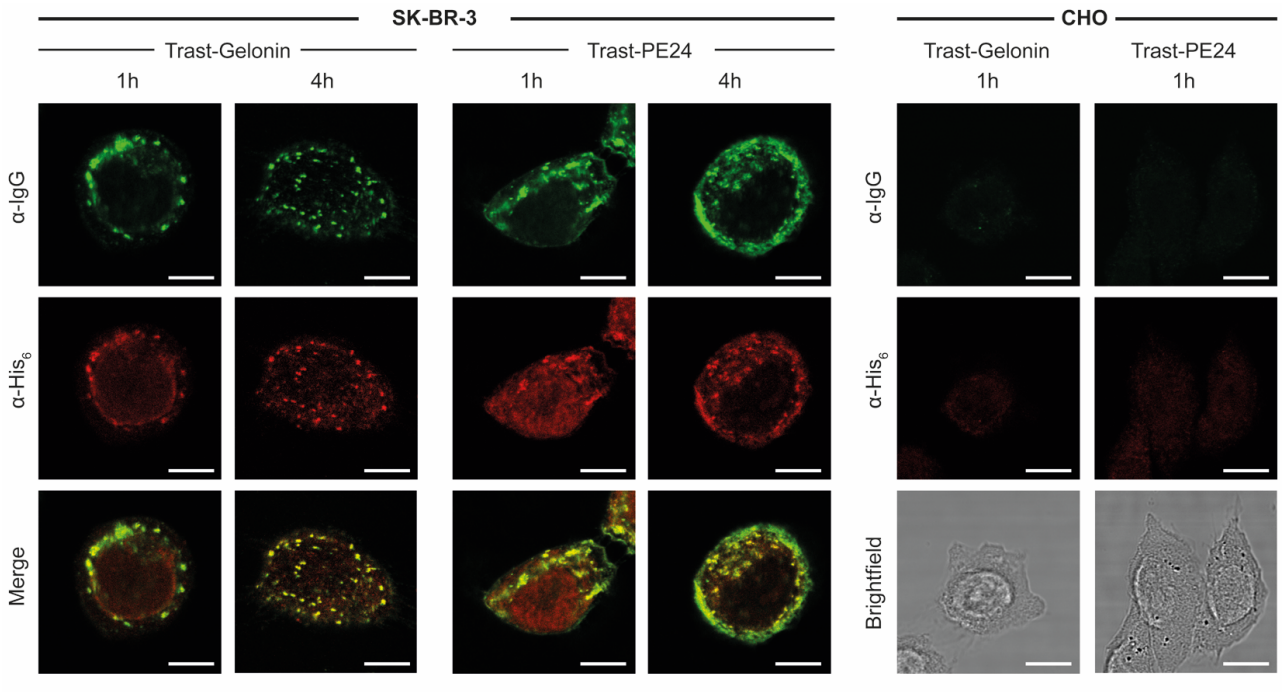

Figure 43: Internalization of trastuzumab ITs and endosomal release of toxins.
SK-BR-3 (HER2 overexpressing) cells were treated for 1h with trastuzumab ITs, washed with low pH glycine buffer to remove surface bound conjugates and stained directly or incubated for another 3h before staining. CHO cells were used as negative cell line. α-hIgG Fab-Alexa 488 (1:500) and α-His6 Alexa 647 antibody (1:1000) were used to specifically visualize the antibody fraction and the toxin fraction of the ITs, respectively. Scale bar = 10 µm.

Unfortunately, unspecific binding of the trastuzumab ITs was observed to the HER2 negative cell line MDA-MB-468 in two independent experiments. In the first one, gelonin was initially marked with the fluorescent tag TAMRA in a SrtA reaction and then ligated to T4 by PTS. When incubated with SK-BR-3 cells, both the WT and the conjugate showed uptake into the cells after 1 h and TAMRA staining confirmed co-localization of the toxin and the Ab (Figure S 3). Unspecific binding of T4-Gelonin-TAMRA was observed, however, on MDA-MB-468 cells. This was confirmed in a second experiment, when the toxin was not labelled with TAMRA but visualized with the α–His_6 Alexa647 antibody. The same picture showed that the gelonin conjugate was internalized into the HER2 negative cell line (Figure S 4). On CHO cells, no unspecific binding was detected, though. The phenomenon should be investigated in more detail on more cell lines and with the solitary toxin to see if it binds to the cell surfaces of some cells by its own.[202]

4.5.4. Cytotoxicity and specificity

As biochemical properties of all ITs looked promising, they were tested in cellular assays to assess their cytotoxicity and specificity. This has already been published.[202] Four different cell lines with different receptor densities on their surfaces were used. A549 have low to medium EGFR expression, MDA-MB-468 show high EGFR expression, SK-BR-3 are HER2 high-expressing cells and CHO-KI were used as

negative cell line because they don't present any of both receptors on their surface. Antibodies, toxins and ITs were incubated with the cells for 72 h before measuring cell viability in a standard MTS assay. Different concentration scales had to be used for gelonin and PE24 in the nanomolar and picomolar range, respectively, because of different inherent toxicities.

On the negative cell line CHO, none of the investigated ITs and controls displayed growth inhibition up to the maximal tested concentrations (Figure 4 left). The single-chain IT with 7D9G targeting HER1 showed potent cell killing of MDA-MB-468 cells compared to the antibody and the toxin alone (Figure 44 top middle). The effective ratio (ER) of IC_{50} value (IC_{50} of IT divided by that of the toxin, Table 1) of 7D9G-Gelonin to MBP-Gelonin of about 771 showed the high selectivity and enhanced uptake of the antibody-toxin conjugate. With a half-maximal inhibition at only 68.0 ± 4.2 pM, this conjugate is highly toxic to this target cell line. Interestingly, the same IT did not show any toxicity in the other EGFR expressing cell line A549, which has a receptor density about 50–fold lower than that of MDA-MB-468.[220] The HER2 targeting T4-Gelonin conjugate showed an even lower inhibitory constant of 11.8 ± 1.6 pM (Table 1) on overexpressing SK-BR-3. Combined with an ER of over 2.5*107 this was the highest selectivity in this whole data set.

Table 1: Cytotoxicity of immunotoxins on target and control cell lines.[202]
Antibodies, toxins and immunotoxins were tested for cytotoxicity in a MTS cell viability assay. IC50 values were calculated by sigmoidal curve fitting using GraphPad Prism (GraphPad Software, Inc.). Values were calculated from triplicate samples.

		CHO		A549		MDA-MB-468		SK-BR-3	
Target	**Protein**	**IC_{50} (nM)**	**ER**	**IC_{50} (pM)**	**ER**	**IC_{50} (pM)**	**ER**	**IC_{50} (pM)**	**ER**
	7D9G-Fc	>300	n.d.	>300000	n.d.	>300000	n.d.	n.d.	n.d.
HER1	**7D9G-Gelonin**	>300	n.d.	>300000	n.d.	**68.0 ± 4.2**	**771**	n.d.	n.d.
	7D9G-PE24	>1	n.d.	**3.9 ± 0.5**	**412**	**0.8 ± 0.1**	**290**	n.d.	n.d.
	Trastuzumab	>300	n.d.	n.d.	n.d.	>300000	n.d.	>300000	n.d.
HER2	**Trast-Gelonin**	>300	n.d.	n.d.	n.d.	n.d.	n.d.	**11.8 ± 1.6**	**>2.5E+7**
	Trast-PE24	>10	n.d.	n.d.	n.d.	59.9 ± 3.2	4	**2.4 ± 0.1**	**233**
	MBP-Gelonin	>300	1	>300000	1	5244 ± 1316	1	>300000	1
	MBP-PE24	>10	1	1644 ± 247	1	239 ± 26	1	568 ± 58	1

Similar results were obtained for the PE24 ITs. In the analyzed concentration range up to 10 nM, no toxicity can be observed in CHO cells for all analytes (Figure 44 left). The 7D9G-PE24 constructs show high potency in both HER1 positive cell lines A549 and MDA-MB-468 compared to the toxin alone with IC_{50} values of 3.9 ± 0.5 and 0.8 ± 0.1 pM, respectively (Table 1). Effective ratios of 412 and 290 for A549 and MDA-MB-468, respectively, show a high contribution of receptor mediated internalization of the antibody fraction to the ultimate toxicity. The sub-picomolar IC_{50} value of 7D9G-PE24 of 0.8 ± 0.1 pM depicts the highest toxicity in this study. In this case, the lower number of surface exposed receptors

on A549 cells did not have such a high impact as for the gelonin construct which indicates that also the efficiency of endosomal escape may play an important role for IT efficacy. Additionally, the Trast-PE24 IT showed a 233-fold decreased IC_{50} of 2.4 ± 0.1 pM compared to the toxin alone.

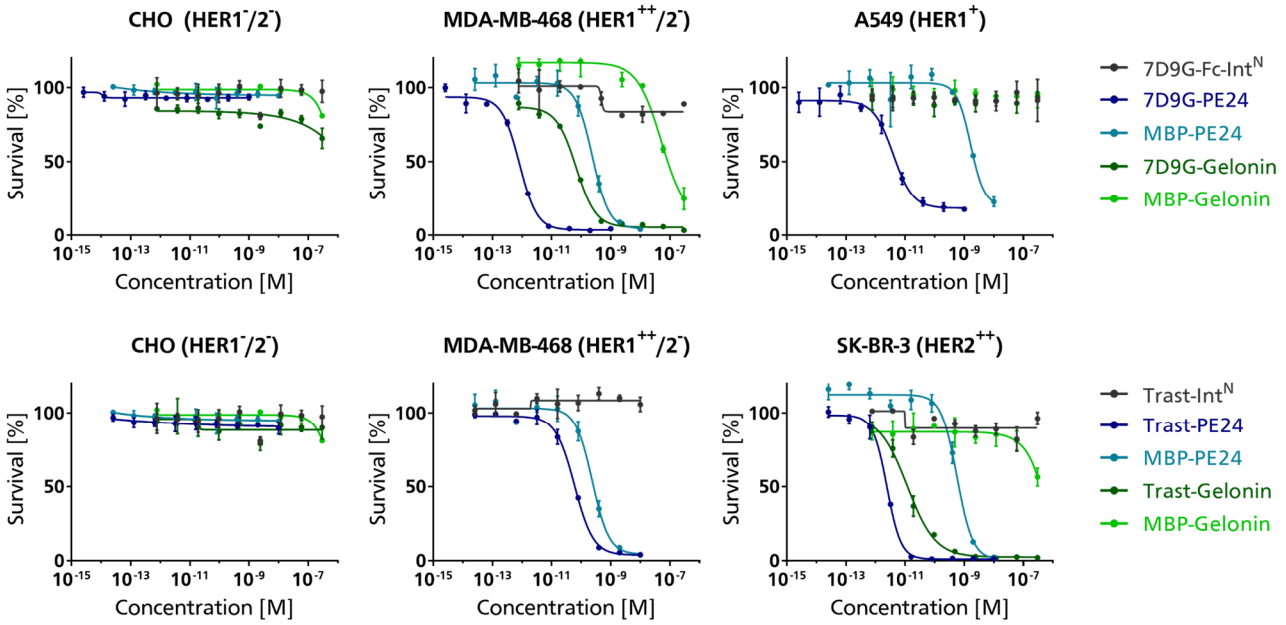

Figure 44 Cytotoxicity assay of ITs.
Different antigen presenting cells were treated for 72 h with antibodies, immunotoxins and toxins alone. The upper row shows data of cell lines treated with HER1 targeting 7D9G conjugates and the lower row shows data of HER2 targeting trastuzumab conjugates. CHO cells were used as negative control because of their lack of HER1 or HER2 expression. The assay was performed in triplicate. The relative survival to untreated cells was plotted against antibody concentrations and IC_{50} values were determined using sigmoidal fitting with GraphPad Prism (GraphPad Software, Inc.).[202]

The toxicity data of T4-PE24 on MDA-MB-468 cells confirms the unspecific internalization in this cell line of transtuzumab ITs, previously shown only for T4-Gelonin. The IC_{50} of T4-PE24 is by a factor of 4 lower than that of MBP-Int^{C}-PE24, which is neglectable compared to toxicities achieved on target cells. Nevertheless, this should be further investigated. Further cell lines should also be tested in cytotoxicity studies for both VHH and trastuzumab ITs.

5. Discussion

5.1. Generation of splicing-active antibodies and cytotoxins

Within the scope of creating functional immunotoxins was the successful cloning and expression of the toxic proteins. The organism of choice for the production was *E. coli* because it is widely used and generally high expression yields are achieved. It is the microorganism of choice for expressions of all kinds of proteins because of the ease to manipulate, low culturing costs and the very fast replication rate.[221] However, there are several factors to be considered for a successful expression resulting in high amounts of pure product. These are the production strain, the vector containing the gene of interest (GOI) and optional tags for higher solubility or purification. Every of these factors can be crucial for the desired outcome.[221]

BL21 and derivatives thereof are routinely used for recombinant protein production in *E. coli*. They are deficient in the proteases Lon and OmpT, which increases protein stability. The addition (DE3) implies the existence of an additional chromosomal copy of the T7 RNA polymerase gene that allows for expression of genes under control of the T7 promoter, which is a high expression promoter.[221] This strain was also chosen in this study because the majority of the proteins had no special requirements for rare codons, secretion into the medium or a difficult disulfide bridge pattern. Only the Int^{C}-ETA construct contained an intramolecular disulfide bond. Since expression yields were low for this construct in the beginning, another strain was tested. In the T7 Shuffle strain oxidizing cytoplasmic conditions prevail and it further overproduces the disufide bond isomerase DsbC that corrects mis-oxidized proteins and also acts as a chaperone for other proteins.[211,222] Unfortunately, no increased expression could be observed for the Int^{C}-ETA fusion protein. Some *E. coli* strains are optimized towards rare codons that are compensated by additional tRNA-synthetase genes. This is only necessary, however, if the GOI has been amplified from its original source and is not adapted to the codon usage of another microorganism. This can be completely ruled out in this study, since all toxin sequences were used with codon optimized sequence.

There are several common expression plasmids that are widely used for heterologous expression. They are mainly characterized by their promoter, the origin of replication and a resistance marker. While the latter was the ampicillin resistance gene β–lactamase in every plasmid, the origin and the promoter varied. The origin has a great impact on the expression yields and interestingly a higher copy number doesn't intuitively lead to a higher expression yield because a high number may impose a metabolic burden that decreases the bacterial growth rate and may produce plasmid instability.[209] In this study, the pMB1 and the ColE1 origin were used, which are both medium copy origins resulting in 15 – 60 and 15 – 20 copies per cell, respectively.[209] Since both show copies in the same range, a great difference in protein yields ensuing from the differences in origins is unlikely.

Two different promoters were used, the T7 and the tac promoter. The latter is an engineered variant of the trp and the lac promoter and is reported to be about 10 times stronger than the lacUV5 promoter. The T7 promoter is commonly used in all pET vectors and constitutes one of the strongest promoters reported. The combination of the promoters with an additional lac operon gives a very tight control of basal expression without addition of IPTG.[209] The tac promoter is used in the MBP-Int^{C}-Toxin constructs, which showed the highest protein yields. This emphasizes that promoter strength is not solely responsible for the good expression. All pET vectors encoding Int^{C}-X and Trx-Int^{C}-X vectors are controlled by a T7 promoter. Expression yields are nevertheless markedly different: Trx-Int^{C}-Toxin > Int^{C}-Trx >> Int^{C}-Toxin. The differences highlight that although similar plasmid backbones and the same strain were used other factors influenced expression a lot.

Beyond the specified regions like promoter and operator sequences, others may influence translation initiation, too. The sequence around the junction of vector and GOI depict a low GC content and a relaxed mRNA structure and differences can result in expression variations of 1000-fold.[223] A 50 bp stretch around the translation start in the MBP construct is characterized by a GC content of 38 %, while in the Int^{C}-X construct the GC content is 8 % higher. In the GOI the divergence in the first 25 bp is even higher with 36 % (MBP) and 64 % (Int^{C}) GC content. Additionally, it was detected that rare codons with A or T at the third position of each codon at the 5' coding region of genes (about 15 - 25 bp) decreases mRNA folding and thereby increases protein expression.[221,224] The MBP gene contained 6/7, the Trx gene 4/7 and the Int^{C} gene 0/7 initial codons with an A/T at the third position. This row correlates with the observed expression yields of the aforementioned constructs. Thus maximizing the folding energy, e.g. by computational tools such as EXENSO (Expression Enhancer Software), RBS CALCULATOR, RBS DESIGNER, UTR DESIGNER and EMOPEC migh result in a uniform high expression.[221]

Last but not least, several fusion tags are routinely used to increase solubility or as purification tag. Most fusion proteins in this study contained a *C*-terminal HA tag that is commonly used for immunostainings in WB or microscopy, followed by a His_6 tag for IMAC purification. Other small tags that have less than 10 aa are the Strep-II and FLAG tag, which both can be applied for purification. They often show a higher purity after a single purification step but are not as cost effective as the His_6 tag.[221] If purity is not achieved after the first step, a tandem His_6-calmodulin fusion tag can be applied, which combines IMAC and HIC that resulted in products with a purity of more than 97% pure after tag cleavage at a thrombin recognition site.[225] While small tags don't interfere much with recombinant protein structure and function, larger tags can be added to increase solubility and production yield. Such fusion tags are normally introduced at the *N*-terminus of cytoplasmic proteins and thereby provide a reliable context for efficient translation initiation.[226] Large fusion tags positively influence protein solubility and expression efficiency. Some of them are thioredoxin (Trx), small ubiquitin-like modifier (SUMO), glutathione S-transferase (GST) and maltose binding protein (MBP), with sizes from 100 to 495 aa.[209,221] MBP was

even found to possess an intrinsic chaperone activity[209]. Both Trx and MBP fusion proteins showed good production yields and solubility up to 200 μM or 9 mg/ml in this study. Thus a *N*-terminal fusion tag had the highest impact on heterologous expression compared to other mentioned factors. Although these tags are often cleaved off after purification to exclude effects on their biological function, this was not possible for MBP. Cleavage by TEV protease resulted in complete precipitation of the remaining Int^{C}-PE24 fragment while MBP stayed in solution. This was already reported and MBP could also affect the properties of the fusion protein.[227] Several exotoxin constructs have the inherent tendency to aggregate as shown in this study and as supported by the fact that all PE ITs of the Pastan group are produced as inclusion bodies.[107,112,119,228] The impact of the MBP tag on splicing efficacy could not be determined in this study because of the precipitation problem upon cleavage. However, up to 70 % of splicing product could be obtained which implies a rather small influence. Recently, an Fh8 tag system called Hitag with a size of only 8 kDa was reported as a robust fusion partner enabling both soluble protein production and the purification of several proteins rapidly and cost-effectively. Another benefit of this system is that the recombinant proteins maintained their solubility after tag removal.[226,229] This kind of fusion partner might be beneficial to further improve expression and purification of protein toxins.

5.2. Intein splicing as suitable method for protein ligation

Different protein conjugation strategies have been reported in previous years, ranging from enzymatic reactions using sortase A[147], microbial transglutaminase (mTG)[98] or SpyLigase[230]. Although sortase A has a high substrate specificity and has already been used to fuse the trastuzumab Fab fragment to gelonin to increase its potency[103], generally a high excess (10-20 fold) of the oligoglycine containing substrate is needed to drive the equilibrium reaction to the side of the desired product.[153] Microbial transglutaminase forms a stable isopeptide bond between the γ-carboxamide group of glutamine and the primary ε-amino group of lysine. Although mTG has been used successfully in the generation of ADCs[99] it shows to be highly promiscuous towards the acyl acceptor[164] and thus makes coupling of proteins with several superficial lysines a trial and error approach. Furthermore, it showed to have a substrate preference for glutamines in a special sequence and structural context that is currently little understood. While IgG1 antibodies have no acyl donor glutamine, they can be specifically conjugated with mTG after deglycosylation or by introduction of a glutamine containing tag.[171,173] In human growth hormone two of several available glutamines are addressed by mTG resulting in a heterogeneous reaction product.[174] The SpyTag/SpyCatcher technology proved to be highly specific with no or only a slight excess of one reaction partner over the other needed for a quantitative turnover to the final product. This method nevertheless has the disadvantage of significant peptide tags (23 aa) remaining in the product.[230,231]

Protein *trans*-splicing thus offers an advantageous combination of specificity, efficiency and speed without inserting large foreign sequences into the final construct. A PTS efficiency of up to 70 % was

achieved, which is fairly high considering the molecular sizes of both splicing partners of 150 and 90 kDa, respectively. In the original assay, the evolved M86 split intein showed up to 90 % splicing efficiency, which was performed with a 30 kDa Int^C protein and an Int^N peptide with less than 2 kDa.[194] Trastuzumab contained a shorter *C*-terminal linker of only 7 aa and glycine at the –1 position of the Int^N, which is favored for the M86 intein. The 7D9G antibody contained a longer linker of 15 aa, providing more flexibility, but had a serine at the –1 position, possibly decreasing PTS efficiency.[232] Thus, optimization of linker length and amino acids composition could further improve the splicing reaction. Interestingly it seemed that splicing at the *C*-terminus of the LC was at least as efficient as at the HC, if not better. Although characterization of the LC and LC/HC conjugates has not been performed here because of comparability to the VHH construct, this should definitively be performed in the future.

Increasing the equivalents of the toxin portion to the antibody could also help increasing the coupling efficiency, although protein solubility could be a limiting factor. Protein solubility of the Int^C containing splicing partner was also critical because inefficient splicing was observed for aggregated portions after concentrating the protein. Efficacy could be successfully increased by SEC purification of smaller aggregates or monomers, respectively. Both gelonin and PE24 showed significant portions of protein aggregates although to a different extent. Especially PE24 built clusters and purification inevitably led to a dramatic loss of protein quantity. Understanding the mechanism of aggregation and the most critical factors could provide more insights into solutions to circumvent this problem. Different models exist and most probably either a reversible association of the native monomer or aggregation of conformationally altered monomers is the reason for the observed aggregation here.[233] The unfolded nature of the Int^C fragment could additionally boost formation of irreversible aggregates of the toxin domains, especially when concentrations increase.[233] Alternatively, aggregation could also be initiated by binding of a monomer to the surface of the reaction vessel, like the cellulose membrane or the plastic surface of the centrifugal filter tubes.[233] Improvements could possibly be achieved by additives that increase protein solubility during concentration like mixtures of 50 mM arginine and glutamine, osmolytes like glycerol or trimethylamine N-oxide (TMAO) or non-ionic detergents like Tween 20.[212] The pH of the storage buffer differed over one unit from the calculated pI of both MBP-Int^C-Gelonin and MBP-Int^C-PE24, so charge related solubility should be given for both proteins.

Increasing the splicing efficacy by choosing a different split intein poses an alternative, as shown for the generation of bispecific antibodies by Han and coworkers in 2017.[186] They used a split *Npu* DnaE intein[234], which was reported to have extremely fast splicing kinetics and could achieve efficient conjugations of antibody scaffolds in the same size range as they were used here. Another engineered *Npu* DnaE split intein was used for direct labelling of antibodies in culture medium.[235] However, the much larger Int^N domain (123 amino acids compared to 11) might impact antibody production yields and stability and would have to be tested.

To this date, this study is the first to ever perform protein ligation reactions on a solid support in a non-covalent manner. There are reports demonstrating conjugations with small molecules but not with two or more protein partners.[195,236] This study showed that it is indeed possible to ligate 150 and 30 kDa proteins together with decent efficacies around 50 %. Several parameters need optimization, including volume ratio of toxin solution to protein A slurry, TCEP equivalents and toxin concentration. In this study a toxin/protein A slurry ration of 3:1 – 6:1 was typically used. This ratio, however, is also dependent on the maximum tolerated toxin concentration that still contains mainly monomers. The binding site of protein A to the Fc domain is located in the interface between C_H2 and C_H3 and binding to the agarose matrix might keep the HC *C*-terminus in close proximity of the beads, making it difficult for the large MBP fusion to attack. There could be an advantage of the LC conjugation because of the additional flexibility governed by the hinge region and the increased distance from the solid support. In both cases, the linker between the antibody and the Int^N fragment plays an important role. In general, linkers can be designed to be rigid (e.g. $(EAAAK)_n$) or flexible (e.g. $(GGGS)_n$) and to have defined lengths.[237] A flexible glycine serine linker was used in this study for all constructs, varying from 7 – 15 aa. While the *C*-termini of an IgG HC point away from the molecule, supporting the idea of using a rigid linker, the *C*-termini of the LC point to the inside of the molecule and thus reinforcing the idea of a flexible linker (see PDB: 1HZH).

5.3. Full-length immunotoxins possess high biological activity

To date, mostly antibody fragments have been linked to toxic proteins to target them to receptor expressing cells.[103,121,228,238] This was mainly driven by the fact that the complete immunotoxin can be produced in prokaryotes and can thus be generated in larger amounts. There are also reports that made use of toxins containing Fc binding domains from protein A or G, which proved to induce cell-specific toxicity when bound to a full antibody.[238,239] Nevertheless, this approach is useful only in screening campaigns and not for therapeutic purposes. Full-length antibodies have other advantages over antibody fragments such as an extended half-life in blood[34], low immunogenicity and increased stability mediated through the glycosylated Fc domain.[240] Additionally, an antibody is naturally bivalent and therefore in the position to trigger efficient cellular uptake through receptor clustering.[200,241] The VHH antibody format that was applied in this study may combine the benefits of both antibody fragments and conventional antibodies. The glycosylated Fc domain adds physicochemical stability and increases the serum half-life. The VHH construct has a simpler structure due to the lack of an additional light chain and retains a bivalent, or in this case, even tetravalent binding to its antigen, leading to an increased receptor-mediated uptake. This may also be the reason for an increased efficacy of the generated ITs in this study, compared to previously reported conjugates.

All produced *Pseudomonas* Exotoxin A conjugates were more potent than the most toxic PE IT reported to date, with an IC_{50} of 7D9G-PE24 of 0.8 pM on MDA-MB-468 cells being more potent by a factor of 24.[122] Although the toxic moiety is comparable in this case, different receptors were targeted and ITs were tested on different cell lines, which may account for some difference in efficacy. More comparability is given for the gelonin conjugates to trastuzumab that were tested on SK-BR-3 cells. The same combination was tested with a Fab-toxin conjugates in 2014 with an EC_{50} of 600 pM on the same cell line which is less potent by a factor of 50 compared to the tested full-length Trast-Gelonin in this study.[103] The endosomal escape mechanism may also play a role in the differences of toxicities between gelonin and PE24. For the latter, a defined escape mechanism *via* a retrograde ER transport has been described in detail,[242] while for gelonin no such mechanism is known. As a consequence, PE24 has the advantage over gelonin of an active transport mechanism that likely contributes to its remarkable potency. Still, IC_{50} values for gelonin are in the low picomolar range.

Contrary to the efficacy, gelonin displayed the higher selectivity. The effective ratio of the IT compared to the toxin alone was higher for both 7D9G and trastuzumab conjugates than the PE24 conjugates. Especially T4-Gelonin showed an extraordinary ER of 2.5×10^7, which emphasizes the increase in toxicity mediated by the specific cellular uptake induced by the antibody fraction of the IT. A number of cell lines negative for the growth receptors would need to be examined for unspecific binding and toxicity to assess the therapeutic windows. Unfortunately, unspecific binding was observed for the trastuzumab ITs, which could be confirmed in both cytotoxic and microscopic experiments. The reason for this phenomenon is unclear because neither gelonin nor the cytotoxic domain III of PE is reported to bind to cell surfaces. More detailed investigations could be performed to specify the type of interaction and potential interaction partners by immunoprecipitations with whole cell lysates or membrane fractions, using the toxins as capturing moiety.

An additional level of specificity may be gained by the protease cleavable linker. Since PE naturally contains a furin cleavable linker, it was used for both constructs. The consensus cleavage sequence of furin is defined as Arg–Leu–Pro–Arg–↓. Inclusion of furin-sensitive linkers in ITs containing ribotoxin[243], caspase-3 or granzyme B[244] and human active truncated Bid[245] has shown significant improvements in cytotoxicity compared with constructs containing stable linkers[237]. Opposing results were reported for a gelonin IT (C6.5-L-rGel), which was more efficient in tumor inhibition than constructs containing furin linkers that was attributed to a higher stability *in vivo*.[104] Furin is a universal protease and essential for survival, as loss of furin was shown to result in cardiac malformation and early postnatal death.[246] This study implies that furin is present in endothelial cells, where most of the recycling of antibodies by FcRn takes place. This recycling involves maturation of vesicles to acidified endosomes and furin might already cleave the toxic payload before recycling of the conjugate back to the extracellular space takes place. This would lead to systemic toxicity. However, this has not been reported for the new RG7787 IT

including the PE24 domain.[109] Nevertheless, shielding the furin cleavage site by designed disulfide bridges from excreted proteases in the blood stream or in the tumor microenvironment extended the serum half-life compared to an IT without the disulfide bond. Additionally it had the same anti-tumor activity, despite being less cytotoxic *in vitro*.[247]

Several proteases are reported to be overexpressed in certain cancers. Using their cleavage sequences would add another level of specificity towards tumor targeting. Some of them are urokinase plasminogen activator (uPA), cathepsin B and membrane-type matrix metalloproteinase (MMP). The selection is reduced by the criterion that the localization has to be endosomal, thus narrowing it down to cathepsins like cathepsin B, D and E.[248] They are already utilized by several ADCs that contain a valine-citrulline linker sequence. Not only the sequence containing the unnatural amino acid citrulline can be used. Genetically encoded sequences containing Phe-Leu, Val-Lys, Phe-Lys or combination sequences (FKFL) were reported to be effectively cleaved by cathepsin B.[249–251] A comparison between different cleavable linkers would be very interesting, especially in an *in vivo* setting, where active monitoring of pharmacokinetics and toxicity can be assessed.

5.4. Conclusions and outlook

In conclusion, highly potent immunotoxins were generated by applying protein *trans*-splicing with split inteins. This method is fast and yields site-specific conjugates with minimal changes to the native sequences. Since this is the first study to build full-length antibody-toxin conjugates by protein ligation, there is still a lot to be improved. However, even conjugates with a TAR of only 1.3 depicted extremely high *in vitro* cytotoxicity. The *in vivo* pharmacokinetic and –dynamic behavior is still unknown and would be very interesting to analyze. Compared to the classical ITs that are in clinical development, the full-length antibodies are expected to have a drastically increased serum half-life. PE24 ITs were designed to be less immunogenic than previous formats, which was confirmed in different studies and clinical trials.[30,109,119] Also gelonin is regarded as low immunogenic. Conjugation to a therapeutically and human antibody is not expected to boost immunogenicity and should thus not pose a problem. What might be problematic for solid tumors, is the large size of the generated ITs of 160 to 210 kDa (with a TAR of 2). Therefore, applications in hematological cancers should be considered first.

This platform is even compatible with bispecific antibodies. Recently, bispecific ADCs targeting c-MET and EGFR were reported to be highly specific and potent.[252] With this concept, receptors can be targeted, that would be activated by dimerization through binding of a bivalent antibody, as reported for c-MET.[253] Additionally, targeting two adjacent receptors with antibody fragments with lower affinity, the selectivity to co-expressing tumor cells is increased.[252,254] Attachment of the small Int^N tag to both heavy chains of a bispecific antibody would be easily achievable and could result in a new therapeutic principle.

6. Literature

(1) Tubbs, A., and Nussenzweig, A. (2017) Endogenous DNA Damage as a Source of Genomic Instability in Cancer. *Cell 168*, 644–656.

(2) Lindahl, T., and Barnes, D. E. (2000) Repair of endogenous DNA damage, in *Cold Spring Harbor Symposia on Quantitative Biology*, pp 127–133.

(3) Michor, F., Iwasa, Y., and Nowak, M. A. (2004) Dynamics of cancer progression. *Nat. Rev. Cancer 4*, 197–205.

(4) Hanahan, D., and Weinberg, R. A. (2011) Hallmarks of cancer: The next generation. *Cell 144*, 646–674.

(5) Gensini, G. F., Conti, A. A., and Lippi, D. (2007) The contributions of Paul Ehrlich to infectious disease. *J. Infect. 54*, 221–224.

(6) Goodman, L. S., Wintrobe, M. M., Dameshek, W., Goodman, M. J., Gilman, A., and Mclennan, M. T. (1946) Nitrogen mustard therapy: Use of Methyl-Bis(Beta-Chloroethyl)amine Hydrochloride and Tris(Beta-Chloroethyl)amine Hydrochloride for Hodgkin's Disease, Lymphosarcoma, Leukemia and Certain Allied and Miscellaneous Disorders. *J. Am. Med. Assoc. 132*, 126–132.

(7) Gilman, A., and Philips, F. S. (1946) The Biological Actions and Therapeutic Applications of the B-Chloroethyl Amines and Sulfides. *Science (80-.). 103*, 409–415.

(8) Heidelberger, C., Chaudhuri, N. K., Danneberg, P., Mooren, D., Griesbach, L., Duschinsky, R., Schnitzer, R. J., Pleven, E., and Scheiner, J. (1957) Fluorinated pyrimidines, a new class of tumour-inhibitory compounds. *Nature 179*, 663–666.

(9) Rosenberg, B., Van Camp, L., Trosko, J. E., and Mansour, V. H. (1969) Platinum compounds: a new class of potent antitumour agents. *Nature 222*, 385–386.

(10) Rosenberg, B., Van Camp, L., and Krigas, T. (1965) Inhibition of cell division in *Escherichia coli* by electrolysis products from a platinum electrode. *Nature 205*, 698–699.

(11) Druker, B. J., Tamura, S., Buchdunger, E., Ohno, S., Segal, G. M., Fanning, S., Zimmermann, J., and Lydon, N. B. (1996) Effects of a selective inhibitor of the Abl tyrosine kinase on the growth of Bcr–Abl positive cells. *Nat. Med. 2*, 561–566.

(12) Blum, G., Gazit, A., and Levitzki, A. (2000) Substrate competitive inhibitors of IGF-1 receptor kinase. *Biochemistry 39*, 15705–15712.

(13) Vassilev, L. T., Vu, B. T., Graves, B., Carvajal, D., Podlaski, F., Filipovic, Z., Kong, N., Kammlott, U., Lukacs, C., Klein, C., Fotouhi, N., and Liu, E. A. (2004) In Vivo Activation of the p53 Pathway by Small-Molecule Antagonists of MDM2. *Science (80-.). 303*, 844–848.

(14) Goossens, N., Nakagawa, S., Sun, X., Hoshida, Y., Program, L. C., and Cancer, T. (2015) Cancer biomarker discovery and validation. *HHS Public Acess 4*, 256–269.

(15) Murphy, K., Travers, P., and Walport, M. (2008) Janeway's Immunobiology 7th ed. Garland Science.

(16) Harding, F. a, Stickler, M. M., Razo, J., and DuBridge, R. B. (2010) The immunogenicity of humanized and fully human antibodies. *Landes Biosci. 2*, 256–265.

(17) Köhler, G., and Milstein, C. (1975) Continuous cultures of fused cells secreting antibody of predefined specificity. *Nature 256*, 495.

(18) Strebhardt, K., and Ullrich, A. (2008) Paul Ehrlich ' s magic bullet concept : 100 years of progress. *Nat. Rev. cancer 8*, 473–480.

(19) Chari, R. V. J., Miller, M. L., and Widdison, W. C. (2014) Antibody-drug conjugates: An emerging concept in cancer therapy. *Angew. Chemie - Int. Ed. 53*, 3796–3827.

(20) Junutula, J. R., Raab, H., Clark, S., Bhakta, S., Leipold, D. D., Weir, S., Chen, Y., Simpson, M., Tsai, S. P., Dennis, M. S., Lu, Y., Meng, Y. G., Ng, C., Yang, J., Lee, C. C., Duenas, E., Gorrell, J., Katta, V., Kim, A., McDorman, K., Flagella, K., Venook, R., Ross, S., Spencer, S. D., Lee Wong, W., Lowman, H. B., Vandlen, R., Sliwkowski, M. X., Scheller, R. H., Polakis, P., and Mallet, W. (2008) Site-specific conjugation of a cytotoxic drug to an antibody improves the therapeutic index. *Nat. Biotechnol. 26*, 925.

(21) Junutula, J. R., Flagella, K. M., Graham, R. A., Parsons, K. L., Ha, E., Raab, H., Bhakta, S., Nguyen, T., Dugger, D. L., Li, G., Mai, E., Lewis Phillips, G. D., Hiraragi, H., Fuji, R. N., Tibbitts, J., Vandlen, R., Spencer, S. D., Scheller, R. H., Polakis, P., and Sliwkowski, M. X. (2010) Engineered Thio-Trastuzumab-DM1 Conjugate with an Improved Therapeutic Index to Target Human Epidermal Growth Factor Receptor 2–Positive Breast Cancer. *Clin. Cancer Res. 16*, 4769 LP-4778.

(22) Younes, A., Gopal, A. K., Smith, S. E., Ansell, S. M., Rosenblatt, J. D., Savage, K. J., Ramchandren, R., Bartlett, N. L., Cheson, B. D., de Vos, S., Forero-Torres, A., Moskowitz, C. H., Connors, J. M., Engert, A., Larsen, E. K., Kennedy, D. A., Sievers, E. L., and Chen, R. (2012) Results of a Pivotal Phase II Study of Brentuximab Vedotin for Patients With Relapsed or Refractory Hodgkin's Lymphoma. *J. Clin. Oncol. 30*, 2183–2189.

(23) Younes, A., Bartlett, N. L., Leonard, J. P., Kennedy, D. A., Lynch, C. M., Sievers, E. L., and Forero-Torres, A. (2010) Brentuximab Vedotin (SGN-35) for Relapsed CD30-Positive Lymphomas. *N. Engl. J. Med. 363*, 1812–1821.

(24) Hurvitz, S. A., Dirix, L., Kocsis, J., Bianchi, G. V, Lu, J., Vinholes, J., Guardino, E., Song, C., Tong, B., Ng, V., Chu, Y.-W., and Perez, E. A. (2013) Phase II Randomized Study of Trastuzumab Emtansine Versus Trastuzumab Plus Docetaxel in Patients With Human Epidermal Growth Factor Receptor 2–Positive Metastatic Breast Cancer. *J. Clin. Oncol. 31*, 1157–1163.

(25) Burris, H. A., Rugo, H. S., Vukelja, S. J., Vogel, C. L., Borson, R. A., Limentani, S., Tan-Chiu, E., Krop, I. E., Michaelson, R. A., Girish, S., Amler, L., Zheng, M., Chu, Y.-W., Klencke, B., and O'Shaughnessy, J. A. (2011) Phase II Study of the Antibody Drug Conjugate Trastuzumab-DM1 for the Treatment of Human Epidermal Growth Factor Receptor 2 (HER2) –Positive Breast Cancer After Prior HER2-Directed Therapy. *J. Clin. Oncol. 29*, 398–405.

(26) Thorpe, P. E., Ross, W. C. J., Cumber, A. J., Hinson, C. A., Edwards, D. C., and Davies, A. J. S. (1978) Toxicity of diphtheria toxin for lymphoblastoid cells is increased by conjugation to antilymphocytic globulin. *Nature 271*, 752–755.

(27) Blythman, H. E., Casellas, P., Gros, O., Gros, P., Jansen, F. K., Paolucci, F., Pau, B., and Vidal, H. (1981) Immunotoxins: hybrid molecules of monoclonal antibodies and a toxin subunit specifically kill tumour cells. *Nature 290*, 145–146.

(28) Antignani, A., and FitzGerald, D. (2013) Immunotoxins: The role of the toxin. *Toxins (Basel). 5*, 1486–1502.

(29) Rust, A., Partridge, L., Davletov, B., and Hautbergue, G. (2017) The Use of Plant-Derived Ribosome Inactivating Proteins in Immunotoxin Development: Past, Present and Future Generations. *Toxins (Basel). 9*, 344.

(30) Mazor, R., Onda, M., Park, D., Addissie, S., Xiang, L., Zhang, J., Hassan, R., and Pastan, I. (2016) Dual B- and T-cell de-immunization of recombinant immunotoxin targeting mesothelin with high cytotoxic activity. *Oncotarget 7*, 29916–29926.

(31) Parkin, J., and Cohen, B. (2001) An overview of the immune system. *Lancet 357*, 1777–1789.

(32) Thomas, A., Teicher, B. A., and Hassan, R. (2016) Antibody–drug conjugates for cancer therapy. *Lancet Oncol. 17*, e254–e262.

(33) Schroeder, H. W., and Cavacini, L. (2010) Structure and function of immunoglobulins. *J. Allergy Clin. Immunol. 125*, S41-52.

(34) Roopenian, D. C., and Akilesh, S. (2007) FcRn: The neonatal Fc receptor comes of age. *Nat. Rev. Immunol. 7*, 715–725.

(35) Kim, J. K., Firan, M., Radu, C. G., Kim, C. H., Ghetie, V., and Ward, E. S. (1999) Mapping the site on human IgG for binding of the MHC class I-related receptor, FcRn. *Eur. J. Immunol. 29*, 2819–25.

(36) Jefferis, R. (2009) Glycosylation as a strategy to improve antibody-based therapeutics. *Nat. Rev. Drug Discov.*

(37) Raju, T. S., and Scallon, B. (2007) Fc glycans terminated with N-acetylglucosamine residues increase antibody resistance to papain. *Biotechnol. Prog. 23*, 964–971.

(38) Seidel, U. J. E., Schlegel, P., and Lang, P. (2013) Natural killer cell mediated antibody-dependent cellular cytotoxicity in tumor immunotherapy with therapeutic antibodies. *Front. Immunol. 4*, 1–8.

(39) Rogers, L. M., Veeramani, S., and Weiner, G. J. (2014) Complement in Monoclonal Antibody Therapy of Cancer. *Immunol. Res. 59*, 203–210.

(40) Ravetch, J. V, and Bolland, S. (2001) IgG Fc Receptors. *Annu. Rev. Immunol 19*, 275–90.

(41) Nimmerjahn, F., and Ravetch, J. V. (2006) Fcγ receptors: Old friends and new family members. *Immunity 24*, 19–28.

(42) Sibéril, S., Dutertre, C. A., Boix, C., Bonnin, E., Ménez, R., Stura, E., Jorieux, S., Fridman, W. H., and Teillaud, J. L. (2006) Molecular aspects of human FcγR interactions with IgG: Functional and therapeutic consequences. *Immunol. Lett.*

(43) Sulica, A., Morel, R., Metes, D., and Herberman, R. B. (2001) Ig-binding Receptors on Human NK Cells as Effector and Regulatory Surface Molecules. *Int. Rev. Immunol. 20*, 371–414.

(44) Kuo, T. T., and Aveson, V. G. (2011) Neonatal Fc receptor and IgG-based therapeutics. *MAbs*.

(45) Sgro, C. (1995) Side-effects of a monoclonal antibody, muromonab CD3/orthoclone OKT3: bibliographic review. *Toxicology*.

(46) Tsurushita, N., Hinton, P. R., and Kumar, S. (2005) Design of humanized antibodies: From anti-Tac to Zenapax. *Methods 36*, 69–83.

(47) Chiu, M. L., and Gilliland, G. L. (2016) Engineering antibody therapeutics. *Curr. Opin. Struct. Biol. 38*, 163–173.

(48) Hudis, C. A. (2007) Trastuzumab — Mechanism of Action and Use in Clinical Practice. *N. Engl. J. Med. 357*, 39–51.

(49) Van Cutsem, E., Köhne, C.-H., Hitre, E., Zaluski, J., Chang Chien, C.-R., Makhson, A., D'Haens, G., Pintér, T., Lim, R., Bodoky, G., Roh, J. K., Folprecht, G., Ruff, P., Stroh, C., Tejpar, S., Schlichting, M., Nippgen, J., and Rougier, P. (2009) Cetuximab and chemotherapy as initial treatment for metastatic colorectal cancer. *N. Engl. J. Med. 360*, 1408–17.

(50) Weiner, G. J. (2010) Rituximab: Mechanism of action. *Semin. Hematol. 47*, 115–123.

(51) Diebolder, C. A., Beurskens, F. J., De Jong, R. N., Koning, R. I., Strumane, K., Lindorfer, M. A., Voorhorst, M., Ugurlar, D., Rosati, S., Heck, A. J. R., Van De Winkel, J. G. J., Wilson, I. A., Koster, A. J., Taylor, R. P., Saphire, E. O., Burton, D. R., Schuurman, J., Gros, P., and Parren, P. W. H. I. (2014) Complement is activated by IgG hexamers assembled at the cell surface. *Science (80-.). 343*, 1260–1263.

(52) Scott, A. M., Wolchok, J. D., and Old, L. J. (2012) Antibody therapy of cancer. *Nat. Rev. Cancer 12*, 278–287.

(53) Ribas, A., and Wolchok, J. D. (2018) Cancer immunotherapy using checkpoint blockade. *Science 359*, 1350–1355.

(54) Wolchok, J. D., Chiarion-Sileni, V., Gonzalez, R., Rutkowski, P., Grob, J.-J., Cowey, C. L., Lao, C. D., Wagstaff, J., Schadendorf, D., Ferrucci, P. F., Smylie, M., Dummer, R., Hill, A., Hogg, D., Haanen, J.,

Carlino, M. S., Bechter, O., Maio, M., Marquez-Rodas, I., Guidoboni, M., McArthur, G., Lebbé, C., Ascierto, P. A., Long, G. V, Cebon, J., Sosman, J., Postow, M. A., Callahan, M. K., Walker, D., Rollin, L., Bhore, R., Hodi, F. S., and Larkin, J. (2017) Overall Survival with Combined Nivolumab and Ipilimumab in Advanced Melanoma. *N. Engl. J. Med. 377*, 1345–1356.

(55) Robert, C., Schachter, J., Long, G. V, Arance, A., Grob, J. J., Mortier, L., Daud, A., Carlino, M. S., McNeil, C., Lotem, M., Larkin, J., Lorigan, P., Neyns, B., Blank, C. U., Hamid, O., Mateus, C., Shapira-Frommer, R., Kosh, M., Zhou, H., Ibrahim, N., Ebbinghaus, S., and Ribas, A. (2015) Pembrolizumab versus Ipilimumab in Advanced Melanoma. *N. Engl. J. Med. 372*, 2521–2532.

(56) Shuptrine, C. W., Surana, R., and Weiner, L. M. (2012) Monoclonal antibodies for the treatment of cancer. *Semin. Cancer Biol. 22*, 3–13.

(57) Skerra, A. (2007) Alternative non-antibody scaffolds for molecular recognition. *Curr. Opin. Biotechnol.*

(58) Stanfield, R. L., Dooley, H., Flajnik, M. F., and Wilson, I. A. (2004) Crystal structure of a shark single-domain antibody V region in complex with lysozyme. *Science (80-.). 305*, 1770–1773.

(59) Zielonka, S., Empting, M., Grzeschik, J., Könning, D., Barelle, C. J., and Kolmar, H. (2015) Structural insights and biomedical potential of IgNAR scaffolds from sharks. *MAbs 7*, 15–25.

(60) Stanfield, R. L., Dooley, H., Verdino, P., Flajnik, M. F., and Wilson, I. A. (2007) Maturation of Shark Single-domain (IgNAR) Antibodies: Evidence for Induced-fit Binding. *J. Mol. Biol. 367*, 358–372.

(61) Müller, M. R., Saunders, K., Grace, C., Jin, M., Piche-Nicholas, N., Steven, J., O'Dwyer, R., Wu, L., Khetemenee, L., Vugmeyster, Y., Hickling, T. P., Tchistiakova, L., Olland, S., Gill, D., Jensen, A., and Barelle, C. J. (2012) Improving the pharmacokinetic properties of biologics by fusion to an anti-HSA shark VNAR domain. *MAbs 4*, 673–685.

(62) Kovaleva, M., Ferguson, L., Steven, J., Porter, a., and Barelle, C. (2014) Shark variable new antigen receptor biologics - a novel technology platform for therapeutic drug development. *Expert Opin. Biol. Ther. 14*, 1527–1539.

(63) Alt, M., Müller, R., and Kontermann, R. E. (1999) Novel tetravalent and bispecific IgG-like antibody molecules combining single-chain diabodies with the immunoglobulin γ1 Fc or CH3 region. *FEBS Lett. 454*, 90–94.

(64) Kovalenko, O. V., Olland, A., Piché-Nicholas, N., Godbole, A., King, D., Svenson, K., Calabro, V., Müller, M. R., Barelle, C. J., Somers, W., Gill, D. S., Mosyak, L., and Tchistiakova, L. (2013) Atypical antigen recognition mode of a shark Immunoglobulin New Antigen Receptor (IgNAR) variable domain characterized by humanization and structural analysis. *J. Biol. Chem. 288*, 17408–17419.

(65) Uth, C., Zielonka, S., Hörner, S., Rasche, N., Plog, A., Orelma, H., Avrutina, O., Zhang, K., and Kolmar, H. (2014) A chemoenzymatic approach to protein immobilization onto crystalline cellulose nanoscaffolds. *Angew. Chemie - Int. Ed. 53*, 12618–12623.

(66) Hamers-Casterman, C., Atarhouch, T., Muyldermans, S., Robinson, G., Hammers, C., Songa, E. B., Bendahman, N., and Hammers, R. (1993) Naturally occurring antibodies devoid of light chains. *Nature 363*, 446–448.

(67) Muyldermans, S. (2013) Nanobodies: Natural Single-Domain Antibodies. *Annu. Rev. Biochem. 82*, 775–797.

(68) De Genst, E., Silence, K., Decanniere, K., Conrath, K., Loris, R., Kinne, J., Muyldermans, S., and Wyns, L. (2006) Molecular basis for the preferential cleft recognition by dromedary heavy-chain antibodies. *Proc. Natl. Acad. Sci. 103*, 4586–4591.

(69) Desmyter, A., Transue, T. R., Ghahroudi, M. A., Thi, M. H. D., Poortmans, F., Hamers, R., Muyldermans, S., and Wyns, L. (1996) Crystal structure of a camel single-domain V(H) antibody fragment in complex with lysozyme. *Nat. Struct. Biol. 3*, 803–811.

(70) Govaert, J., Pellis, M., Deschacht, N., Vincke, C., Conrath, K., Muyldermans, S., and Saerens, D. (2012) Dual beneficial effect of interloop disulfide bond for single domain antibody fragments. *J. Biol. Chem. 287*, 1970–1979.

(71) Akazawa-Ogawa, Y., Takashima, M., Lee, Y. H., Ikegami, T., Goto, Y., Uegaki, K., and Hagihara, Y. (2014) Heat-induced irreversible denaturation of the camelid single domain vhh antibody is governed by chemical modifications. *J. Biol. Chem. 289*, 15666–15679.

(72) Ewert, S., Cambillau, C., Conrath, K., and Plückthun, A. (2002) Biophysical properties of camelid VHH domains compared to those of human VH3 domains. *Biochemistry 41*, 3628–3636.

(73) Revets, H., De Baetselier, P., and Muyldermans, S. (2005) Nanobodies as novel agents for cancer therapy. *Expert Opin. Biol. Ther. 5*, 111–124.

(74) Goldman, E. R., Andersen, G. P., Liu, J. L., Delehanty, J. B., Sherwood, L. J., Osborn, L. E., Cummins, L. B., and Hayhurst, A. (2006) Facile generation of heat-stable antiviral and antitoxin single domain antibodies from a semisynthetic llama library. *Anal. Chem. 78*, 8245–8255.

(75) Monegal, A., Ami, D., Martinelli, C., Huang, H., Aliprandi, M., Capasso, P., Francavilla, C., Ossolengo, G., and De Marco, A. (2009) Immunological applications of single-domain llama recombinant antibodies isolated from a naïve library. *Protein Eng. Des. Sel. 22*, 273–280.

(76) Wesolowski, J., Alzogaray, V., Reyelt, J., Unger, M., Juarez, K., Urrutia, M., Cauerhff, A., Danquah, W., Rissiek, B., Scheuplein, F., Schwarz, N., Adriouch, S., Boyer, O., Seman, M., Licea, A., Serreze, D. V., Goldbaum, F. a., Haag, F., and Koch-Nolte, F. (2009) Single domain antibodies: Promising experimental and therapeutic tools in infection and immunity. *Med. Microbiol. Immunol. 198*, 157–174.

(77) De Meyer, T., Muyldermans, S., and Depicker, A. (2014) Nanobody-based products as research and diagnostic tools. *Trends Biotechnol. 32*, 263–270.

(78) Smolarek, D., Bertrand, O., and Czerwinski, M. (2012) Variable fragments of heavy chain antibodies (VHHs): A new magic bullet molecule of medicine? *Postepy Hig. Med. Dosw. 66*, 348–358.

(79) Van Audenhove, I., and Gettemans, J. (2016) Nanobodies as Versatile Tools to Understand, Diagnose, Visualize and Treat Cancer. *EBioMedicine 8*, 40–48.

(80) Roovers, R. C., Vosjan, M. J. W. D., Laeremans, T., El Khoulati, R., De Bruin, R. C. G., Ferguson, K. M., Verkleij, A. J., Van Dongen, G. a M. S., and Van Bergen En Henegouwen, P. M. P. (2011) A biparatopic anti-EGFR nanobody efficiently inhibits solid tumour growth. *Int. J. Cancer 129*, 2013–2024.

(81) Frei, E. (1972) Combination Cancer Therapy: Presidential Address. *Cancer Res. 32*, 2593 LP-2607.

(82) Solal-Céligny, P. (2006) Safety of rituximab maintenance therapy in follicular lymphomas. *Leuk. Res. 30*, S16–S21.

(83) Orth, J. D., Krueger, E. W., Weller, S. G., and McNiven, M. A. (2006) A novel endocytic mechanism of epidermal growth factor receptor sequestration and internalization. *Cancer Res. 66*, 3603–3610.

(84) Owen, S. C., Patel, N., Logie, J., Pan, G., Persson, H., Moffat, J., Sidhu, S. S., and Shoichet, M. S. (2013) Targeting HER2 + breast cancer cells: Lysosomal accumulation of anti-HER2 antibodies is influenced by antibody binding site and conjugation to polymeric nanoparticles. *J. Control. Release 172*, 395–404.

(85) Panowski, S., Bhakta, S., Raab, H., Polakis, P., and Junutula, J. R. (2014) Site-specific antibody drug conjugates for cancer therapy. *MAbs 6*, 34–45.

(86) Lewis Phillips, G. D., Li, G., Dugger, D. L., Crocker, L. M., Parsons, K. L., Mai, E., Blättler, W. A., Lambert, J. M., Chari, R. V. J., Lutz, R. J., Wong, W. L. T., Jacobson, F. S., Koeppen, H., Schwall, R. H., Kenkare-Mitra, S. R., Spencer, S. D., and Sliwkowski, M. X. (2008) Targeting HER2-positive breast cancer with trastuzumab-DM1, an antibody-cytotoxic drug conjugate. *Cancer Res. 68*, 9280–9290.

(87) Perez, H. L., Cardarelli, P. M., Deshpande, S., Gangwar, S., Schroeder, G. M., Vite, G. D., and

Borzilleri, R. M. (2014) Antibody-drug conjugates: Current status and future directions. *Drug Discov. Today 19*, 869–881.

(88) Scotti, C., Iamele, L., and Vecchia, L. (2015) Antibody–drug conjugates: targeted weapons against cancer. *Antib. Technol. J.* 1–13.

(89) Remillard, S., Rebhun, L., Howie, G., and Kupchan, S. (1975) Antimitotic activity of the potent tumor inhibitor maytansine. *Science (80-.). 189*, 1002–5.

(90) Elgersma, R. C., Coumans, R. G. E., Huijbregts, T., Menge, W. M. P. B., Joosten, J. A. F., Spijker, H. J., De Groot, F. M. H., Van Der Lee, M. M. C., Ubink, R., Van Den Dobbelsteen, D. J., Egging, D. F., Dokter, W. H. A., Verheijden, G. F. M., Lemmens, J. M., Timmers, C. M., and Beusker, P. H. (2015) Design, synthesis, and evaluation of linker-duocarmycin payloads: Toward selection of HER2-targeting antibody-drug conjugate SYD985. *Mol. Pharm. 12*, 1813–1835.

(91) Doronina, S. O., Toki, B. E., Torgov, M. Y., Mendelsohn, B. a, Cerveny, C. G., Chace, D. F., DeBlanc, R. L., Gearing, R. P., Bovee, T. D., Siegall, C. B., Francisco, J. a, Wahl, A. F., Meyer, D. L., and Senter, P. D. (2003) Development of potent monoclonal antibody auristatin conjugates for cancer therapy. *Nat. Biotech. 21*, 778–784.

(92) Lencer, W. I., and Blumberg, R. S. (2005) A passionate kiss, then run: Exocytosis and recycling of IgG by FcRn. *Trends Cell Biol.*

(93) Zhu, Z., Ramakrishnan, B., Li, J., Wang, Y., Feng, Y., Prabakaran, P., Colantonio, S., Dyba, M. A., Qasba, P. K., and Dimitrov, D. S. (2014) Site-specific antibody-drug conjugation through an engineered glycotransferase and a chemically reactive sugar. *MAbs 6*, 1190–1200.

(94) Kim, M. T., Chen, Y., Marhoul, J., and Jacobson, F. (2014) Statistical modeling of the drug load distribution on trastuzumab emtansine (Kadcyla), a lysine-linked antibody drug conjugate. *Bioconjug. Chem. 25*, 1223–1232.

(95) Lazar, A. C., Wang, L., Blä, W. A., Amphlett, G., Lambert, J. M., and Zhang, W. (2005) Analysis of the composition of immunoconjugates using size-exclusion chromatography coupled to mass spectrometry. *RAPID Commun. MASS Spectrom. Rapid Commun. Mass Spectrom 19*, 1806–1814.

(96) Boylan, N. J., Zhou, W., Proos, R. J., Tolbert, T. J., Wolfe, J. L., and Laurence, J. S. (2013) Conjugation site heterogeneity causes variable electrostatic properties in Fc conjugates. *Bioconjug. Chem. 24*, 1008–1016.

(97) Junutula, J. R., Bhakta, S., Raab, H., Ervin, K. E., Eigenbrot, C., Vandlen, R., Scheller, R. H., and Lowman, H. B. (2008) Rapid identification of reactive cysteine residues for site-specific labeling of antibody-Fabs. *J. Immunol. Methods 332*, 41–52.

(98) Strop, P. (2014) Versatility of microbial transglutaminase. *Bioconjug. Chem. 25*, 855–862.

(99) Dennler, P., Chiotellis, A., Fischer, E., Brégeon, D., Belmant, C., Gauthier, L., Lhospice, F., Romagne, F., and Schibli, R. (2014) Transglutaminase-Based Chemo-Enzymatic Conjugation Approach Yields Homogeneous Antibody–Drug Conjugates. *Bioconjug. Chem. 25*, 569–578.

(100) Beerli, R. R., Hell, T., Merkel, A. S., and Grawunder, U. (2015) Sortase enzyme-mediated generation of site-specifically conjugated antibody drug conjugates with high In Vitro and In Vivo potency. *PLoS One 10*.

(101) Alewine, C., Hassan, R., and Pastan, I. (2015) Advances in Anticancer Immunotoxin Therapy. *Oncologist 20*, 176–185.

(102) Shin, M. C., Min, K. A., Cheong, H., Moon, C., Huang, Y., He, H., and Yang, V. C. (2016) Preparation and Characterization of Gelonin-Melittin Fusion Biotoxin for Synergistically Enhanced Anti-Tumor Activity. *Pharm. Res. 33*, 2218–2228.

(103) Kornberger, P., and Skerra, A. (2014) Sortase-catalyzed in vitro functionalization of a HER2-

specific recombinant Fab for tumor targeting of the plant cytotoxin gelonin. *MAbs 6*, 354–366.

(104) Cao, Y., Marks, J. D., Marks, J. W., Cheung, L. H., Kim, S., and Rosenblum, M. G. (2009) Construction and characterization of novel, recombinant immunotoxins targeting the Her2/neu oncogene product: In vitro and in vivo studies. *Cancer Res. 69*, 8987–8995.

(105) Weldon, J. E., and Pastan, I. (2011) A guide to taming a toxin - Recombinant immunotoxins constructed from Pseudomonas exotoxin A for the treatment of cancer. *FEBS J. 278*, 4683–4700.

(106) Allahyari, H., Heidari, S., Ghamgosha, M., Saffarian, P., and Amani, J. (2017) Immunotoxin: A new tool for cancer therapy. *Tumor Biol. 39*, 101042831769222.

(107) Song, S., Xue, J., Fan, K., Kou, G., Zhou, Q., Wang, H., and Guo, Y. (2005) Preparation and characterization of fusion protein truncated Pseudomonas Exotoxin A (PE38KDEL) in Escherichia coli. *Protein Expr. Purif. 44*, 52–57.

(108) ClinicalTrials.gov. (2011) SS1P and Pentostatin Plus Cyclophosphamide for Mesothelioma; Identifier NCT01362790; *Identifier NCT01362790*.

(109) ClinicalTrials.gov. (2016) Mesothelin-Targeted Immunotoxin LMB-100 in People With Malignant Mesothelioma; Identifier NCT02798536; *Identifier NCT02798536*.

(110) Domenighini, M., and Rappuoli, R. (1996) Three conserved consensus sequences identify the NAD-binding site of ADP-ribosylating enzymes, expressed by eukaryotes, bacteria and T-even bacteriophages. *Mol. Microbiol. 21*, 667–74.

(111) Michalska, M., and Wolf, P. (2015) Pseudomonas Exotoxin A: Optimized by evolution for effective killing. *Front. Microbiol. 6*, 1–7.

(112) Siegall, C. B., Chaudhary, V. K., FitzGerald, D. J., and Pastan, I. (1989) Functional analysis of domains II, Ib, and III of Pseudomonas exotoxin. *J. Biol. Chem. 264*, 14256–14261.

(113) El Hage, T., Lorin, S., Decottignies, P., Djavaheri-Mergny, M., and Authier, F. (2010) Proteolysis of Pseudomonas exotoxin A within hepatic endosomes by cathepsins B and D produces fragments displaying in vitro ADP-ribosylating and apoptotic effects. *FEBS J. 277*, 3735–3749.

(114) Decker, T., Oelsner, M., Kreitman, R. J., Salvatore, G., Wang, Q. C., Pastan, I., Peschel, C., and Licht, T. (2004) Induction of caspase-dependent programmed cell death in B-cell chronic lymphocytic leukemia by anti-CD22 immunotoxins. *Blood 103*, 2718–2726.

(115) Zhang, L., Zhao, J., Wang, T., Yu, C.-J., Jia, L.-T., Duan, Y.-Y., Yao, L.-B., Chen, S.-Y., and Yang, A.-G. (2008) HER2-targeting recombinant protein with truncated pseudomonas exotoxin A translocation domain efficiently kills breast cancer cells. *Cancer Biol. Ther. 7*, 1226–31.

(116) Prior, T. I., Kunwar, S., and Pastan, I. (1996) Studies on the activity of barnase toxins in vitro and in vivo. *Bioconjug. Chem. 7*, 23–29.

(117) Taupiac, M. P., Bébien, M., Alami, M., and Beaumelle, B. (1999) A deletion within the translocation domain of Pseudomonas exotoxin A enhances translocation efficiency and cytotoxicity concomitantly. *Mol. Microbiol. 31*, 1385–93.

(118) Morlon-Guyot, J., Mere, J., Bonhoure, A., and Beaumelle, B. (2009) Processing of Pseudomonas aeruginosa Exotoxin A Is Dispensable for Cell Intoxication. *Infect. Immun. 77*, 3090–3099.

(119) Bauss, F., Lechmann, M., Krippendorff, B. F., Staack, R., Herting, F., Festag, M., Imhof-Jung, S., Hesse, F., Pompiati, M., Kollmorgen, G., da Silva Mateus Seidl, R., Bossenmaier, B., Lau, W., Schantz, C., Stracke, J. O., Brinkmann, U., Onda, M., Pastan, I., Bosslet, K., and Niederfellner, G. (2016) Characterization of a re-engineered, mesothelin-targeted Pseudomonas exotoxin fusion protein for lung cancer therapy. *Mol. Oncol. 10*, 1317–1329.

(120) Onda, M., Beers, R., Xiang, L., Lee, B., Weldon, J. E., Kreitman, R. J., and Pastan, I. (2011) Recombinant immunotoxin against B-cell malignancies with no immunogenicity in mice by removal of

B-cell epitopes. *Proc. Natl. Acad. Sci. 108*, 5742–5747.

(121) Weldon, J. E., Xiang, L., Zhang, J., Beers, R., Walker, D. A., Onda, M., Hassan, R., and Pastan, I. (2013) A Recombinant Immunotoxin against the Tumor-Associated Antigen Mesothelin Reengineered for High Activity, Low Off-Target Toxicity, and Reduced Antigenicity. *Mol. Cancer Ther. 12*, 48–57.

(122) Hollevoet, K., Mason-Osann, E., Liu, X. -f., Imhof-Jung, S., Niederfellner, G., and Pastan, I. (2014) In Vitro and In Vivo Activity of the Low-Immunogenic Antimesothelin Immunotoxin RG7787 in Pancreatic Cancer. *Mol. Cancer Ther. 13*, 2040–2049.

(123) Stirpe, F., Olsnes, S., and Pihl, A. (1980) Gelonin , a New Inhibitor of Protein Synthesis , Nontoxic to Intact Cells. *J. Biol. Chem. 255*, 6947–6953.

(124) Madan, S., and Ghosh, P. C. (1992) Interaction of gelonin with macrophages: Effect of lysosomotropic amines. *Exp. Cell Res. 198*, 52–58.

(125) Rosenblum, M. G., Marks, J. W., and Cheung, L. H. (1999) Comparative cytotoxicity and pharmacokinetics of antimelanoma immunotoxins containing either natural or recombinant gelonin. *Cancer Chemother. Pharmacol. 44*, 343–348.

(126) Barbieri, L., Valbonesi, P., Bonora, E., Gorini, P., Bolognesi, A., and Stirpe, F. (1997) Polynucleotide:adenosine glycosidase activity of ribosome-inactivating proteins: Effect on DNA, RNA and poly(A). *Nucleic Acids Res. 25*, 518–522.

(127) Das, M. K., Sharma, R. S., and Mishra, V. (2012) Induction of apoptosis by ribosome inactivating proteins: Importance of N-glycosidase activity. *Appl. Biochem. Biotechnol.*

(128) Pirie, C. M., Hackel, B. J., Rosenblum, M. G., and Wittrup, K. D. (2011) Convergent potency of internalized gelonin immunotoxins across varied cell lines, antigens, and targeting moieties. *J. Biol. Chem. 286*, 4165–4172.

(129) Yang, N. J., Liu, D. V., Sklaviadis, D., Gui, D. Y., Vander Heiden, M. G., and Wittrup, K. D. (2015) Antibody-mediated neutralization of perfringolysin o for intracellular protein delivery. *Mol. Pharm. 12*, 1992–2000.

(130) Selbo, P. K., Sandvig, K., Kirveliene, V., and Berg, K. (2000) Release of gelonin from endosomes and lysosomes to cytosol by photochemical internalization. *Biochim. Biophys. Acta - Gen. Subj. 1475*, 307–313.

(131) Pirie, C. M., Liu, D. V, and Wittrup, K. D. (2013) Targeted cytolysins synergistically potentiate cytoplasmic delivery of gelonin immunotoxin. *Mol. Cancer Ther. 12*, 1774–82.

(132) Thorpe, P. E., Brown, A. N. F., Ross, W. C. J., Cumber, A. J., Detre, S. I., Edwards, D. C., Davies, A. J. S., and Stirpe, F. (1981) Cytotoxicity Acquired by Conjugation of an Anti-Thy1.1 Monoclonal Antibody and the Ribosome-Inactivating Protein, Gelonin. *Eur. J. Biochem. 116*, 447–454.

(133) Berg, K., Nordstrand, S., Selbo, P. K., Tran, D. T. T., Angell-Petersen, E., and Høgset, A. (2011) Disulfonated tetraphenyl chlorin (TPCS2a), a novel photosensitizer developed for clinical utilization of photochemical internalization. *Photochem. Photobiol. Sci. 10*, 1637–1651.

(134) Berstad, M. B., Cheung, L. H., Berg, K., Peng, Q., Fremstedal, a S. V, Patzke, S., Rosenblum, M. G., and Weyergang, a. (2015) Design of an EGFR-targeting toxin for photochemical delivery: in vitro and in vivo selectivity and efficacy. *Oncogene* 1–11.

(135) Fuchs, H., Weng, A., and Gilabert-Oriol, R. (2016) Augmenting the Efficacy of Immunotoxins and Other Targeted Protein Toxins by Endosomal Escape Enhancers. *Toxins (Basel). 8*, 200.

(136) Fuchs, H., Niesler, N., Trautner, A., Sama, S., Jerz, G., Panjideh, H., and Weng, A. (2017) Glycosylated Triterpenoids as Endosomal Escape Enhancers in Targeted Tumor Therapies. *Biomedicines 5*, 14.

(137) Kerr, D. E., Wu, G. Y., Wu, C. H., and Senter, P. D. (1997) Listeriolysin O potentiates immunotoxin

and bleomycin cytotoxicity. *Bioconjug. Chem. 8*, 781–784.

(138) Shin, M. C., Zhang, J., David, A. E., Trommer, W. E., Kwon, Y. M., Min, K. A., Kim, J. H., and Yang, V. C. (2013) Chemically and biologically synthesized CPP-modified gelonin for enhanced anti-tumor activity. *J. Control. Release 172*, 169–178.

(139) Pagliaro, L. C., Liu, B., Munker, R., Andreeff, M., Freireich, E. J., Scheinberg, D. A., and Rosenblum, M. G. (1998) Humanized M195 monoclonal antibody conjugated to recombinant gelonin: An anti-CD33 immunotoxin with antileukemic activity. *Clin. Cancer Res. 4*, 1971–1976.

(140) Zhou, H., Marks, J. W., Hittelman, W. N., Yagita, H., Cheung, L. H., Rosenblum, M. G., and Winkles, J. A. (2011) Development and Characterization of a Potent Immunoconjugate Targeting the Fn14 Receptor on Solid Tumor Cells. *Mol. Cancer Ther. 10*, 1276–1288.

(141) Zhou, H., Ekmekcioglu, S., Marks, J. W., Mohamedali, K. A., Asrani, K., Phillips, K. K., Brown, S. A. N., Cheng, E., Weiss, M. B., Hittelman, W. N., Tran, N. L., Yagita, H., Winkles, J. A., and Rosenblum, M. G. (2013) The TWEAK receptor Fn14 is a therapeutic target in melanoma: Immunotoxins targeting Fn14 receptor for malignant melanoma treatment. *J. Invest. Dermatol. 133*, 1052–1062.

(142) Zhou, H., Hittelman, W. N., Yagita, H., Cheung, L. H., Martin, S. S., Winkles, J. A., and Rosenblum, M. G. (2013) Antitumor activity of a humanized, bivalent immunotoxin targeting Fn14-positive solid tumors. *Cancer Res. 73*, 4439–4450.

(143) Tsukiji, S., and Nagamune, T. (2009) Sortase-mediated ligation: A gift from gram-positive bacteria to protein engineering. *ChemBioChem*.

(144) Ton-That, H., Liu, G., Mazmanian, S. K., Faull, K. F., and Schneewind, O. (1999) Purification and characterization of sortase, the transpeptidase that cleaves surface proteins of Staphylococcus aureus at the LPXTG motif. *Proc. Natl. Acad. Sci. 96*, 12424–12429.

(145) Chen, I., Dorr, B. M., and Liu, D. R. (2011) A general strategy for the evolution of bond-forming enzymes using yeast display. *Proc. Natl. Acad. Sci. U. S. A. 108*, 11399–11404.

(146) Dorr, B. M., Ham, H. O., An, C., Chaikof, E. L., and Liu, D. R. (2014) Reprogramming the specificity of sortase enzymes. *Proc. Natl. Acad. Sci. 111*, 13343–13348.

(147) Schmohl, L., and Schwarzer, D. (2014) Sortase-mediated ligations for the site-specific modification of proteins. *Curr. Opin. Chem. Biol. 22*, 122–128.

(148) Popp, M. W.-L., and Ploegh, H. L. (2011) Making and Breaking Peptide Bonds: Protein Engineering Using Sortase. *Angew. Chemie Int. Ed. 50*, 5024–5032.

(149) Paterson, B. M., Alt, K., Jeffery, C. M., Price, R. I., Jagdale, S., Rigby, S., Williams, C. C., Peter, K., Hagemeyer, C. E., and Donnelly, P. S. (2014) Enzyme-mediated site-specific bioconjugation of metal complexes to proteins: Sortase-mediated coupling of copper-64 to a single-chain antibody. *Angew. Chemie - Int. Ed. 53*, 6115–6119.

(150) Hagemeyer, C. E., Alt, K., Johnston, A. P. R., Such, G. K., Ta, H. T., Leung, M. K. M., Prabhu, S., Wang, X., Caruso, F., and Peter, K. (2015) Particle generation, functionalization and sortase A-mediated modification with targeting of single-chain antibodies for diagnostic and therapeutic use. *Nat. Protoc. 10*, 90–105.

(151) Stefan, N., Gébleux, R., Waldmeier, L., Hell, T., Escher, M., Wolter, F. I., Grawunder, U., and Beerli, R. R. (2017) Highly potent, anthracycline-based antibody drug conjugates generated by enzymatic, site-specific conjugation. *Mol. Cancer Ther.* molcanther.0688.2016.

(152) Dickgiesser, S., Rasche, N., Nasu, D., Middel, S., Hörner, S., Avrutina, O., Diederichsen, U., and Kolmar, H. (2015) Self-Assembled Hybrid Aptamer-Fc Conjugates for Targeted Delivery: A Modular Chemoenzymatic Approach. *ACS Chem. Biol.*

(153) Guimaraes, C. P., Witte, M. D., Theile, C. S., Bozkurt, G., Kundrat, L., Blom, A. E. M., and Ploegh,

H. L. (2013) Site-specific C-terminal and internal loop labeling of proteins using sortase-mediated reactions. *Nat. Protoc. 8*, 1787–1799.

(154) Griffin, M., Casadio, R., and Bergamini, C. M. (2002) Transglutaminases: Nature's biological glues. *Biochem. J. 368*, 377–396.

(155) Zemskov, E. A., Janiak, A., Hang, J., Waghray, A., and Belkin, A. M. (2006) The role of tissue transglutaminase in cell-matrix interactions. *Front Biosci 11*, 1057–1076.

(156) Akimov, S. S., Krylov, D., Fleischmana, L. F., and Belkin, A. M. (2000) Tissue transglutaminase is an integrin-binding adhesion coreceptor for fibronectin. *J. Cell Biol. 148*, 825–838.

(157) Kashiwagi, T., Yokoyama, K. ichi, Ishikawa, K., Ono, K., Ejima, D., Matsui, H., and Suzuki, E. ichiro. (2002) Crystal structure of microbial transglutaminase from Streptoverticillium mobaraense. *J. Biol. Chem. 277*, 44252–44260.

(158) Ohtsuka, T., Umezawa, Y., Nio, N., and Kubota, K. (2001) Comparison of deamidation activity of transglutaminases. *J. Food Sci. 66*, 25–29.

(159) Salis, B., Spinetti, G., Scaramuzza, S., Bossi, M., Saccani Jotti, G., Tonon, G., Crobu, D., and Schrepfer, R. (2015) High-level expression of a recombinant active microbial transglutaminase in Escherichia coli. *BMC Biotechnol. 15*.

(160) Kieliszek, M., and Misiewicz, A. (2014) Microbial transglutaminase and its application in the food industry. A review. *Folia Microbiol. (Praha). 59*, 241–250.

(161) Pasternack, R., Dorsch, S., Otterbach, J. T., Robenek, I. R., Wolf, S., and Fuchsbauer, H. L. (1998) Bacterial pro-transglutaminase from Streptoverticillium mobaraense - Purification, characterisation and sequence of the zymogen. *Eur. J. Biochem. 257*, 570–576.

(162) Zotzel, J., Keller, P., and Fuchsbauer, H. L. (2003) Transglutaminase from Streptomyces mobaraensis is activated by an endogenous metalloprotease. *Eur. J. Biochem. 270*, 3214–3222.

(163) Zotzel, J., Pasternack, R., Pelzer, C., Ziegert, D., Mainusch, M., and Fuchsbauer, H. L. (2003) Activated transglutaminase from Streptomyces mobaraensis is processed by a tripeptidyl aminopeptidase in the final step. *Eur. J. Biochem. 270*, 4149–4155.

(164) Gundersen, M. T., Keillor, J. W., and Pelletier, J. N. (2014) Microbial transglutaminase displays broad acyl-acceptor substrate specificity. *Appl. Microbiol. Biotechnol. 98*, 219–230.

(165) Fontana, A., Spolaore, B., Mero, A., and Veronese, F. M. (2008) Site-specific modification and PEGylation of pharmaceutical proteins mediated by transglutaminase. *Adv. Drug Deliv. Rev.*

(166) Spolaore, B., Raboni, S., Ramos Molina, A., Satwekar, A., Damiano, N., and Fontana, A. (2012) Local unfolding is required for the site-specific protein modification by transglutaminase. *Biochemistry 51*, 8679–8689.

(167) Tominaga, J., Kemori, Y., Tanaka, Y., Maruyama, T., Kamiya, N., and Goto, M. (2007) An enzymatic method for site-specific labeling of recombinant proteins with oligonucleotides. *Chem. Commun. (Camb).* 401–403.

(168) Takahara, M., Hayashi, K., Goto, M., and Kamiya, N. (2013) Tailing DNA aptamers with a functional protein by two-step enzymatic reaction. *J. Biosci. Bioeng. 116*, 660–665.

(169) Buchardt, J., Selvig, H., Nielsen, P. F., and Johansen, N. L. (2010) Transglutaminase-mediated methods for site-selective modification of human growth hormone. *Biopolymers 94*, 229–235.

(170) Takazawa, T., Kamiya, N., Ueda, H., and Nagamune, T. (2004) Enzymatic labeling of a single chain variable fragment of an antibody with alkaline phosphatase by microbial transglutaminase. *Biotechnol. Bioeng. 86*, 399–404.

(171) Jeger, S., Zimmermann, K., Blanc, A., Grünberg, J., Honer, M., Hunziker, P., Struthers, H., and Schibli, R. (2010) Site-specific and stoichiometric modification of antibodies by bacterial

transglutaminase. *Angew. Chemie - Int. Ed. 49*, 9995–9997.

(172) Strop, P., Liu, S. H., Dorywalska, M., Delaria, K., Dushin, R. G., Tran, T. T., Ho, W. H., Farias, S., Casas, M. G., Abdiche, Y., Zhou, D., Chandrasekaran, R., Samain, C., Loo, C., Rossi, A., Rickert, M., Krimm, S., Wong, T., Chin, S. M., Yu, J., Dilley, J., Chaparro-Riggers, J., Filzen, G. F., O'Donnell, C. J., Wang, F., Myers, J. S., Pons, J., Shelton, D. L., and Rajpal, A. (2013) Location matters: Site of conjugation modulates stability and pharmacokinetics of antibody drug conjugates. *Chem. Biol. 20*, 161–167.

(173) Siegmund, V., Schmelz, S., Dickgiesser, S., Beck, J., Ebenig, A., Fittler, H., Frauendorf, H., Piater, B., Betz, U. A. K., Avrutina, O., Scrima, A., Fuchsbauer, H. L., and Kolmar, H. (2015) Locked by Design: A Conformationally Constrained Transglutaminase Tag Enables Efficient Site-Specific Conjugation. *Angew. Chemie - Int. Ed. 54*, 13420–13424.

(174) Mero, A., Spolaore, B., Veronese, F. M., and Fontana, A. (2009) Transglutaminase-mediated PEGylation of proteins: Direct identification of the sites of protein modification by mass spectrometry using a novel monodisperse PEG. *Bioconjug. Chem. 20*, 384–389.

(175) Perler, F. B. (2002) InBase: the Intein Database. *Nucleic Acids Res. 30*, 383–384.

(176) Paulus, H. (2001) Inteins as enzymes. *Bioorg. Chem. 29*, 119–129.

(177) Mills, K. V., Johnson, M. A., and Perler, F. B. (2014) Protein splicing: How Inteins escape from precursor proteins. *J. Biol. Chem. 289*, 14498–14505.

(178) Shah, N. H., and Muir, T. W. (2014) Inteins: nature's gift to protein chemists. *Chem. Sci. 5*, 446–461.

(179) Pietrokovski, S. (2001) Intein spread and extinction in evolution. *Trends Genet.*

(180) Volkmann, G., and Mootz, H. D. (2013) Recent progress in intein research: From mechanism to directed evolution and applications. *Cell. Mol. Life Sci. 70*, 1185–1206.

(181) Martin, D. D., Xu, M. Q., and Evans, T. C. (2001) Characterization of a naturally occurring trans-splicing intein from Synechocystis sp. PCC6803. *Biochemistry 40*, 1393–1402.

(182) Iwai, H., Züger, S., Jin, J., and Tam, P. H. (2006) Highly efficient protein trans-splicing by a naturally split DnaE intein from Nostoc punctiforme. *FEBS Lett. 580*, 1853–1858.

(183) Wu, H., Hu, Z., and Liu, X.-Q. (1998) Protein trans-splicing by a split intein encoded in a split DnaE gene of Synechocystis sp. PCC6803. *Proc. Natl. Acad. Sci. 95*, 9226–9231.

(184) Shibuya, Y., Haga, N., Asano, R., Nakazawa, H., Hattori, T., Takeda, D., Sugiyama, A., Kurotani, R., Kumagai, I., Umetsu, M., and Makabe, K. (2016) Generation of camelid VHH bispecific constructs via in-cell intein-mediated protein trans-splicing. *Protein Eng. Des. Sel.* 1–7.

(185) Braner, M., Kollmannsperger, A., Wieneke, R., and Tampé, R. (2016) 'Traceless' tracing of proteins – high-affinity trans-splicing directed by a minimal interaction pair. *Chem. Sci.* 2646–2652.

(186) Han, L., Chen, J., Ding, K., Zong, H., Xie, Y., Jiang, H., Zhang, B., Lu, H., Yin, W., Gilly, J., and Zhu, J. (2017) Efficient generation of bispecific IgG antibodies by split intein mediated protein trans-splicing system. *Sci. Rep. 7*, 8360.

(187) Debelouchina, G. T., and Muir, T. W. (2017) A molecular engineering toolbox for the structural biologist. *Q. Rev. Biophys. 50*, e7.

(188) Muir, T. W., Sondhi, D., and Cole, P. A. (1998) Expressed protein ligation: a general method for protein engineering. *Proc. Natl. Acad. Sci. U. S. A. 95*, 6705–10.

(189) Mootz, H. D. (2009) Split inteins as versatile tools for protein semisynthesis. *ChemBioChem 10*, 2579–2589.

(190) Ludwig, C., Schwarzer, D., Zettler, J., Garbe, D., Janning, P., Czeslik, C., and Mootz, H. D. (2009) Semisynthesis of Proteins Using Split Inteins. *Methods Enzymol.* 1st ed. Elsevier Inc.

(191) Vila-Perelló, M., and Muir, T. W. (2010) Biological Applications of Protein Splicing. *Cell 143*, 191–200.

(192) Youngeun, K., A., C. M., and A., C. J. (2006) Selective Immobilization of Proteins onto Solid Supports through Split-Intein-Mediated Protein Trans-Splicing. *Angew. Chemie Int. Ed. 45*, 1726–1729.

(193) Giriat, I., and Muir, T. W. (2003) Protein Semi-Synthesis in Living Cells. *J. Am. Chem. Soc. 125*, 7180–7181.

(194) Appleby-Tagoe, J. H., Thiel, I. V., Wang, Y., Wang, Y., Mootz, H. D., and Liu, X. Q. (2011) Highly efficient and more general cis- and trans-splicing inteins through sequential directed evolution. *J. Biol. Chem. 286*, 34440–34447.

(195) Puthenveetil, S., Musto, S., Loganzo, F., Tumey, L. N., O'Donnell, C. J., and Graziani, E. (2016) Development of Solid-Phase Site-Specific Conjugation and Its Application toward Generation of Dual Labeled Antibody and Fab Drug Conjugates. *Bioconjug. Chem. 27*, 1030–1039.

(196) Tebbutt, N., Pedersen, M. W., and Johns, T. G. (2013) Targeting the ERBB family in cancer: Couples therapy. *Nat. Rev. Cancer*.

(197) Ganti, R., Skapek, S. X., Zhang, J., Fuller, C. E., Wu, J., Billups, C. A., Breitfeld, P. P., Dalton, J. D., Meyer, W. H., and Khoury, J. D. (2006) Expression and genomic status of EGFR and ErbB-2 in alveolar and embryonal rhabdomyosarcoma. *Mod. Pathol. 19*, 1213–1220.

(198) Herbst, R. S., and Shin, D. M. (2002) Monoclonal antibodies to target epidermal growth factor receptor-positive tumors. *Cancer 94*, 1593–1611.

(199) Schmitz, K. R., Bagchi, A., Roovers, R. C., Bergen, P. M. P. Van, and Ferguson, K. M. (2013) Structural Evaluation of EGFR Inhibition Mechanisms for Nanobodies/VHH Domains - Supplement. *Structure 21*, 1–11.

(200) Heukers, R., Vermeulen, J. F., Fereidouni, F., Bader, A. N., Voortman, J., Roovers, R. C., Gerritsen, H. C., and van Bergen En Henegouwen, P. M. P. (2013) Endocytosis of EGFR requires its kinase activity and N-terminal transmembrane dimerization motif. *J. Cell Sci. 126*, 4900–12.

(201) Roovers, R. C., Laeremans, T., Huang, L., De Taeye, S., Verkleij, A. J., Revets, H., de Haard, H. J., and van Bergen en Henegouwen, P. M. P. (2007) Efficient inhibition of EGFR signaling and of tumour growth by antagonistic anti-EFGR Nanobodies. *Cancer Immunol. Immunother. 56*, 303–317.

(202) Pirzer, T., Becher, K. S., Rieker, M., Meckel, T., Mootz, H. D., and Kolmar, H. (2018) Generation of Potent Anti-HER1/2 Immunotoxins by Protein Ligation Using Split Inteins. *ACS Chem. Biol. 13*, 2058–2066.

(203) Concepcion, J., Witte, K., Wartchow, C., Choo, S., Yao, D., Persson, H., Wei, J., Li, P., Heidecker, B., Ma, W., Varma, R., Zhao, L.-S., Perillat, D., Carricato, G., Recknor, M., Du, K., Ho, H., Ellis, T., Gamez, J., Howes, M., Phi-Wilson, J., Lockard, S., Zuk, R., and Tan, H. (2009) Label-free detection of biomolecular interactions using BioLayer interferometry for kinetic characterization. *Comb. Chem. High Throughput Screen. 12*, 791–800.

(204) Gainkam, L. O. T., Huang, L., Caveliers, V., Keyaerts, M., Hernot, S., Vaneycken, I., Vanhove, C., Revets, H., De Baetselier, P., and Lahoutte, T. (2008) Comparison of the Biodistribution and Tumor Targeting of Two 99mTc-Labeled Anti-EGFR Nanobodies in Mice, Using Pinhole SPECT/Micro-CT. *J. Nucl. Med. 49*, 788–795.

(205) De Lorenzo, C., Tedesco, A., Terrazzano, G., Cozzolino, R., Laccetti, P., Piccoli, R., and D'Alessio, G. (2004) A human, compact, fully functional anti-ErbB2 antibody as a novel antitumour agent. *Br. J. Cancer 91*, 1200–1204.

(206) Mohammed, A. F., Abdul-Wahid, A., Huang, E. H. B., Bolewska-Pedyczak, E., Cydzik, M., Broad, A. E., and Gariépy, J. (2012) The Pseudomonas aeruginosa exotoxin A translocation domain facilitates the routing of CPP-protein cargos to the cytosol of eukaryotic cells. *J. Control. Release 164*, 58–64.

(207) Verdurmen, W. P. R., Luginb??hl, M., Honegger, A., and Pl??ckthun, A. (2015) Efficient cell-specific uptake of binding proteins into the cytoplasm through engineered modular transport systems. *J. Control. Release 200*, 13–22.

(208) Zhao, J., Zhang, L. H., Jia, L. T., Zhang, L., Xu, Y. M., Wang, Z., Yu, C. J., Peng, W. D., Wen, W. H., Wang, C. J., Chen, S. Y., and Yang, A. G. (2004) Secreted antibody/granzyme B fusion protein stimulates selective killing of HER2-overexpressing tumor cells. *J. Biol. Chem. 279*, 21343–21348.

(209) Rosano, G. L., and Ceccarelli, E. A. (2014) Recombinant protein expression in Escherichia coli: Advances and challenges. *Front. Microbiol. 5*, 1–17.

(210) Lobstein, J., Emrich, C. A., Jeans, C., Faulkner, M., Riggs, P., and Berkmen, M. (2012) SHuffle, a novel Escherichia coli protein expression strain capable of correctly folding disulfide bonded proteins in its cytoplasm. *Microb. Cell Fact. 11*.

(211) Chen, J., Song, J. L., Zhang, S., Wang, Y., Cui, D. F., and Wangt, C. C. (1999) Chaperone activity of DsbC. *J. Biol. Chem. 274*, 19601–19605.

(212) Lebendiker, M., and Danieli, T. (2014) Production of prone-to-aggregate proteins. *FEBS Lett. 588*, 236–246.

(213) Kamath, A. V., and Iyer, S. (2015) Preclinical Pharmacokinetic Considerations for the Development of Antibody Drug Conjugates. *Pharm. Res.*

(214) Bornstein, G. G. (2015) Antibody Drug Conjugates: Preclinical Considerations. *AAPS J. 17*, 525–534.

(215) Huynh, K., and Partch, C. L. (2015) Analysis of protein stability and ligand interactions by thermal shift assay. *Curr. Protoc. protein Sci. 79*, 28.9.1-28.9.14.

(216) Vermeer, A. W. P., and Norde, W. (2000) The thermal stability of immunoglobulin: Unfolding and aggregation of a multi-domain protein. *Biophys. J. 78*, 394–404.

(217) Pastrana, D. V., and FitzGerald, D. J. (2006) A nonradioactive, cell-free method for measuring protein synthesis inhibition by Pseudomonas exotoxin. *Anal. Biochem. 353*, 266–271.

(218) Austin, C. D., Mazière, A. M. De, Pisacane, P. I., Dijk, S. M. van, Eigenbrot, C., Sliwkowski, M. X., Klumperman, J., and Scheller, R. H. (2004) Endocytosis and Sorting of ErbB2 and the Site of Action of Cancer Therapeutics Trastuzumab and Geldanamycin. *Mol. Biol. Cell 15*, 5268–5282.

(219) Smith, D. C., Spooner, R. A., Watson, P. D., Murray, J. L., Hodge, T. W., Amessou, M., Johannes, L., Lord, J. M., and Roberts, L. M. (2006) Internalized pseudomonas exotoxin A can exploit multiple pathways to reach the endoplasmic reticulum. *Traffic 7*, 379–393.

(220) Sellmann, C., Doerner, A., Knuehl, C., Rasche, N., Sood, V., Krah, S., Rhiel, L., Messemer, A., Wesolowski, J., Schuette, M., Becker, S., Toleikis, L., Kolmar, H., and Hock, B. (2016) Balancing Selectivity and Efficacy of Bispecific EGFR x c-MET Antibodies and Antibody-Drug Conjugates. *J. Biol. Chem.* jbc.M116.753491.

(221) Jia, B., and Jeon, C. O. (2016) High-throughput recombinant protein expression in Escherichia coli : current status and future perspectives.

(222) Bessette, P. H., Aslund, F., Beckwith, J., and Georgiou, G. (1999) Efficient folding of proteins with multiple disulfide bonds in the Escherichia coli cytoplasm. *Proc. Natl. Acad. Sci. 96*, 13703–13708.

(223) Mirzadeh, K., Martínez, V., Toddo, S., Guntur, S., Herrgård, M. J., Elofsson, A., Nørholm, M. H. H., and Daley, D. O. (2015) Enhanced Protein Production in Escherichia coli by Optimization of Cloning Scars at the Vector-Coding Sequence Junction. *ACS Synth. Biol. 4*, 959–965.

(224) Goodman, D. B., Church, G. M., and Kosuri, S. (2013) Causes and effects of N-terminal codon bias in bacterial genes. *Science (80-.). 342*, 475–479.

(225) McCluskey, A. J., Poon, G. M. K., and Gariépy, J. (2007) A rapid and universal tandem-purification

strategy for recombinant proteins. *Protein Sci. 16*, 2726–2732.

(226) Costa, S., Almeida, A., Castro, A., and Domingues, L. (2014) Fusion tags for protein solubility, purification, and immunogenicity in Escherichia coli: The novel Fh8 system. *Front. Microbiol.*

(227) Zhao, X., Li, G., and Liang, S. (2013) Several affinity tags commonly used in chromatographic purification. *J. Anal. Methods Chem.*

(228) Kawa, S., Onda, M., Ho, M., Kreitman, R. J., Bera, T. K., and Pastan, I. (2011) The improvement of an anti-CD22 immunotoxin: Conversion to single-chain and disulfide stabilized form and affinity maturation by alanine scan. *MAbs 3*, 479–486.

(229) Costa, S. J., Coelho, E., Franco, L., Almeida, A., Castro, A., and Domingues, L. (2013) The Fh8 tag: A fusion partner for simple and cost-effective protein purification in Escherichia coli. *Protein Expr. Purif. 92*, 163–170.

(230) Veggiani, G., Zakeri, B., and Howarth, M. (2014) Superglue from bacteria: Unbreakable bridges for protein nanotechnology. *Trends Biotechnol.*

(231) Zakeri, B., and Howarth, M. (2010) Spontaneous intermolecular amide bond formation between side chains for irreversible peptide targeting. *J. Am. Chem. Soc. 132*, 4526–4527.

(232) Ludwig, C., Schwarzer, D., and Mootz, H. D. (2008) Interaction studies and alanine scanning analysis of a semi-synthetic split intein reveal thiazoline ring formation from an intermediate of the protein splicing reaction. *J. Biol. Chem. 283*, 25264–25272.

(233) Philo, J. S., and Arakawa, T. (2009) Mechanisms of protein aggregation. *Curr. Pharm. Biotechnol. 10*, 348–51.

(234) Zettler, J., Schütz, V., and Mootz, H. D. (2009) The naturally split Npu DnaE intein exhibits an extraordinarily high rate in the protein trans-splicing reaction. *FEBS Lett. 583*, 909–914.

(235) Stevens, A. J., Brown, Z. Z., Shah, N. H., Sekar, G., Cowburn, D., and Muir, T. W. (2016) Design of a Split Intein with Exceptional Protein Splicing Activity. *J. Am. Chem. Soc. 138*, 2162–2165.

(236) Houen, G., Olsen, D. T., Hansen, P. R., Petersen, K. B., and Barkholt, V. (2003) Preparation of bioconjugates by solid-phase conjugation to ion exchange matrix-adsorbed carrier proteins. *Bioconjug. Chem. 14*, 75–79.

(237) Chen, X., Zaro, J. L., and Shen, W. C. (2013) Fusion protein linkers: Property, design and functionality. *Adv. Drug Deliv. Rev. 65*, 1357–1369.

(238) Fukuhara, T., Kim, J., Hokaiwado, S., Nawa, M., Okamoto, H., Kogiso, T., Watabe, T., and Hattori, N. (2017) A novel immunotoxin reveals a new role for CD321 in endothelial cells. *PLoS One* 1–12.

(239) Klausz, K., Kellner, C., Derer, S., Valerius, T., Staudinger, M., Burger, R., Gramatzki, M., and Peipp, M. (2015) The novel multispecies Fc-specific Pseudomonas exotoxin A fusion protein α-Fc-ETA' enables screening of antibodies for immunotoxin development. *J. Immunol. Methods 418*, 75–83.

(240) Zheng, K., Bantog, C., and Bayer, R. (2011) The impact of glycosylation on monoclonal antibody conformation and stability. *MAbs 3*.

(241) Moody, P. R., Sayers, E. J., Magnusson, J. P., Alexander, C., Borri, P., Watson, P., and Jones, A. T. (2015) Receptor Crosslinking: A General Method to Trigger Internalization and Lysosomal Targeting of Therapeutic Receptor:Ligand Complexes. *Mol. Ther. 23*, 1888–1898.

(242) Jackson, M. E., Simpson, J. C., Girod, A., Pepperkok, R., Roberts, L. M., and Lord, J. M. (1999) The KDEL retrieval system is exploited by Pseudomonas exotoxin A, but not by Shiga-like toxin-1, during retrograde transport from the Golgi complex to the endoplasmic reticulum. *J. Cell Sci. 112 (Pt 4*, 467–75.

(243) Goyal, A., and Batra, J. K. (2000) Inclusion of a furin-sensitive spacer enhances the cytotoxicity of ribotoxin restrictocin containing recombinant single-chain immunotoxins. *Biochem. J. 345*, 247–254.

(244) Wang, T., Zhao, J., Ren, J. L., Zhang, L., Wen, W. H., Zhang, R., Qin, W. W., Jia, L. T., Yao, L. B., Zhang, Y. Q., Chen, S. Y., and Yang, A. G. (2007) Recombinant immunoproapoptotic proteins with furin site can translocate and kill HER2-positive cancer cells. *Cancer Res. 67*, 11830–11839.

(245) Wang, F., Ren, J., Qiu, X. C., Wang, L. F., Zhu, Q., Zhang, Y. Q., Huan, Y., Meng, Y. L., Yao, L. B., Chen, S. Y., Xu, Y. M., and Yang, A. G. (2010) Selective cytotoxicity to HER2-positive tumor cells by a recombinant e23sFv-TD-tBID protein containing a furin cleavage sequence. *Clin. Cancer Res. 16*, 2284–2294.

(246) Kim, W., Essalmani, R., Szumska, D., Creemers, J. W. M., Roebroek, A. J. M., D'Orleans-Juste, P., Bhattacharya, S., Seidah, N. G., and Prat, A. (2012) Loss of Endothelial Furin Leads to Cardiac Malformation and Early Postnatal Death. *Mol. Cell. Biol. 32*, 3382–3391.

(247) Kaplan, G., Lee, F., Onda, M., Kolyvas, E., Bhardwaj, G., Baker, D., and Pastan, I. (2016) Protection of the furin cleavage site in low-toxicity immunotoxins based on Pseudomonas exotoxin A. *Toxins (Basel)*. *8*, 1–14.

(248) Choi, K. Y., Swierczewska, M., Lee, S., and Chen, X. (2012) Protease-activated drug development. *Theranostics 2*, 156–179.

(249) Dubowchik, G. M., Firestone, R. A., Padilla, L., Willner, D., Hofstead, S. J., Mosure, K., Knipe, J. O., Lasch, S. J., and Trail, P. A. (2002) Cathepsin B-Labile Dipeptide Linkers for Lysosomal Release of Doxorubicin from Internalizing Immunoconjugates: Model Studies of Enzymatic Drug Release and Antigen-Specific In Vitro Anticancer Activity 855–869.

(250) Chu, D. S. H., Johnson, R. N., and Pun, S. H. (2012) Cathepsin B-sensitive polymers for compartment-specific degradation and nucleic acid release. *J. Control. Release 157*, 445–454.

(251) Zhong, Y. J., Shao, L. H., and Li, Y. (2013) Cathepsin B-cleavable doxorubicin prodrugs for targeted cancer therapy (Review). *Int. J. Oncol. 42*, 373–383.

(252) Sellmann, C., Doerner, A., Knuehl, C., Rasche, N., Sood, V., Krah, S., Rhiel, L., Messemer, A., Wesolowski, J., Schuette, M., Becker, S., Toleikis, L., Kolmar, H., and Hock, B. (2016) Balancing selectivity and efficacy of bispecific Epidermal Growth Factor Receptor (EGFR) x c-MET antibodies and antibody-drug conjugates. *J. Biol. Chem. 291*, 25106–25119.

(253) Liu, L., Zeng, W., Wortinger, M. A., Yan, S. B., Cornwell, P., Peek, V. L., Stephens, J. R., Tetreault, J. W., Xia, J., Manro, J. R., Credille, K. M., Ballard, D. W., Brown-Augsburger, P., Wacheck, V., Chow, C. K., Huang, L., Wang, Y., Denning, I., Davies, J., Tang, Y., Vaillancourt, P., and Lu, J. (2014) LY2875358, a neutralizing and internalizing anti-MET bivalent antibody, inhibits HGF-dependent and HGF-independent MET activation and tumor growth. *Clin. Cancer Res. 20*, 6059–6070.

(254) Mazor, Y., Hansen, A., Yang, C., Chowdhury, P. S., Wang, J., Stephens, G., Wu, H., and Dall'Acqua, W. F. (2015) Insights into the molecular basis of a bispecific antibody's target selectivity. *MAbs 7*, 461–469.

7. Appendix

7.1. Supplementary Information

7.1.1. Figures

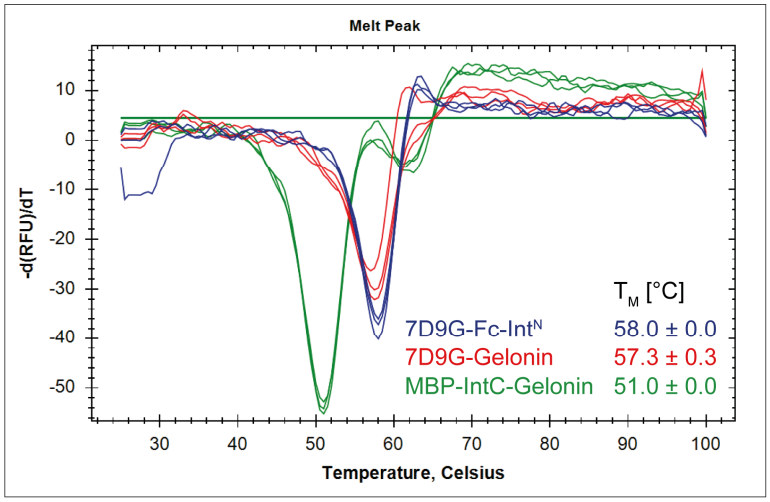

Figure S 1: Melting curve determination of 7D9G-Gelonin IT by thermal shift assay.
The measurement was performed in triplicate and all curves are depicted. Blue = 7D9G-Fc-Int^{N}; Red = 7D9G-Gelonin; Green = MBP-Int^{C}-Gelonin. The depicted T_M was calculated from all three curves and the standard deviation is given.

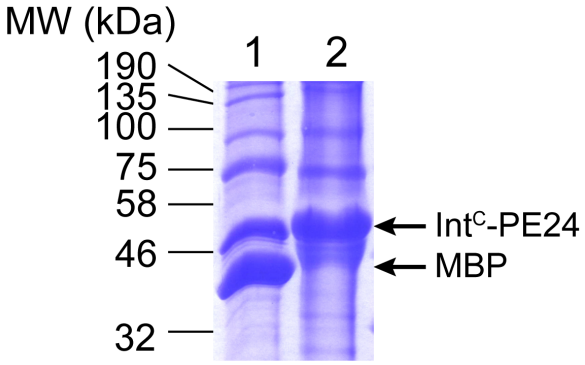

Figure S 2: TEV cleavage of MBP-Int^{C}-PE24.
A TEV cleavage site was introduced between MBP and IntC and cleavage was conducted O/N at RT. A fraction precipitated during the reaction and was analyzed by SDS-PAGE. 1 = soluble fraction mainly containing free MBP. 2 = precipitate mainly containing Int^{C}-PE24.

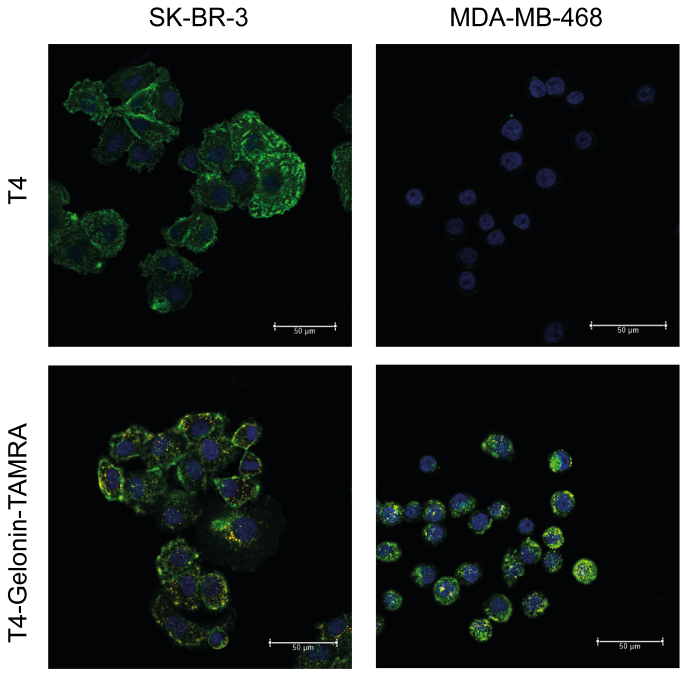

Figure S 3: Cell binding and internalization studies of trastuzumab and T4-Gelonin-TAMRA.
SK-BR-3 cells (HER2$^+$) and MDA-MB-468 (HER$^-$) cells were incubated with antibodies and visualized by staining with α–hIgG-Fab Alexa488 (green) detection antibody. Gelonin was labelled with TAMRA (red) through SrtA reaction of MBP-Int^C-Gelonin containing a LPTEGS tag and GGG-TAMRA. The labelled toxin was then spliced to T4 in a standard PTS reaction. Colocalized signals are depicted in yellow.

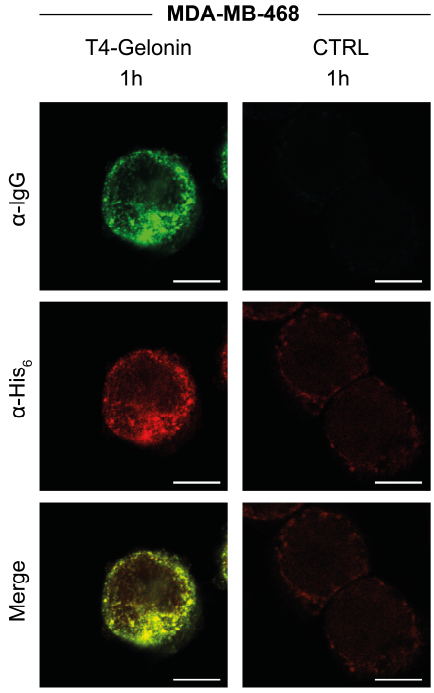

Figure S 4: Unspecific binding of trastuzumab ITs on MDA-MB-468 cells.
MDA-MB-468 cells (HER2 negative) were treated for 1h with T4-Gelonin, washed with low pH glycine buffer to remove surface bound conjugates and stained directly. CTRL cells were not incubated with a sample antibody but stained with secondary antibodies. α-hIgG Fab-Alexa 488 (1:500) and α-His6 Alexa 647 antibody (1:1000) were used to specifically visualize the antibody fraction and the toxin fraction of the ITs, respectively. Scale bar = 10 µm.

7.1.2. Protein Sequences

Int^{C}

STGKRVPIKDLLGEKDFEIWAINEQTMKLESAKVSRVFCTGKKLVYTLKTRLGRTIKATANHRFLTIDGWKRLD
ELSLKEHIALPRKLESSSLQLAPEIEKLPQSDIYWDPIVSITETGVEEVFDLTVPGLRNFVANDIIVHN|SIEGSGS

Int^{N}

CISGDSLISLA

FCS

DKTHKASGGRHRQPRGWEQLGGGGGS

Gelonin

GLDTVSFSTKGATYITYVNFLNELRVKLKPEGNSHGIPLLRKKCDDPGKCFVLVALSNDNGQLAEIAIDVTSVYV
VGYQVRNRSYFFKDAPDAAYEGLFKNTIKTRLHFGGSYPSLEGEKAYRETTDLGIEPLRIGIKKLDENAIDNYKP
TEIASSLLVVIQMVSEAARFTFIENQIRNNFQQRIRPANNTISLENKWGKLSFQIRTSGANGMFSEAVELERAN
GKKYYVTAVDQVKPKIALLKFVDKDPKYPYDVPDYAHHHHHHLPETGS

PE24

PTGAEFLGDGGDISFSTRGTQNWTVERLLQAHRQLEERGYVFVGYHGTFLEAAQSIVFGGVRARSQDLDAIW
RGFYIAGDPALAYGYAQDQEPDARGRIRNGALLRVYVPRSSLPGFYRTSLTLAAPEAAGEVERLIGHPLPLRLD
AITGPEEEGGRLETILGWPLAERTVVIPSAIPTDPRNVGGDLDPSSIPDKEQAISALPDYASQPGKPPYPYDVPDY
AHHHHHHKDEL

Trx

SDKIIHLTDDSFDTDVLKADGAILVDFWAHWCGPCKMIAPILDEIADEYQGKLTVAKLNIDHNPGTAPKYGIRG
IPTLLLFKNGEVAATKVGALSKGQLKEFLDANLAGS

MBP

MKTEEGKLVIWINGDKGYNGLAEVGKKFEKDTGIKVTVEHPDKLEEKFPQVAATGDGPDIIFWAHDRFGGYA
QSGLLAEITPDKAFQDKLYPFTWDAVRYNGKLIAYPIAVEALSLIYNKDLLPNPPKTWEEIPALDKELKAKGKSA
LMFNLQEPYFTWPLIAADGGYAFKYENGKYDIKDVGVDNAGAKAGLTFLVDLIKNKHMNADTDYSIAEAAFN
KGETAMTINGPWAWSNIDTSKVNYGVTVLPTFKGQPSKPFVGVLSAGINAASPNKELAKEFLENYLLTDEGLE
AVNKDKPLGAVALKSYEEELAKDPRIAATMENAQKGEIMPNIPQMSAFWYAVRTAVINAASGRQTVDEALKD
AQTNSSSNNNNNNNNNN

7D12

AAQVKLEESGGGSVQTGGSLRLTCAASGRTSRSYGMGWFRQAPGKEREFVSGISWRGDSTGYADSVKGRFTI
SRDNAKNTVDLQMNSLKPEDTAIYYCAAAAGSAWYGTLYEYDYWGQGTQVTVSS

9G8

EVQLVESGGGLVQAGGSLRLSCAASGRTFSSYAMGWFRQAPGKEREFVVAINWSSGSTYYADSVKGRFTISR
DNAKNTMYLQMNSLKPEDTAVYYCAAGYQINSGNYNFKDYEYDYWGQGTQVTVSS

Hinge

GSEPKSCDKTHTCPPCP

Fc (IgG1)

APELLGGPSVFLFPPKPKDTLMISRTPEVTCVVVDVSHEDPEVKFNWYVDGVEVHNAKTKPREEQYNSTYRVV
SVLTVLHQDWLNGKEYKCKVSNKALPAPIEKTISKAKGQPREPQVYTLPPSRDELTKNQVSLTCLVKGFYPSDI
AVEWESNGQPENNYKTTPPVLDSDGSFFLYSKLTVDKSRWQQGNVFSCSVMHEALHNHYTQKSLSLSP

Trastuzumab-HC

EVQLVESGGGLVQPGGSLRLSCAASGFNIKDTYIHWVRQAPGKGLEWVARIYPTNGYTRYADSVKGRFTISAD
TSKNTAYLQMNSLRAEDTAVYYCSRWGGDGFYAMDYWGQGTLVTVSSASTKGPSVFPLAPSSKSTSGGTAA
LGCLVKDYFPEPVTVSWNSGALTSGVHTFPAVLQSSGLYSLSSVVTVPSSSLGTQTYICNVNHKPSNTKVDKKV
EPPKSCDKTHTCPPCPAPELLGGPSVFLFPPKPKDTLMISRTPEVTCVVVDVSHEDPEVKFNWYVDGVEVHNA
KTKPREEQYNSTYRVVSVLTVLHQDWLNGKEYKCKVSNKALPAPIEKTISKAKGQPREPQVYTLPPSRDELTKN
QVSLTCLVKGFYPSDIAVEWESNGQPENNYKTTPPVLDSDGSFFLYSKLTVDKSRWQQGNVFSCSVMHEALH
NHYTQKSLSLSPGK

Trastuzumab-LC

DIQMTQSPSSLSASVGDRVTITCRASQDVNTAVAWYQQKPGKAPKLLIYSASFLYSGVPSRFSGSRSGTDFTLT
ISSLQPEDFATYYCQQHYTTPPTFGQGTKVEIKRTVAAPSVFIFPPSDEQLKSGTASVVCLLNNFYPREAKVQW
KVDNALQSGNSQESVTEQDSKDSTYSLSSTLTLSKADYEKHKVYACEVTHQGLSSPVTKSFNRGEC

7.2. List of figures

7.3. Abbreviations

aa	Amino acids
Ab	Antibody
ADCC	Antibody-dependent cellular cytotoxicity
ADCs	Antibody-drug-conjugates
ADPr	ADP-ribosyltransferase
AP	Alkaline phosphatase
APC	Antigen presenting cell
APS	Ammonium persulfate
BSA	Bovine serum albumin
C	Constant domain
CDC	Complement dependent cytotoxicity
CDR	Complementarity-determining regions
CV	Column volume
DAR	Drug/antibody ratio
ddH_2O	Double deionized water (autoclaved)
dH_2O	Deionized water
DMF	N,N-Dimethylformamid
DMSO	Dimethyl sulfoxide
DSC	Differential scanning calorimetry
DT	Diphtheria toxin
DTT	Dithiotreitol
EDTA	Ethylenediaminetetraacetic acid
EEE	Endosomal escape enhancer
eEF2	Eukaryotic elongation factor-2
EGFR, HER1	Epidermal growth factor receptor
EPL	Expressed protein ligation
ER	Endoplasmic reticulum
ETA	*Pseudomonas* Exotoxin A
Fab	Antigen binding fragment
FACS	Fluorescence-activated cell sorting
FcRn	Neonatal Fc receptor
FcγR	Fc gamma receptor
FR	Framework
FT	Flow-through
GOI	Gene of interest
HC	Heavy chain
HCAb	Heavy-chain antibody
HER2	Human epidermal growth factor receptor 2
HV	Hypervariable loop

Int^N	N-terminal intein part
IPTG	Isopropyl β-D-1 thiogalactopyranoside
ISB	Intein splicing buffer
LC	Light chain
mAb	Monoclonal antibody
mTG	Microbial transglutaminase
NK cell	Natural killer cell
PAMP	Pathogen-associated molecular patterns
PBS	Phosphate buffered saline
PE	*Pseudomonas* Exotoxin A
PEI	Polyethylenimine
PK	Pharmakokinetics
PRR	Pattern recognition receptors
RIP	Ribosome inactivating protein
RRL	Rabbit reticulocyte lysate
rRNA	Ribosomal RNA
RT	Room temperature
scFv	Single chain variable fragment
SDS	Sodium dodecyl sulfate
TAR	Toxin/antibody ratio
TCEP	Tris(2-carboxyethyl)phosphin
T-DM1	Trastuzumab-emtansin
TEMED	Tetramethylethylenediamine
TFA	Trifluoressigsäure
Tris	Tris(hydroxymethyl)aminomethan
V	Variable domain
VHH	V_H of heavy chain antibody
vNAR	New Antigen Receptor

7.4. Danksagung

Zum Schluss dieser Arbeit möchte ich mich bei einer Reihe von Personen bedanken, ohne die diese Arbeit nicht möglich gewesen wäre.

Herrn Prof. Dr. Harald Kolmar möchte ich für die Möglichkeit danken, meine Dissertation in seiner Arbeitsgruppe und unter seiner Anleitung durchzuführen. Ich möchte ihm für sein Vertrauen danken und dass er meine Meinung stets respektiert hat. Unter anderem hat dies zu einer Kehrtwende des Themas nach etwa einem Jahr geführt, wobei der Impuls zum Themenwechsel von mir kam und er mich dabei voll und ganz unterstützt hat. Außerdem danke ich ihm für die Unterstützung und die Möglichkeit an Konferenzen teilzunehmen, um meine Forschungsergebnisse zu präsentieren.

Herrn Prof. Dr. Henning Mootz danke ich herzlich für die Übernahme der Korreferentenaufgabe. Dank seiner Expertise auf dem Feld der Inteine machte diese Arbeit erst möglich.

Herrn Dr. Siegfried Neumann danke ich für seine Tipps und seine Arbeit als erster Fachprüfer.

Herrn PD Dr. Tobias Meckel danke ich für seine Arbeit als zweitem Fachprüfer und für die Hilfe bei gestochen scharfen konfokalen Mikroskopieaufnahmen, sowie den interessanten Gesprächen über Wissenschaft, Musik und andere interessante Themen.

Kira-Sophie Becher aus dem Arbeitskreis von Prof. Mootz danke ich sehr, da wir in diesem Projekt eng zusammengearbeitet haben und sie mir einige Tipps und Hilfestellungen bei den Inteinen gab.

Dr. Andreas Christmann danke ich für die zahlreichen Tipps in allen wissenschaftlichen Belangen, sowie vertrauensvollen Gesprächen über den Fortgang einer Doktorarbeit. Diese haben mich unter anderem darin bestärkt diese erfolgreich abzuschließen.

Aileen Ebenig möchte ich für die frühmorgentlichen Gespräche danken, wenn die meisten anderen noch tief geschlummert haben. Auch auf ihre Hilfe in der Zellkultur konnte ich stets vertrauen.

Bei Desislava Yanakieva möchte ich mir für die hervorragende und selbstständige Arbeit während ihrer Masterarbeit bedanken und dass sie sich trotz wenig aussichtsreichem Thema nicht hat entmutigen lassen. Das sah man auch daran, dass sie sogar zur Doktorarbeit blieb. Vielen Dank auch in dieser Zeit für die zahlreichen wissenschaftlichen Diskussionen, die Hilfe in der Zellkultur und die tolle Gesellschaft beim Konferenzbesuch in Lissabon.

Für letzteres möchte ich mich auch bei Hendrik Schneider bedanken, der mir auch im Labor mit zahlreichen „Chemikertipps“ weitergeholfen hat. Ihm rechne ich auch seine unendliche Geduld mit HPLCs, Lyophille und zahlreichen Pumpen hoch an!

Bei Bastian Becker und Simon Englert möchte ich mich ebenfalls für Kniffe und Tricks bei der Peptidsynthese, HPLC und MS Analysen danken.

Marcel Rieker danke ich für die grandiose Gesellschaft beim Wandern im Kleinwalsertal sowie auf weiteren anschließenden Touren mit dem Höhepunkt der Hüttenwanderung in Österreich. Wissenschaftliche Diskussionen im Privaten haben auch für diese Arbeit essentielle Anregungen gebracht. Nicht zuletzt sein guter Draht zu Merck hat außerdem das ein oder andere ermöglicht, das sonst nicht zu realisieren gewesen wäre.

Des Weiteren möchte ich mich bei den Hefe-Dudes Steffen Hinz, Julius Grzeschik und Lukas „Klausi“ Deweid bedanken, die mir bei FACS Problemen und anderen Hefe-Methoden weitergeholfen haben. Die „interessanten“ musikalischen Ausflüge in ihrem Labor haben mir außerdem viele Male ein Lächeln auf die Lippen gezaubert.

Dem gesamten Bio-Labor danke ich für den doch überwiegend guten, rocklastigen Musikgeschmack. Musik macht doch so manche Arbeit deutlich leichter.

Ein großer Dank geht auch an die Kicker-Gruppe bestehend aus Hendrik, Klausi, Basti und unserem Frischling Arturo Macarron. Was wäre die Promotion nur ohne das alltägliche Kickern gewesen?

Barbara Diestelmann danke ich für die Gespräche in den Mittagspausen über selbstgekochtes Essen und Fertigsuppen. Außerdem natürlich für die vielen organisatorischen Aufgaben, die sie für uns gemeistert hat.

Auch allen anderen Mitgliedern des AK Kolmar möchte ich natürlich herzlich danken, alle aufzuzählen würde die Seitenzahl nochmal verdoppeln, weshalb ich dies hier verallgemeinern muss.

Zum Schluss möchte ich mich bei meiner Familie bedanken, die mich von Geburt an in allem unterstützt hat, was ich angefangen hab. In schwierigen Zeiten konnte ich mich immer auf sie verlassen. Zu dieser Familie darf ich seit letztem Jahr auch meine langjährige Freundin und jetzt Frau Kerstin zählen, die ich über alles Liebe und ohne die ich diese Promotion wohl nicht abgeschlossen hätte. In schweren Zeiten, die es zur Genüge gab, war sie mein Fels in der Brandung und lies mich weitermachen. Vielen, vielen Dank dafür!

7.5. Curriculum vitae

Name:	Thomas Pirzer
Geburtsdatum:	27.05.1990
Geburtsort:	Haßfurt
Staatsangehörigkeit:	deutsch
Familienstand:	verheiratet

Ausbildung:

10/2012 – 10/2014	TU Darmstadt – Promotion zum Dr. rer. nat. Promotion am Clemens-Schöpf-Institut für Organische Chemie und Biochemie unter Prof. Dr. Harald Kolmar: *Generation of anti-HER1/2 Immunotoxins by Protein Ligation using Split Inteins*
10/2012 – 10/2014	Johannes-Gutenberg-Universität Mainz – Wissenschaftlicher Mitarbeiter Wissenschaftlicher Mitarbeiter am Institut für Toxikologie unter Prof. Dr. Bernd Kaina:
10/2012 – 10/2014	TU Darmstadt - Master of Science Studiengang: Biomolecular Engineering Masterarbeit am Paul-Ehrlich-Institut in Langen unter Prof. Dr. Gerald G. Schumann: *The Role of Reprogramming Factors and Gene Delivery Method in Transcriptional Regulation and Mobilization of Endogenous LINE-1 Retrotransposons in Human Induced Pluripotent Stem Cells* Abschlussnote: sehr gut (1,18)
10/2009 – 12/2012	TU Darmstadt - Bachelor of Science Studiengang: Biomolecular Engineering Bachelorarbeit am Clemens-Schöpf-Institut für Organische Chemie und Biochemie unter Prof. Dr. Harald Kolmar: *Analyse der inhibitorischen Eigenschaften eines Matriptase I-Inhibitors durch Alanin-Scanning-Mutagenese* Abschlussnote: sehr gut (1,35)
09/2000 – 06/2009	Abitur am Regiomontanus-Gymnasium in Haßfurt

7.6. Affirmations

Thomas Pirzer Darmstadt, 14.06.2018

Eidesstattliche Erklärung

Ich erkläre hiermit, dass ich meine Dissertation selbstständig und nur mit den angegebenen Hilfsmitteln angefertigt habe.

_____

Thomas Pirzer

Eidesstattliche Erklärung

Ich erkläre hiermit, noch keinen Promotionsversuch unternommen zu haben.

_____

Thomas Pirzer

Thomas Pirzer Darmstadt, 14.06.2018

Erklärung

Ich erkläre hiermit, dass die elektronische Version der Doktorarbeit mit der schriftlichen Version übereinstimmt. Die elektronische Version liegt dem Prüfungssekretariat vor.

_____

Thomas Pirzer